NASA-CR-192346

ASTRO
SCIENCES

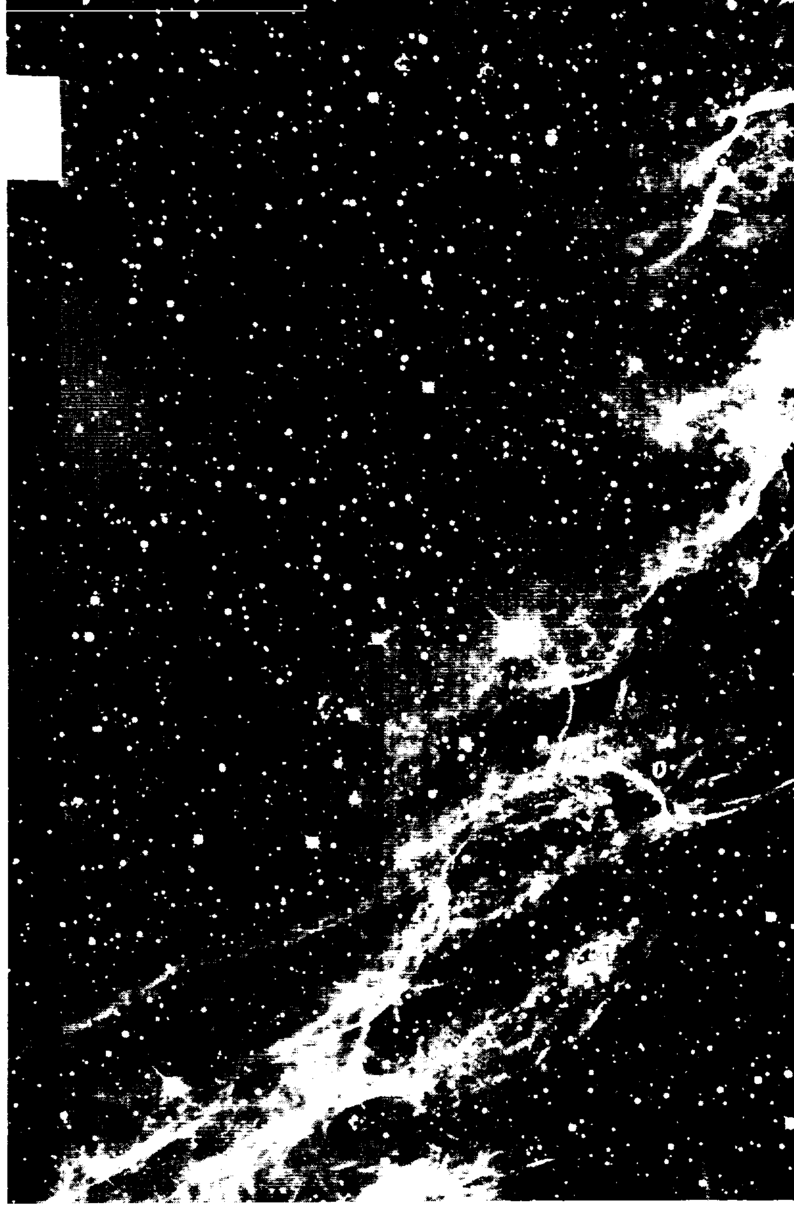

(NASA-CR-192346) MERCURY ORBITER MISSION STUDY (IIT Research Inst.) 177 p

N93-71610

Unclas

Z9/18 0150733

Report No. M-26

MERCURY ORBITER MISSION STUDY

Report No. M-26

MERCURY ORBITER MISSION STUDY

by

David A. Klopp

and

William C. Wells

Astro Sciences
IIT RESEARCH INSTITUTE
Chicago, Illinois 60616

for

Office of Space Science and Applications
NASA Headquarters
Washington, D. C.

Contract No. NASW-2144

APPROVED BY:

D L Roberts

D. L. Roberts, Manager
Astro Sciences

June 1971

MERCURY ORBITER MISSION STUDY

SUMMARY

This report provides a preliminary analysis of an unmanned Mercury orbiter mission which might be flown in the early 1980's. In addition to investigating the applicability of solar electric low-thrust technology to such a mission, the study also identifies scientific objectives for a Mercury orbiter, provides estimates of science payloads appropriate to a Mercury orbiter, and compares several mission concepts for an early orbiter mission.

Approximately 35 specific "measurables" are identified as relevant to the scientific exploration of Mercury. These measurables are listed in Summary Figure 1. Three groupings are shown in the figure: (1) those measurables likely to be investigated by an orbiter mission, (2) those likely to be investigated by a combination of orbiter and lander missions, and (3) those likely to be investigated by lander missions alone. The figure also provides an evaluation of the utility of various measurement techniques in studying these measurables. The major role expected of an orbiter is that of obtaining global surface imagery of one to three km resolution, which is not likely to be provided by flyby missions. Visual imagery experiments performed from an orbiter would be most useful in investigating surface elevations, lithologic contacts, surface topography, surface appearance, and the orientation of Mercury's rotation axis. Lander and orbiting spacecraft working together would prove most valuable for objectives requiring both

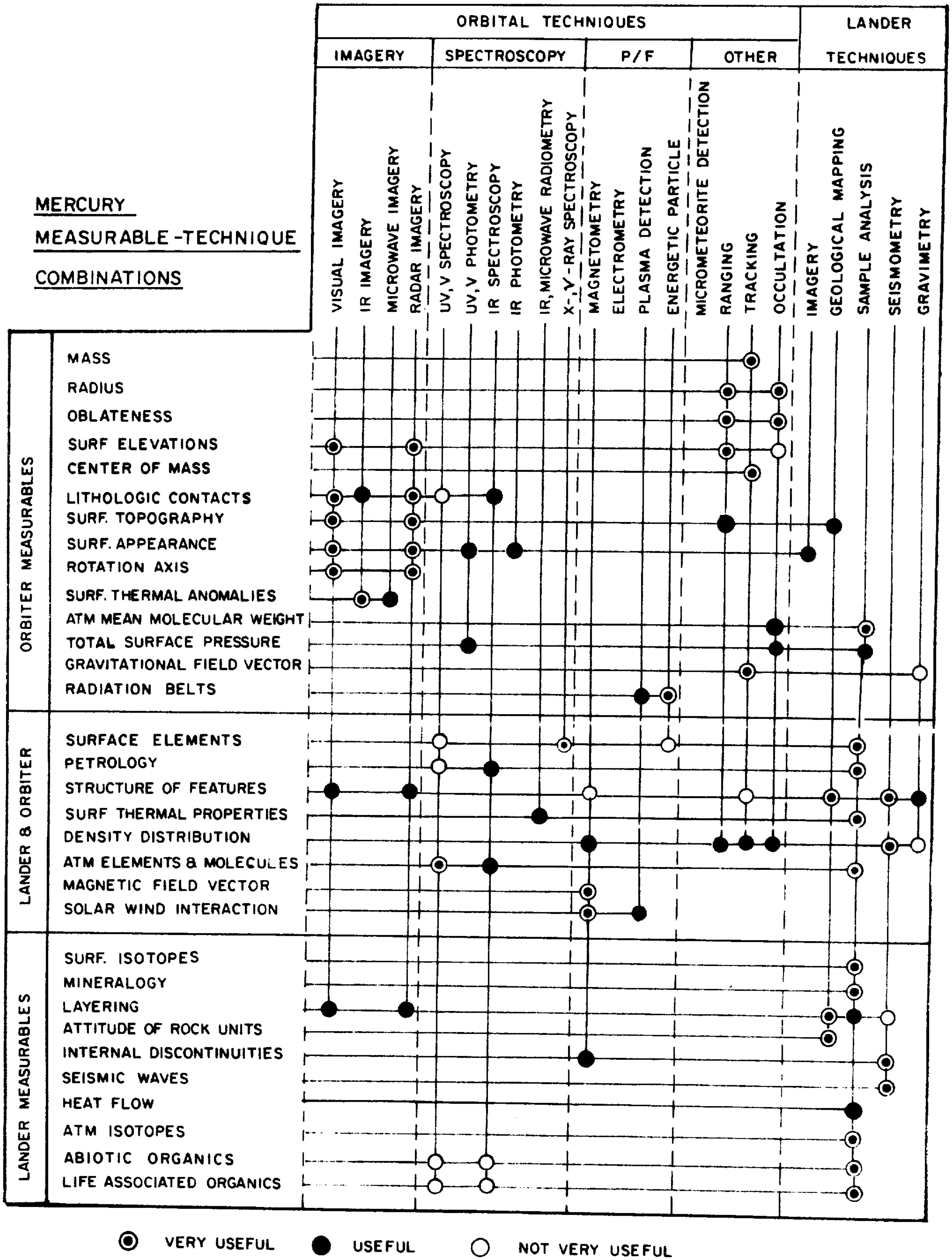

SUMMARY FIGURE I.

extensive surface mapping and ground truth measurements, such as the study of surface elemental composition and petrology, the structure of observed surface features, and the structure of the interior. The determination of surface isotopic abundances and surface minerology and the detection and study of pre-biotic phases of extraterrestrial life require lander missions, but not orbiters.

Specific measurements have been defined (in terms of desired resolution, planetary coverage, lighting conditions, etc.) for those measurables which can be investigated from an orbiting spacecraft. These measurement definitions then form the basis for estimating the weight, power, and data rate requirements of the scientific instrumentation of various orbiter missions. Five mission classes, shown in Summary Figure 2, have been identified:

A. A "particles and fields" spacecraft of nearly 200 kg, carrying 22 kg of particles and fields instrumentation along with a few low data-rate non-imaging planetology instruments in a moderately eccentric orbit of medium inclination.

B. A "minimum planetology" spacecraft of about 250 kg carrying 27 kg of science instruments including a television camera and an infrared spectrometer. The emphasis is upon regional scale (3 km resolution) surface examination conducted from a low-altitude circular polar orbit.

MISSON	SPACECRAFT MODEL(S)		SCIENCE	ORBITER	PERIAPSE ALTITUDE	ϵ	INCLINATION	ORBIT PERIOD
A	PARTICLES AND FIELDS		22 kg	198 kg	500 km	0.6	50°	7.4^h
B	MINIMUM PLANETOLOGY		27	267	500	0	90	1.9
C	BASELINE PLANETOLOGY		67	437	500	0	90	1.9
D	BROAD FIRST LOOK	(A)	22	198	500	0.6	50	7.4
		(C)	67	437	500	0	90	1.9
E	MAXIMUM PLANETOLOGY	(B)	44	303	2000	0	0	3.4
		(C)	67	437	500	0	90	1.9

SUMMARY FIGURE 2. CANDIDATE ORBITER MISSION SET

C. A "baseline planetology" spacecraft of somewhat more than 400 kg carrying nearly 70 kg of science instruments. Here the emphasis is upon regional and local (150 meters resolution) scale imagery, although the payload also includes three spectrometers, a radiometer, and an altimeter. A low-altitude circular polar orbit is used as with the smaller planetology spacecraft.

D. A "broad first look" dual satellite concept consisting of the baseline planetology orbiter and the particles and fields orbiter.

E. A "maximum planetology" dual satellite concept consisting of the baseline planetology satellite and the minimum planetology satellite in a circular equatorial orbit of higher altitude to provide repetitive coverage of equatorial and mid-latitude surface areas.

The capabilities and characteristics of these orbiter concepts are described in the report.

The case for a ballistic Mercury orbiter is shown in Summary Figure 3, which portrays orbiting spacecraft mass as a function of orbit eccentricity with launch vehicle class as a parameter. A Titan IIID(7)/Centaur class vehicle is required to perform the particles and fields mission, an Intermediate-20 to perform the minimum planetology mission, and an Intermediate-20/Centaur to perform the baseline planetology mission.

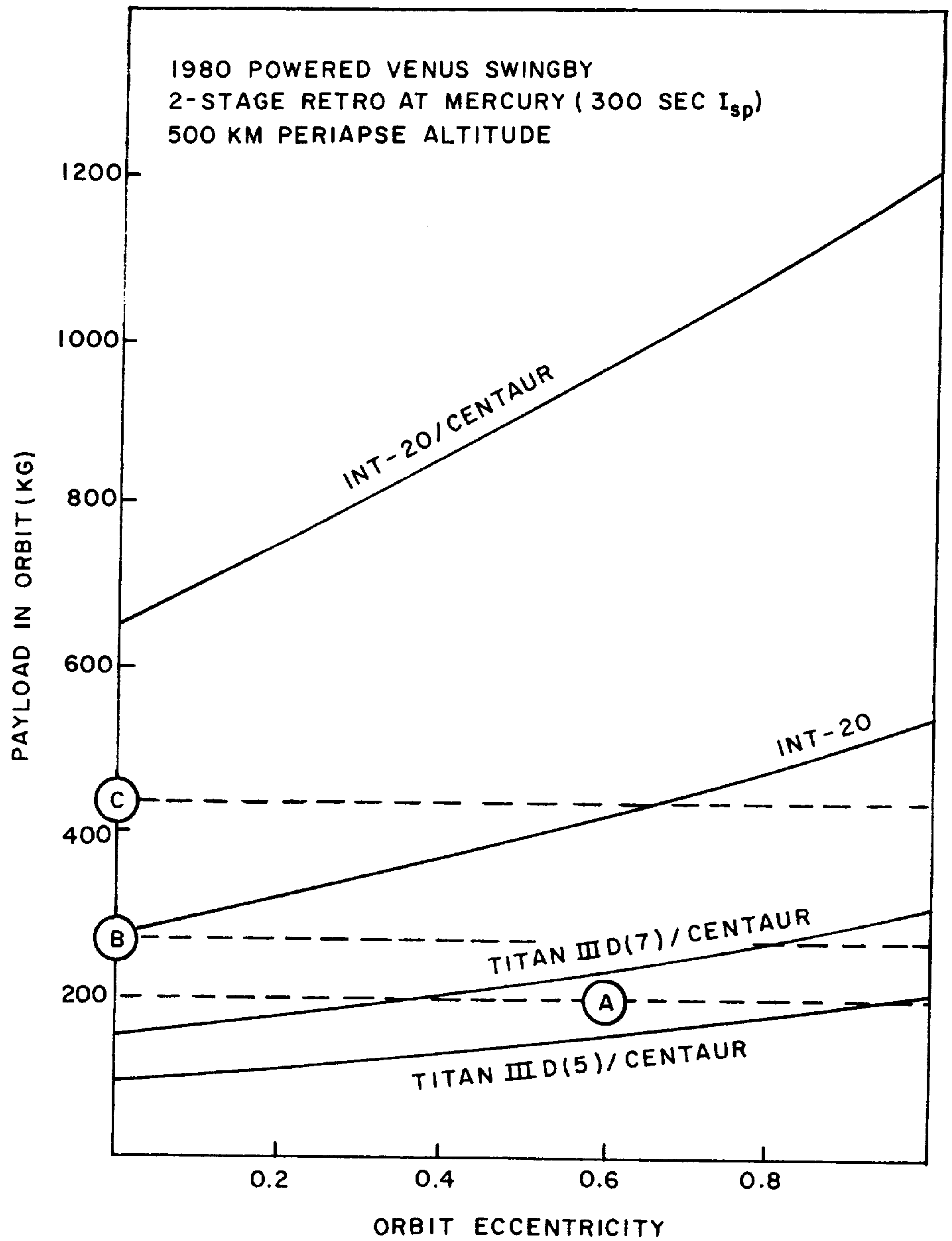

SUMMARY FIGURE 3. BALLISTIC MODE DELIVERY CAPABILITIES

The dual satellite missions both require the Intermediate-20/ Centaur. The results shown apply only to a ballistic launch in November 1980 with a gravity-assist maneuver performed at Venus on the way to Mercury. The swingby maneuver involves an impulsive ΔV of about 0.9 km/sec to prevent the spacecraft from entering the atmosphere of Venus. The flight time for this mission is 124 days. Many other ballistic opportunities are discussed in the report, but this particular opportunity presents very nearly the best available case (for 1980 through 1993) for the ballistic mission mode. Actually, the 1988 powered Venus swingby opportunity is a slightly better opportunity in the sense that the particles and fields orbiter can be delivered with a Titan IIID(5)/Centaur. No changes occur in the launch vehicle requirements for the other mission classes. The 1988 opportunity, however, involves a 300 day flight time.

The case for the solar electric low-thrust flight mode is shown in Summary Figure 4, which gives payload mass in orbit as a function of interplanetary flight time based on a 500 km altitude circular orbit at Mercury and a Titan IIID(5)/Centaur class launch vehicle. The solar electric stage is assumed to have a specific mass of 30 kg per kw and the thrust is assumed variable in jet power and direction but operates at a constant specific impulse. The upper curve in the figure applies to a solar electric state of optimum power level and specific impulse, while the lower curve applies to a 15 kw solar electric stage with a specific impulse of 2500 sec. The optimum specific impulse for the 15 kw stage is less than 2500 sec, but 2500 sec is regarded as the lowest feasible value for the specific impulse. In both cases, the orbital payload which can be delivered increases with increasing flight time. However, if the power level is restricted to 15 kw a flight time of 370 days or longer is required for the baseline planetology mission

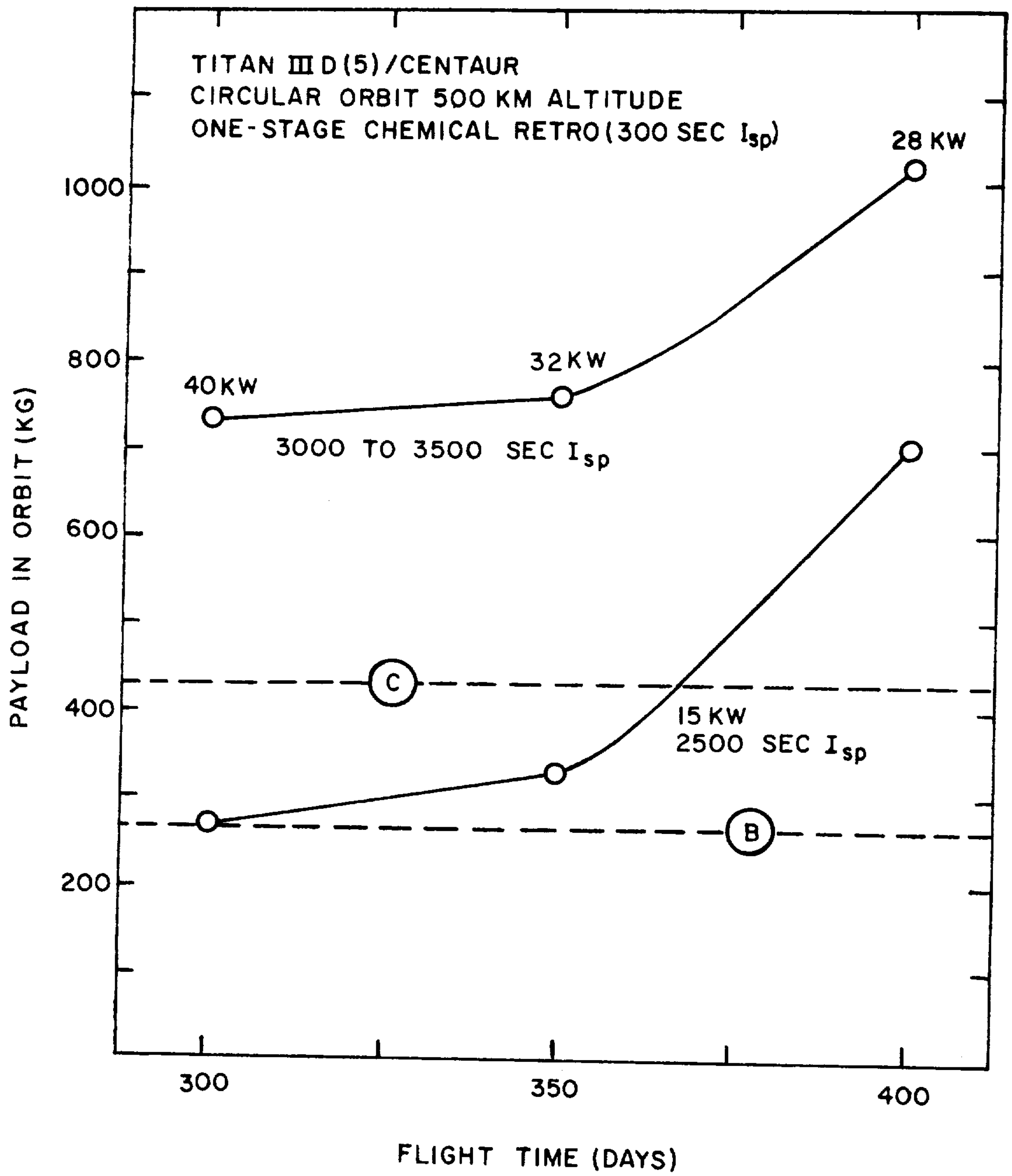

SUMMARY FIGURE 4. SOLAR ELECTRIC MODE DELIVERY CAPABILITIES (TITAN III D(5)/CENTAUR-1982 LAUNCH)

(Mission "C" is represented by the horizontal dashed line at 437 kg). Only a 300 day flight time is required for the minimum planetology mission. The dual satellite mission could be flown with the 15 kw solar electric stage, but would require flight times in excess of 400 days. The results shown are based on using 1982 launch opportunities, and are presumed to be representative of what can be achieved by using the solar electric low-thrust mode.

Both the ballistic mode and solar electric mode results presented here are based on an impulsive orbit capture maneuver at Mercury using a chemical system of 300 sec specific impulse. For the low approach velocities of the solar electric mode, a single stage retro is adequate, while for the higher approach velocities of the ballistic mode, a two-stage retro has been assumed. That is, in the solar electric mode, the interplanetary low-thrust stage is jettisoned prior to the orbit capture maneuver. Estimates have been made of the effects of retaining the low-thrust stage and performing a low-thrust spiral capture rather than utilizing a chemical retro system. The spiral capture maneuver increases both the orbital payload and the total flight time, relative to the impulsive capture maneuver. For a total flight time of 350 days, a low-thrust spiral capture increases the injected payload from 760 to 950 kg for the solar electric mission, but this increase drops off to only 50 kg at 400 days flight time. These payload increases are not felt to compensate for the increased complexity (in particular with regard to solar panel orientation during the spiral capture) of performing a low-thrust capture maneuver. This conclusion appears to be sensitive to the altitude of the desired final orbit. If a high-altitude orbit at Mercury were acceptable, the low-thrust capture might offer more advantage than suggested here.

The results summarized here indicate that even for the most favorable launch opportunities, an Intermediate-20 class launch vehicle is required to deliver a minimal surface-imaging science package into Mercury orbit using a ballistic mission mode with multiple chemical propulsion stages. Employment of a 15 kw solar electric low-thrust interplanetary stage permits delivery of a larger, more capable surface-imaging science package with a Titan IIID(5)/Centaur or even a Titan IIIC/Centaur (at over 400 day flight time).

MERCURY ORBITER MISSION STUDY

TABLE OF CONTENTS

TABLE OF CONTENTS (Continued)

TABLE OF CONTENTS (Continued)

LIST OF FIGURES

LIST OF FIGURES (Continued)

LIST OF FIGURES (Continued)

LIST OF TABLES

SECTION 1

INTRODUCTION

MERCURY ORBITER MISSION STUDY

1. INTRODUCTION

This report presents a preliminary analysis of an unmanned Mercury orbiter mission which might be flown in the early 1980's. The primary objective is to investigate the applicability of solar electric low-thrust technology to an early Mercury orbiter mission. The following secondary objectives are also considered:

a. Identify those scientific objectives which might be accomplished by an early Mercury orbiter.

b. Assess the role of orbiter missions in the exploration of Mercury.

c. Provide preliminary estimates of useful science payloads which appear to be appropriate to an early Mercury orbiter mission.

d. Identify problem areas which require further study and analysis.

Earlier studies have emphasized the large energy requirements of Mercury flybys, orbiters, and round-trip missions if performed using a direct or Venus swingby ballistic trajectory.

Summarizing the important works of other authors which preceeded the work reported here, and in large measure helped focus attention upon the specific technical areas addressed during this study, the most influential studies have been those of:

a. Manning (1966, 1967a, 1967b, 1969), who identified the energy requirements of ballistic flights to Mercury (both direct and Venus swingby) and who also emphasized the difficulty of obtaining adequate visual imagery of Mercury's surface from a ballistic flyby,

b. Zola (1969), who obtained optimized solar electric low-thrust interplanetary trajectories suitable for Mercury orbiter missions and indicated the payload benefits accruing from use of solar electric low-thrust propulsion systems, and

c. Horsewood and Mann (1970), who supplemented Zola's results by obtaining optimized Mercury flyby solar electric low-thrust trajectories.

Two recent developments have enhanced the timeliness and utility of the research effort reported here. The most significant of these is the launch and successful operation of the SERT II flight test. This test, launched in early 1970, demonstrated that Kaufman thrusters using mercury as the ion propellant are workable space propulsion systems, and that their space performance can be predicted adequately using vacuum-facility tests on the ground. Furthermore, the achieved duration of thrusting time (more than 150 days) suggests that interplanetary flight times on the order of 500 days are probably within technological reach. Simultaneously with this technological development, the computational procedures for optimizing low-thrust trajectories have been improved. A modified form of the CHEBYTOP computer program (Hahn, Johnson, and Itzen, 1969) has been used in the computation of all low-thrust Earth-Mercury trajectories examined in the course of work reported here, together with the "actual" orbit of the planet Mercury. Thus the computation of such parameters as thrust vector direction and terminal approach velocity relative to Mercury were performed using a more realistic model than in studies such as those of Zola and of Horsewood and Mann.

This report presents in detail the scientific objectives of Mercury exploration and relates payload weight to various levels of scientific achievement. This science emphasis is reflected in the organization of the report, in which the next section (2) discusses the scientific exploration of Mercury with the following section (3) presenting estimates of science payloads and their capabilities. In particular, section 2 reviews the present scientific perception of Mercury, and defines both specific scientific objectives likely to be achieved by unmanned exploration of Mercury and measurement techniques most useful in pursuit of these objectives. Section 3 describes the orbiting spacecraft, its subsystems, and its science instrument payload demanded by the scientific exploration objectives postulated in the previous section. Section 4 discusses operational constraints upon orbit selection. The interplanetary transfer mode is considered in section 5, which presents the general characteristics of Earth-Mercury trajectories (direct ballistic, Venus swingby, and solar electric low-thrust). The latter mission mode is emphasized, as Manning (1966, 1967a, 1967b) has already discussed comprehensively the direct and swingby ballistic modes.

Section 6 compares the suitability of the various modes for orbiter missions by considering the Venus swingby launch opportunity in 1980 and low-thrust opportunities in 1982. The exploration capabilities, in the context of a Mercury orbiter mission, are related to the employment of specific launch vehicles and mission modes. A representative orbiter mission (1982 Titan IIID(5)/Centaur launch with a 15 kw solar electric interplanetary stage) is considered in more detail in section 7 to show the interplay between the degree of mission achievement and the time in orbit, communications capability, and other mission parameters. In effect, a time profile of the mission is presented. Finally, section 8 presents conclusions and recommendations arising from the study. Implications for advanced technology and recommendations for further analysis are stressed.

SECTION 2

MERCURY EXPLORATION

2. MERCURY EXPLORATION

This section reviews and summarizes the existing scientific knowledge and speculation concerning the planet Mercury. The existing knowledge provides a framework for the definition of specific measurements aimed at observing Mercury's structure, composition, and dynamic processes. The suggested measurements are then related to the use of unmanned flybys, orbiters, and landers.

2.1 Review of Existing Knowledge

2.1.1 Orbital and Physical Characteristics

Mercury is the smallest planet in the solar system and lies closest to the Sun. Mercury's small cross-sectional area would fit within the Atlantic Ocean, and is irradiated by the Sun with a greater intensity than any other planet. Except for Pluto, the orbit of Mercury shows both the greatest eccentricity and inclination to the ecliptic plane. This pronounced eccentricity causes the apparent solar intensity at Mercury to vary by more than a factor of two throughout Mercury's year.

Until 1965 Mercury was believed to be locked to the Sun in a synchronous rotation, i.e., the same side of Mercury was thought to continuously face the Sun. Using the large Arecibo antenna, Pettingill and Dyce (1965) examined radar reflections from Mercury and deduced from the doppler spread in frequency that the period of rotation was not 88 days, as previously thought, but rather 59($\pm$ 5) days. This astonishing result led to a re-examination (McGovern, Gross, and Rasool, 1965; Columbo and Shapiro, 1966; Chapman, 1967; Camichel and Dollfus, 1968) of earlier visual observations of Mercury. The earlier observations, which estimated the rotation period by the recurrence of surface features on the disk of Mercury at intervals of one or more rotations, were found to be consistent with a 59-day rotation period. Smith and Reese (1968) have recently derived a rotation period of 58.7 days by observing the motion of surface features across the disk at intervals less than a single rotation. It is now generally agreed that the rotation period is exactly 2/3 of the orbital period, a conclusion supported both by observations and theoretical calculations of the interplay between solar torques and a presumed asymmetry in Mercury's principal moments of inertia.

Dyce, Pettengill, and Shapiro (1967) have concluded from radar measurements that the axis of rotation is pointing to within 28 degrees of the normal to the orbital plane. Peale (1969) has suggested that the rotation axis is normal to either the orbital plane or the ecliptic plane; the difference between the two is about seven degrees. The orbital elements used in the study reported here are shown in Table 1. In the absence of more definitive data, the rotation axis has been taken as normal to the orbital plane. A projection of Mercury's orbit onto the ecliptic plane is shown in Figure 1. It may be noted that the orbital velocity of Mercury's is much higher at perihelion than at aphelion, and this has a significant effect upon the selection of ballistic launch opportunities for orbiter missions.

The reciprocal mass of Mercury (i.e., the ratio of the mass of the Sun to the mass of Mercury) legislated by the General Assembly of the International Astronomical Union is 6,000,000. This value is generally accepted as being within the range of "measured" values. For example, Ash, Shapiro, and Smith (1967) using radar data deduce a value of 6,029,000 or 6,021,000, depending upon whether the analysis is based on a Newtonian or general relativity model, respectively. In either case, the formal standard error is 55,000. These authors also

TABLE 1

ORBITAL ELEMENTS & PHYSICAL PROPERTIES

OF MERCURY

A. ORBITAL ELEMENTS

Semi-Major Axis	0.3871 AU
Eccentricity	0.2056 AU
Periapse Radius	0.3076 AU
Apoapse Radius	0.4667 AU
Inclination of Orbital Plane	7.004 deg
Orbital Period	87.969 days
Rotation Period	58.646 days
Synodic Period	115.88 days

B. PHYSICAL PROPERTIES

Mass	0.55 Earth mass
Radius	2440 km
Derived Density	5.45 g/cm^3
Surface Gravity	0.38 Earth g
Escape Velocity	4.26 km/sec
Maximum Surface Temperature	700°K
Minimum Surface Temperature	100°K

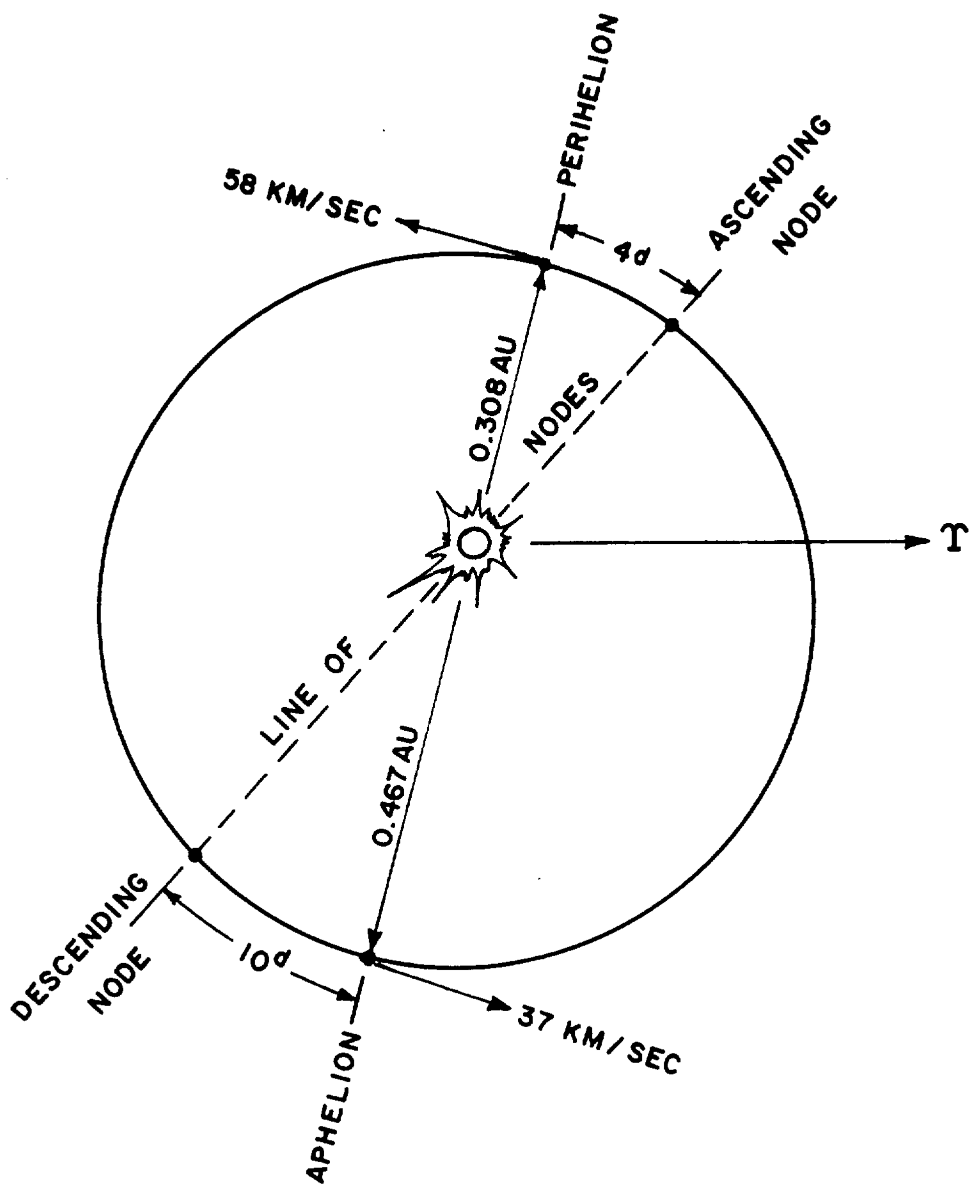

FIGURE I. MERCURY'S ORBIT

deduce values for the average equatorial radius of Mercury, namely 2,440 km or 2,434 km, again depending upon the type of model used in the data analysis. Here the formal standard error is 2.4 km, which does not reflect possible systematic errors. Melbourne and O'Handley (1968) have obtained a value of 2,446 $\pm$ 1 km. It appears that consideration of systematic errors would result in a radius of 2,440 $\pm$ 6 km. Because Mercury rotates slowly, dynamic flattening is not expected and none has been observed within the accuracy of the measurements.

Using measured values of the radius and reciprocal mass, together with well-known solar and terrestrial data, the ratio of the density of Mercury to that of Earth may be calculated. Ash, Shapiro, and Smith (1967) arrive at the value 0.995 $\pm$ 0.009 if a Newtonian model is used, and 0.986 $\pm$ 0.009 if a general relativity model is used. That is, the density of Mercury is very nearly equal to that of the Earth. This result is discussed in greater detail below when attention is turned to the internal structure of Mercury. Suffice it to say that the deduced density of Mercury is generally thought to imply that Mercury contains a large percentage of iron. The radius and mass values can also be used to derive estimates of the surface gravity. The gravitational acceleration at the surface of Mercury is found to be 371 cm/sec^2, approximately equal to the surface gravity at Mars despite the much larger Martian radius. The escape velocity at Mercury is 4.26 km/sec, compared to 11.2 km/sec at Earth.

As mentioned above, it was thought for many years that Mercury was locked to the Sun in a synchronous rotation, just as the Moon is locked to the Earth. The primordial rotation rate of the Moon has been altered by tidal friction finally leading to a lunar rotation rate equal to its orbital period. The natural assumption was that the Sun-Mercury system evolved in a similar manner. The startling discovery of the non-synchronous 59-day rotation period of Mercury stimulated a succession of papers dealing with the possibilities of various rotation resonances in the Sun-Mercury system. The general method of approach is to assume that Mercury is subject to two types of solar torques; a tidal torque and a torque arising from a postulated asymmetry in Mercury's equatorial shape. If Mercury's principal moments of inertia are represented by A, B, and C, where C is the moment about the spin or rotation axis and A and B are the moments lying in the equatorial plane, the asymmetry is measured by the quantity (B-A)/C, where B traditionally is taken as the larger of A or B. Colombo and Shapiro (1966) show that the time-averaged value of the torque due to asymmetry reaches particularly high values, i.e., shows resonances, at rotation rates corresponding to integral and half-integral multiples of the orbital period. Hence Mercury may be trapped in the resonance associated with a rotation angular velocity equal to 3/2 of the orbital angular velocity. Goldreich and Peale (1966, 1968) estimate that the 3/2 resonance state will be stable if (B-A)/C is greater than 10^{-8}. For comparison, it is helpful to note that the known value of (B-A)/C for the Moon is about 2×10^{-4}.

One of the major theoretical difficulties is the avoidance of capture in a higher resonance state, say 2 or 5/2, assuming that the primordial rotation rate was high and gradually slowed down by the action of tidal torque. The calculation of resonance state capture probabilities is sensitive to the analytical model used to describe the tidal torque; a situation aggravated by the paucity of satisfactory tidal models. Even now there is no theoretical model which accurately predicts the shape of the tidally-distorted Earth. Nonetheless, using a variety of simple tidal models, Goldreich and Peale have estimated resonance capture probabilities for Mercury with provocative results. For example, using a Darwin tidal model with a frequency-independent dissipation function, the capture probabilities in the 5/2, 2, and 3/2 states are 0.03, 0.15, and 0.73, respectively. Thus it is now generally accepted, both on observational and theoretical grounds, that the rotational angular velocity of Mercury is exactly 3/2 the mean orbital angular velocity. Measurements of the planetary figure and radius are desired to supplement theoretical calculations.

2.1.2 Surface Features and Properties

Attempts to observe surface features and properties of Mercury from the Earth have been made at all wavelengths penetrating the Earth's atmosphere, i.e., from visible to radio wavelengths. Visual and radar observations are used to infer surface features and other properties; infrared and passive microwave observations are used to infer temperatures and thermal properties.

It is difficult to study visual surface features on Mercury by Earth-based observation. Mercury is never further than 28 degrees from the Sun when viewed from Earth. Thus Mercury must be observed shortly before sunrise or shortly after sunset, using relatively long line of sight segments in the Earth's turbulent atmosphere, or during the daylight hours, when the bright sky background reduces the apparent contrast.

Chapman (1967) has constructed a map of the visible surface features, reproduced here in Figure 2, based on many drawings and photographs of earlier researchers and assuming a 58.646-day rotation period. Some care must be taken in interpreting drawings produced earlier than 1965 when the rotation period was thought to be 88 days. The figure shown here adopts the astronomical convention of placing South at the top of the map. The main features appear as dark streaks, many of which are aligned in a NW-SE or a SW-NE direction. Positional accuracy and surface resolution correspond to about ten degrees on Mercury's surface (about 400 km). It is unlikely that Earth-based visual observations will ever result in resolution better than about 200 km.

The visual geometric albedo of Mercury is usually taken as 0.096, which is sufficiently close to that of the Moon (0.11) that within experimental error the albedo of Mercury is the same as the Moon. A recent microdensimetric analysis (Hämeen-Antilla, Pikkarainen, and Camichel, 1970) of the best available photographs of Mercury show that Mercury's photometric function is almost identical to that of the Moon. In fact, except at large phase angles, the two photometric functions are identical within experimental error. Even at large phase angles, where Mercury's surface appears to be somewhat brighter than the Moon's surface, the difference is almost within error limits. Because of the similarity in visual properties, most astronomers and other scientists believe that Mercury's surface must be very similar to that of the Moon.

Pikkarainen (1969) has computed the visual brightness of the Moon and Mercury by using a surface model with craters of parabolic cross section, a Lommel-Seeliger reflection law, and a measured phase function for basalt powder. The calculations depend upon two parameters; the fraction of the surface covered

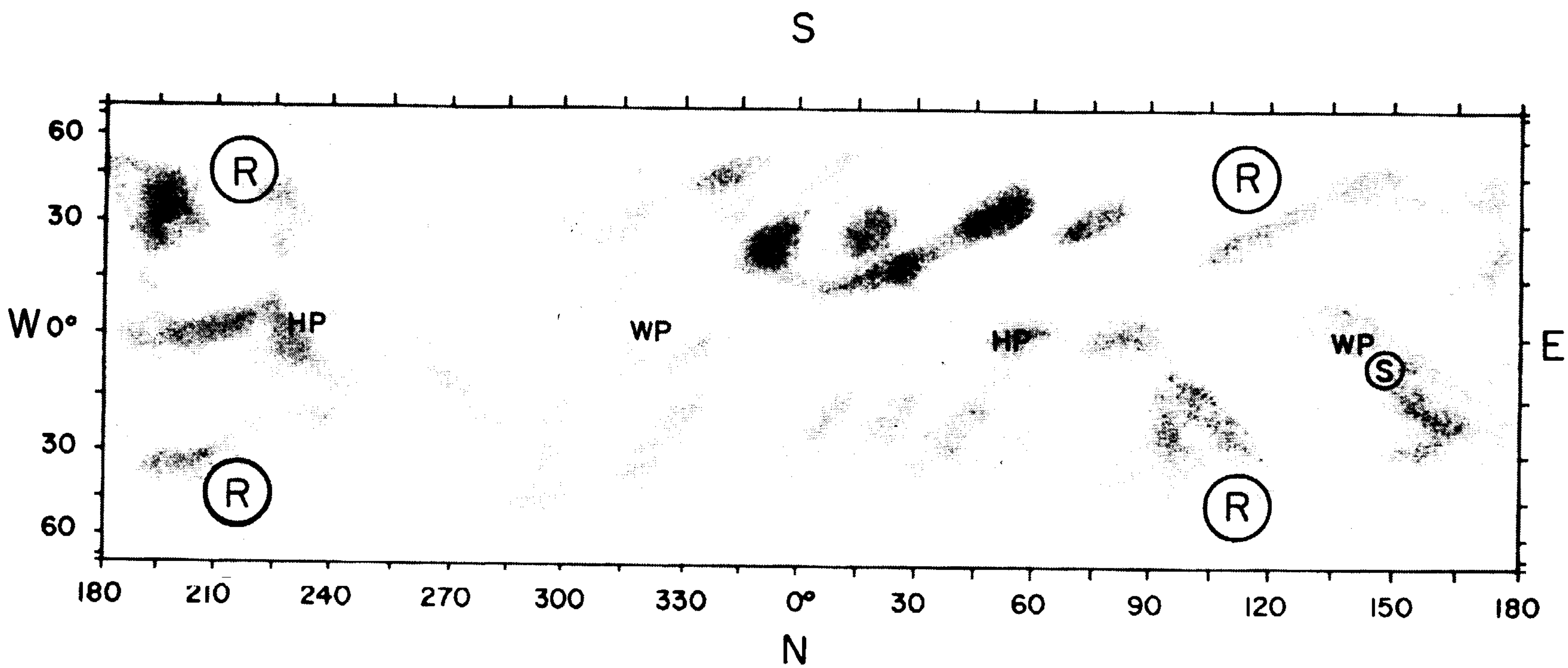

ORTHOGRAPHIC EQUAL AREA PROJECTION

HP = HOT POLES
WP = WARM POLES

R = ROUGH AREAS } AS DEDUCED
S = SMOOTH AREA } FROM RADAR

ZERO DEGREES LONGITUDE DEFINED AS THE CENTRAL MERIDIAN OF THE TOTAL DISK AS SEEN FROM CELESTIAL LONGITUDE ZERO DEGREES ON JULIAN DAY 2424417.5 (24 SEP 1925).

FIGURE 2. MAP OF MERCURY (AFTER CHAPMAN 1967)

by craters, and the ratio of crater depth to diameter. By varying these two parameters to find the best possible fit to the experimental data, Pikkarainen finds that the Moon is twenty percent covered by craters and that the "average" crater depth is one-half the diameter. Similarly, for Mercury, he finds that the surface is fifty percent covered by craters and the "average" crater depth is one-eighth the diameter. Pikkarainen therefore concludes that Mercury has more craters than the Moon, per unit surface area, and that the craters are, on the whole, shallower than lunar craters. Unfortunately, the basic argument is somewhat akin to estimating the size of an elephant by measuring the circumference of his trunk, and Pikkarainen provides no data on the sensitivity of his conclusions to changes in crater density or depth.

Radar returns from Mercury may also be used to infer surface characteristics. Pettingill, Dyce, and Campbell (1967) find that at a wavelength of 70 cm the radar cross section of Mercury is between six and seven percent of the physical cross section (as compared to seven percent for the Moon), and that the delay scattering law for Mercury is very similar to that of the Moon (normalized to Mercury's radius). Thus the radar data support the hypothesis that the surface of Mercury is similar to that of the Moon. Goldstein (1970) has analyzed radar returns at 12.5 cm and deduced the presence of two rough areas and one smooth area on Mercury's surface. The existence of rough areas is inferred by the depolarization of the return signal. As shown on Figure 2, the smooth area lies on the equator near 150° longitude. The rough areas occur at longitudes of about 110 and 210 degrees with latitudes of about 45 degrees, but the data are ambiguous in determining the appropriate hemisphere. Therefore, in the figure each rough area is depicted in both the Northern and Southern hemispheres.

Thermal observations of Mercury prior to realization of the 59-day rotation rate were considerably more confusing than the visual data. Earth-based thermal measurements (infrared and passive microwave) are as difficult to perform as accurate visual observations, and for the same reason - i.e., the nearby Sun is an intense interferring source. Microwave measurements in the early 1960's, at about 4 cm by Howard, Barrett, and Haddock (1962) and at 11 cm by Kellerman (1965), were interpreted on the basis of an 88-day rotation rate. The hot sunlit side was assumed to continuously face the Sun, the cold dark side continuously shielded from the Sun's warmth. It was therefore expected that the subsolar point, which was assumed to be fixed on Mercury's surface, would experience surface temperatures in the range 600-700°K while the cold dark side would be very cold indeed, nearly 0°K. The observations were not consistent with this picture, suggesting a cold side temperature on the order of 200°K. It was concluded that some indirect mechanism, such as internal conduction or atmospheric convection, was transporting heat from the sunlit to the dark side. Field (1964) went so far as to suggest that hemispheric winds in an argon atmosphere could explain the observations. The 88-day rotation rate was so widely accepted that no one publicly suggested that heat could be transported from the hot to the cold side by a physical rotation of the planet.

Once the 59-day rotation rate was discovered, Soter and Ulrichs (1967) recognized the existence of "hot" poles and "warm" poles. Assuming that the spin axis is normal to the orbital plane, a given point on the equator is always sub-solar at a specific position in the orbit. Because of Mercury's appreciable orbital eccentricity, a different total energy flux falls on each equatorial longitude. There are two perihelion sub-solar points, 180 degrees apart in longitude, such that each of these two points, called "hot" poles, are sub-solar at alternate perihelion passages. The hot poles are identified by the letters HP in Figure 2. The orbital angular velocity slightly exceeds the constant rotation angular velocity whenever Mercury is within 26 degrees of perihelion, leading to a highly nonuniform motion of the Sun as seen from Mercury. An observer at one of the hot poles would see the Sun rise in the East and climb at a decreasing rate. At mid-morning (22 Earth days after sunrise) the Sun is 22 degrees from the zenith. Still slowing down, the Sun grows in size and passes the zenith shortly before noon. Reversing its motion, the Sun passes backward through the zenith at high noon (44 days after sunrise) appearing sixty percent larger than at sunrise. Shortly after noon, the Sun again reverses its motion and passes through the zenith for the third time. Since the total amount of retrograde motion is less than the Sun's apparent diameter, a casual observer would regard the Sun as essentially hovering at the zenith for about ten days. As afternoon progresses, the Sun shrinks slowly in size and approaches the western horizon at an increasing rate, sunset occurring 88 Earth days after sunrise. At high noon, the surface temperature at the hot poles has been estimated as 700°K.

The behavior of the Sun, as seen from the warm poles, is equally unconventional. The Sun rises slowly in the East and promptly sets because of its retrograde motion. Rising again, the Sun climbs slowly, shrinking in size. At mid-morning the Sun is only 22 degrees above the horizon. Decreasing further in size, but gaining speed, the Sun passes rapidly through the zenith at noon, appearing forty percent smaller at high noon than at sunrise. The afternoon motion is symmetric with the morning motion, the Sun setting (twice) about 88 days after sunrise. As should be apparent when contrasting the Sun's motion as seen from a warm pole to that seen from a hot pole, a warm pole receives considerably less solar energy than a hot pole. In fact, the two warm poles receive less energy than any other equatorial longitude. The warm poles are actually "cool" poles. The warm pole noon-time surface temperature has been estimated as 570°K.

Night-time temperatures depend upon the thermal inertia of the surface material and the relative roles played by thermal conduction and thermal radiation during cooling. It is difficult to relate Earth-based observations to surface temperatures at any specific point on Mercury's surface. Virtually all Earth-based thermal observations detect radiation from the whole of Mercury's disk, i.e., the observed temperatures are disk-averaged temperatures. Also, the longer the wavelength used, the more important is the contribution of the subsurface temperature distribution. The most recent measurements (Murdock and Ney, 1970) indicate an average dark-side temperature of 111($\pm$3)°K, which should be interpreted as very nearly the surface temperature since wavelengths of 3.75 to 12 μm were used. The most sophisticated contemporary thermophysical model of lunar soil, due to Winter and Saari (1969), regards both the thermal conductivity and specific heat as functions of temperature. Assuming that the pertinent surface properties of Mercury are identical to those of the Moon, Winter and Saari calculate that the night-time infrared brightness temperature at either of Mercury's hot poles varies from 150°K at sunset to 59°K just prior to dawn. These values are in substantial agreement with the homogeneous models (in which the thermophysical properties of the soil are constants independent of temperature or depth) of Soter and Ulrichs (1967) and of Morrison and Sagan (1967), and with the average dark-side temperature given above. It may be noted that most, if not all, homogeneous models predict that night-time temperatures at the warm poles are essentially the same as at the hot poles; only the day-time temperatures are different.

The inescapable conclusion of all visual infrared, radar, and passive microwave observations of Mercury is that the surface properties of Mercury are essentially identical to those of the Moon.

2.1.3 Internal Structure

As noted earlier, the mean density of Mercury is nearly equal to that of the Earth. This does not at all imply that the gross composition of Mercury is similar to that of Earth -- indeed, the opposite is true. For a meaningful comparison, the density must be corrected to similar pressure-temperature conditions. This correction, in general, depends upon the planetary structure, in particular the degree to which the iron or iron-nickel (zero pressure density of about 7.9 g/cm^3) has separated from the silicates (zero pressure density of about 3.3 g/cm^3). The two possible extremes of separation are a homogeneous structure (no separation) and a core structure (implying an iron or iron-nickel core with a silicate mantle). If the planetary moment of inertia is known, it provides an integral condition upon the degree of separation. Since Mercury is considerably smaller than the Earth, the internal pressure is presumed considerably less, and since the mean densities are comparable it is generally agreed that Mercury must have a much heavier bulk composition than the Earth.

Reynolds and Summers (1969) have constructed compositional models of the terrestrial planets. The elements considered are silicon, magnesium, aluminum, calcium, iron, nickel, and oxygen, which together comprise more than 95 percent by mass of observed terrestrial, lunar, and meteoric materials. These elements are grouped into three different materials in the Reynolds-Summers model: (1) "iron", a metallic Fe Ni mixture of 95 percent Fe and 5 percent Ni, (2) "rock", a mixture of the light oxides MgO, SiO_2, CaO, and Al_2O_3, and (3) the oxides of iron. Two Mercury models were constructed, a core model and an homogeneous model. Upper and lower limits for the total iron content were established in each case. For the core model, in which the core comprised 68 percent of the total planet mass, the total iron content ranged from 67 to 69 percent. For the homogeneous model, the total iron content ranged from 66 to 71 percent. For comparison, the iron content associated with models of the other terrestrial planets (Earth, Venus, Mars), range from 24 to 38 percent. Kozlovskaya (1969) has also constructed core and homogeneous Mercury models with similar results. The homogeneous models are preferred, both by Reynolds and Summers and by Koslovskaya. This preference is substantiated by Majeva (1969), who speculates on the thermal history of Mercury. It is likely that the maximum heating of Mercury took place two or three aeons ago, and that at no time has the temperature approached the melting point of silicates or metallic iron. Thus Mercury, which is now cooling, should have neither a core nor a crust.

Although the presence (or absence) of a core in Mercury is of no small interest, particularly with regard to the evolution of Mercury as a planet, the high percentage of iron is of much greater import. Apparently Mercury contains twice as much iron (in terms of percentage composition) as any other planet in the solar system. Lyttleton (1969) held out some hope that the inferred mass of Mercury was in error by fifty percent, a hope stimulated by the withdrawal of some earlier mass data and the possibility of a systematic error in the radar measurements analysis by Ash, Shapiro, and Smith (1967). However, Melbourne and O'Handley (1968) have improved the radar analysis, and Lieske and Null (1969) have determined the mass of Mercury independently by observations of Icarus. Thus it appears that the mass of Mercury is known with sufficient accuracy, barring a revelation analogous to the discovery of the 59-day rotation rate, to infer confidently that Mercury's composition is indeed anomolous. Thus Mercury, the planetary freak, provides a crucial test for candidate theories explaining the origin and evolution of the solar system. The high iron content of Mercury appears to be explicable only as a consequence of an inergetic early Sun volatizing most of Mercury's silicates and blowing them away with the atmosphere.

2.1.4 Atmospheric and Other Properties

A number of unsuccessful attempts have been made to detect an atmosphere on Mercury by searching for absorption features in the observed infrared spectrum. Primary attention has been focused on a search for CO_2. Belton, Hunten, and McElroy (1967) performed high resolution observations of the spectrum near 1.05 μm. After analysis of their own data, and a review of earlier data at different regions of the spectrum, they arrive at an upper limit of 5 m-atm on the CO_2 abundance, corresponding to a surface partial pressure of 0.35 mb. It should be emphasized that no positive detection of CO_2 has occurred. It is the absence of such detection that permits an assessment of upper limits on the abundance. In a similar manner, upper limits have been set on the atmospheric abundance of O_2 and H_2O. The maximum amounts present of these species are considerably less than the upper limit on CO_2.

At one time, Dollfus (1961) estimated an atmospheric pressure of about 1 mb on Mercury, based on visual polarization measurements. However, O'Leary and Rea (1967) have reinterpreted the polarization data and conclude that an atmosphere need not be invoked to explain the data. In fact, they suggest that the albedo, color, polarization, and photometric data can be explained most easily by assuming that Mercury's surface is very similar to the Moon, with darkening and roughening due to bombardment by the solar wind and by micrometeorites. The surface pressure must be no more than about 10^{-5} mb if solar protons are to reach the surface. This corresponds very closely to the value 10^{-6} mb suggested by Belton, Hunten, and McElroy.

Because of its slow rotation rate, Mercury is presumed to have no magnetic field. This is even more likely if Mercury has no iron core, as has been suggested above. Nevertheless, Good (1967) has noticed a propensity for solar flares to be observed when Mercury is in a preferred orientation relative to the Sun and the Earth. By assuming that solar flare protons are deflected in the direction of Earth by Mercury's magnetosphere, Good estimates that Mercury's dipole moment is on the order of one-tenth of the Earth's dipole moment. This implies that the magnetic field strength on Mercury's surface would be about 0.5 gauss, slightly larger than the Earth's surface field.

Finally, a note should be added on the possibility of Hermean satellites. None, of course, have been observed. If any exist, they would have to be smaller than about 50 km in diameter to have escaped detection.

This section has summarized the present inventory of knowledge and responsible opinion dealing with the planet Mercury. The main points are (1) that the bulk composition of Mercury is quite different from the other terrestial planets, (2) that the surface of Mercury is very similar to that of the Moon, and (3) that, like the Moon, Mercury has no appreciable atmosphere. The next section defines specific scientific objectives in connection with unmanned exploration of Mercury, and suggests measurement techniques most likely to be useful in achieving them. These objectives should be interpreted in light of the existing knowledge and theory summarized above.

2.2 Science Objectives

The process of defining the scientific objectives of Mercury exploration may be understood most readily by picturing an objective "tree", representing successive levels of detail. An initial list of major goals is first identified, then defined in greater detail by a set of subgoals. Each subgoal is defined in greater detail by major objectives, each major objective by specific objectives, each specific objective by measurables. That is, once the major goals are identified, branches are added until specific accomplishments and measurables are identified at the tips of the tree. There are several levels of branches between the goals and the measurables. The contribution of the measurables to the objectives are established by the relative contribution of each of the branches to the next higher branch. However, the determination of "value", which can only be done subjectively, is specifically avoided in this model. The model used here was derived in an early study (Klopp, 1970) dealing with planetary exploration in a more general manner than is appropriate for this study.

The scientific goal of planetary exploration is the understanding of the origin and evolution of the solar system. This involves determining the present status of the planets, searching for evidence of extraterrestrial life, determining the present status of the Sun, and determining the present status of the interplanetary medium. The emphasis is on present status, since the origin and evolution of the solar system are not directly observable. Exploration of Mercury is regarded here as assisting in the determination of the present status of the planets and the search for extraterrestrial life. This is not to say that a Mercury orbiter mission cannot be expected to contribute to our knowledge of the Sun and interplanetary medium. However, it is assumed that the value of performing a Mercury orbiter (or even flyby) mission is derived primarily from what we can learn about Mercury, not the Sun or the interplanetary medium.

The objective "tree" for Mercury exploration is presented in Figure 3. Some branches have been omitted from the more general model as not appropriate for Mercury. For example, the subgoal dealing with Mercury's atmosphere is considered to have only one major objective: determining the atmospheric composition. In the more general model there are three major atmospheric objectives dealing with composition, structure, and active processes. Similarly, although the general model identifies nearly one hundred measurables, only one-third of these are relevant to Mercury. The figure shows that most of the Mercury measurables pertain to planetology. The Mercury measurables are:

1. Surface elements - abundance measurements of O, Si, Al, Mg, H, Na, Fe, Cu, and Ni on Mercury's surface are particularly desired.

2. Surface isotopic ratios - notably Li^7/Li^6, B^{11}/B^{10}, Li/Be, B/Be, and D^2/H^1.

3. Petrology - identification of rock types.

4. Mineralogy - identification of characteristic crystallographic structures.

5. Mass - reduce present error in Mercury's mass.

6. Radius - measurements of equatorial radius.

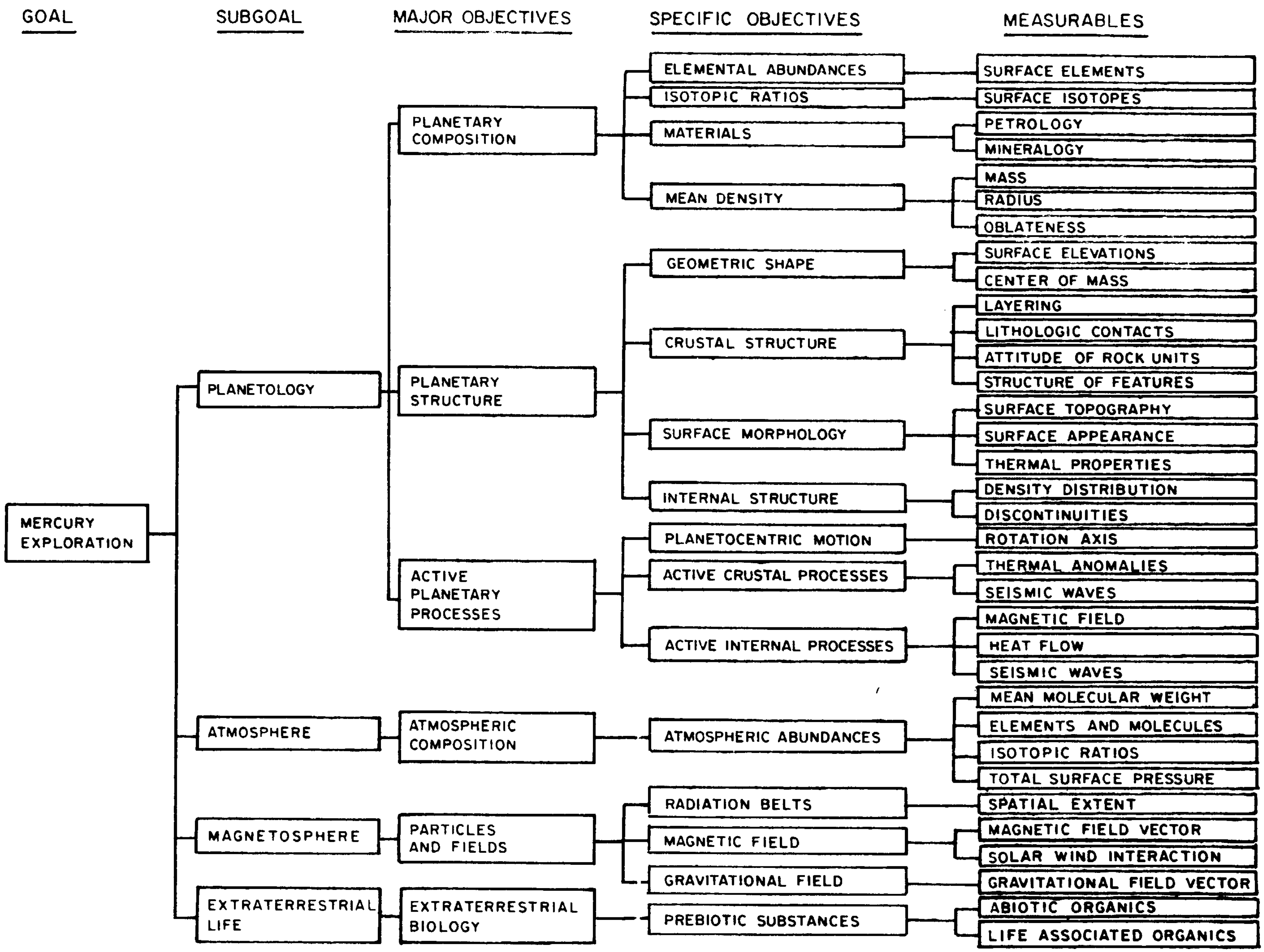

FIGURE 3. OBJECTIVES OF MERCURY EXPLORATION

7. Oblateness - defined as $(r_e - r_p)/r_e$ where r_e is the average equatorial radius and r_p is the polar radius.

8. Surface elevations - height of surface above some datum; to define regional deviations from basic planet shape.

9. Center of mass- determined by tracking of orbiting spacecraft.

10. Layering - the structure of parallel, tabular rock units.

11. Contacts - the interface between two adjacent rock units.

12. Attitude of rock units - orientation of rock units, usually expressed in terms of the dip and strike.

13. Structure of features - geometric relationship between and within rock units, such as folds, domes, and graben.

14. Surface topography - the shape of the surface.

15. Surface appearance - the texture, reflectivity, and color of the surface.

16. Thermal properties - includes thermal conductivity, specific heat, and electrical conductivity of the surface.

17. Density distribution - interior density distribution as a function of radius.

18. Discontinuities - includes density discontinuities and phase changes in the interior of Mercury.

19. Rotation axis - orientation of Mercury's axis of rotation; the period itself is known with sufficient accuracy.

20. Thermal anomalies - areas of the surface or crust which are at a different temperature than their general surroundings.

21. Seismic waves - detection would be positive evidence of active crustal processes.

22. Magnetic field - mapping of magnetic field might lead to inferences concerning dynamic processes in the interior.

23. Heat flow - surface measurements of both thermal gradient and thermal conductivity.

24. Seismic waves - in addition to crustal processes, as in 21 above, may be used to infer nature of active internal processes.

25. Mean molecular weight - average molecular weight of atmosphere.

26. Elements and molecules - measurements of atmospheric abundances with emphasis on Ar, Kr, and outgassing volatiles.

27. Isotopic ratios - atmospheric isotopic ratios; Ar^{40}/Ar^{38} of most interest.

28. Total surface pressure - atmospheric pressure at surface.

29. Spatial extent of radiation belts - pertains to detection of protons or electrons in magnetosphere.

30. Magnetic field vector - magnetic mapping of magnetosphere.

31. Solar wind interaction - emphasis on possible bow shock and correlation with magnetic field.

32. Gravitational field vector - surface and orbital mapping of gravitational field and anomalies.

33. Abiotic organics - search for organic materials such as formaldehyde.

34. Life-associated organics - search for organic materials of biological origin, such as amino acids.

These measurables are defined in considerably more detail in Klopp et al. (1969).

2.3 Relevant Mission Types

Having defined the scientific objectives of Mercury exploration, it is possible to suggest ways in which the scientific objectives might be achieved. In particular, which objectives might be achieved by flybys, by orbiters, and by landers?

2.3.1 Flybys

A flyby past Mercury is very likely to provide greatly improved upper limits on Mercury's magnetic field and atmospheric pressure. Visual imagery may provide detection of surface features on the order of one to ten kilometers in size, depending upon the imaging system capabilities and the flyby trajectory. This represents roughly two orders of magnitude improvement over Earth-based observations, but only a small fraction of Mercury's surface can be observed at high resolution from a single flyby.

If an Earth occultation experiment is to be performed at Mercury both the direct and Venus swingby missions generally require a dark-side flyby of Mercury. Of course, a dark-side flyby provides for limited visual observation of Mercury's surface, and a natural conflict arises between enthusiasts for occultation experiments and devotees of Mercury surface imaging experiments. Despite Manning's identification (Manning, 1969) of the possibibility of nearly complete visual coverage of Mercury by utilizing sunlit-side flybys in 1973, 1974, and 1975, current NASA planning indicates that a dark-side flyby trajectory will be employed for the 1973 Venus/Mercury Mariner mission. The visual coverage which might have been provided by a light-side passage during the 1973 mission cannot be repeated, in terms of longitude, until 1982. It seems likely, therefore, that orbiters, rather than flybys, will be the first missions to provide extensive coverage of Mercury's surface. In addition to scientific data, even a single flyby would be invaluable in providing data essential for the optimum design of subsequent orbiter missions.

2.3.2 Orbiters

A spacecraft orbiting Mercury can provide imagery of all of Mercury's surface. A low altitude orbiter can pass over virtually every point on Mercury's surface and can stay at Mercury long enough to obtain proper illumination conditions. In contrast, flyby spacecraft move rapidly past Mercury, at a relatively high altitude, and can observe limited areas of the planet (particularly if occultation experiments are being conducted since these involve dark-side flybys). Thus the major role expected of an orbiter is that of obtaining complete surface imagery.

This emphasis on imaging experiments is shown in Figure 4 in which appropriate combinations of measurables and instrument techniques are identified for orbiters and landers. The upper third of the figure deals with those measurables which can be investigated by experiments involving only an orbiter. Various experimental techniques are listed at the top of the table, the symbol at the intersection of the measurable row and the technique column depicts the utility of that technique in investigating that measurable. The absence of a symbol indicates that the technique is not appropriate to the measurable. For example, no one would be likely to use visual imagery of Mercury to determine Mercury's mass. Tracking the spacecraft orbiting

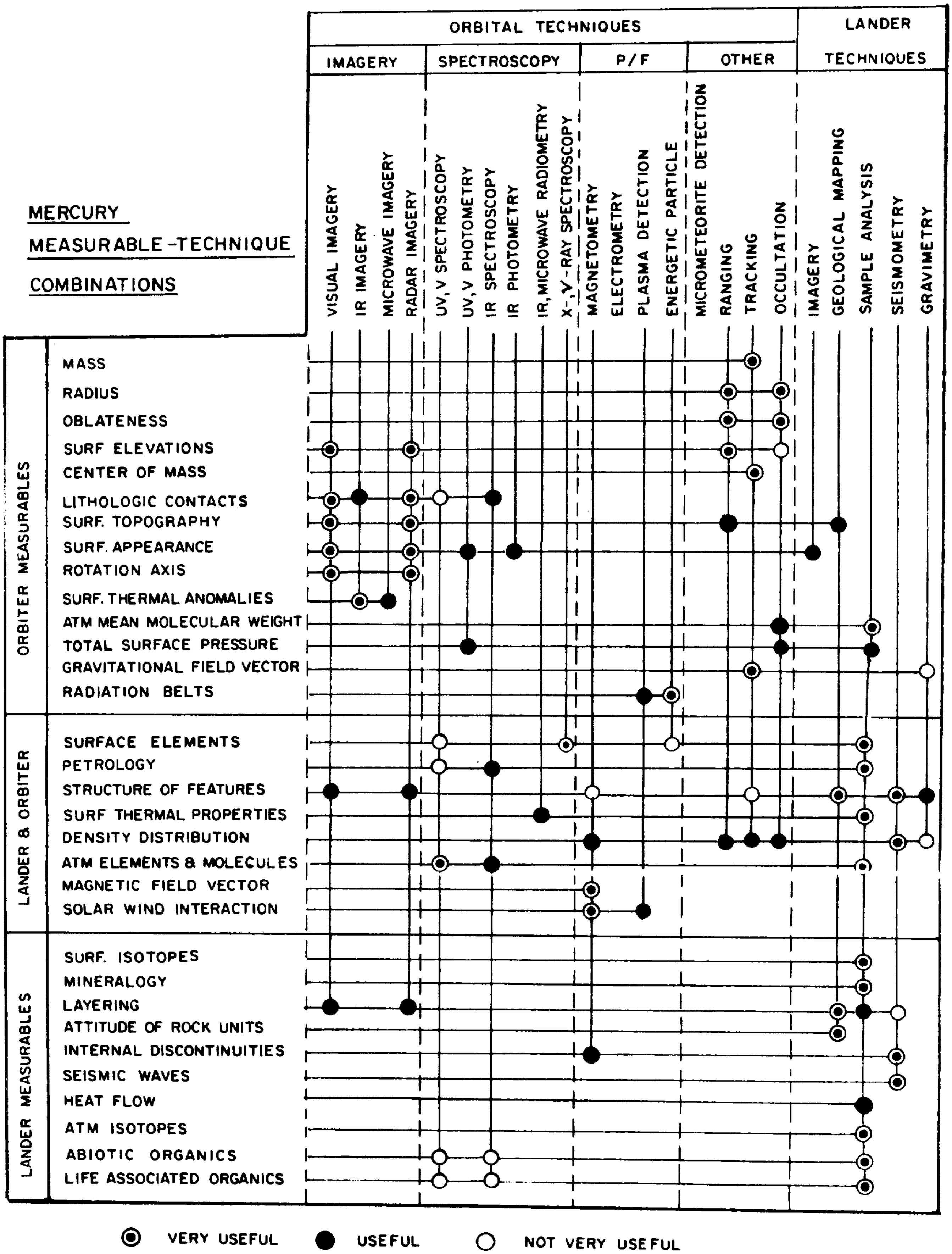
MERCURY
MEASURABLE-TECHNIQUE
COMBINATIONS
ORBITAL TECHNIQUES
LANDER TECHNIQUES
IMAGERY
SPECTROSCOPY
P/F
OTHER
VISUAL IMAGERY
IR IMAGERY
MICROWAVE IMAGERY
RADAR IMAGERY
UV, V SPECTROSCOPY
UV, V PHOTOMETRY
IR SPECTROSCOPY
IR PHOTOMETRY
IR, MICROWAVE RADIOMETRY
X-, γ-RAY SPECTROSCOPY
MAGNETOMETRY
ELECTROMETRY
PLASMA DETECTION
ENERGETIC PARTICLE
MICROMETEORITE DETECTION
RANGING
TRACKING
OCCULTATION
IMAGERY
GEOLOGICAL MAPPING
SAMPLE ANALYSIS
SEISMOMETRY
GRAVIMETRY
ORBITER MEASURABLES
MASS
RADIUS
OBLATENESS
SURF ELEVATIONS
CENTER OF MASS
LITHOLOGIC CONTACTS
SURF. TOPOGRAPHY
SURF. APPEARANCE
ROTATION AXIS
SURF. THERMAL ANOMALIES
ATM MEAN MOLECULAR WEIGHT
TOTAL SURFACE PRESSURE
GRAVITATIONAL FIELD VECTOR
RADIATION BELTS
LANDER & ORBITER
SURFACE ELEMENTS
PETROLOGY
STRUCTURE OF FEATURES
SURF THERMAL PROPERTIES
DENSITY DISTRIBUTION
ATM ELEMENTS & MOLECULES
MAGNETIC FIELD VECTOR
SOLAR WIND INTERACTION
LANDER MEASURABLES
SURF. ISOTOPES
MINERALOGY
LAYERING
ATTITUDE OF ROCK UNITS
INTERNAL DISCONTINUITIES
SEISMIC WAVES
HEAT FLOW
ATM ISOTOPES
ABIOTIC ORGANICS
LIFE ASSOCIATED ORGANICS
VERY USEFUL
USEFUL
NOT VERY USEFUL

FIGURE 4.

Mercury would be much more meaningful for mass determination. Figure 4 graphically emphasizes the conclusion that visual imaging experiments are likely to be very useful in investigating surface elevations, lithologic contacts, surface topography, surface appearance, and the orientation of the axis of Mercury's rotation. Other very useful experimental techniques include ranging, tracking, and occultation. However, previous flyby experiments may have resulted in adequate mass, radius, and oblateness determinations, hence these techniques may be less useful than implied by the figure.

Additional useful experiments which might be performed by an orbiter include mapping of lithologic contacts by infrared imagery and spectroscopy, study of surface appearance by UV, visible, and IR photometry, mapping of thermal anomalies by infrared and passive microwave imaging techniques, determination of the atmospheric pressure and mean molecular weight by radio occultation experiments, detection of gravitational anomalies by spacecraft tracking, and detection of radiation belts. In addition to such scientific objectives, an orbiter mission would be expected to play a key role in providing engineering data for any subsequent lander missions.

2.3.3 Landers

Lander missions are required to satisfy those scientific objectives which can only be achieved by surface sampling. As shown in the bottom third of Figure 4, these include the determination of surface isotopic abundances and surface mineralogy and the detection and study of pre-biotic phases of extraterrestrial life. Seismometer experiments are also likely to play an important role in lander exploration.

Lander and orbiting spacecraft working together are likely to prove most valuable in connection with those scientific objectives involving extensive mapping of the surface but which also require some ground truth measurements. In particular, as indicated by the middle third of Figure 4, orbiter-lander combinations would be most useful for study of surface elemental composition and petrology, the structure of the observed surface features, and the structure of the interior.

2.4 Orbiter Measurement Specifications

In principle, each measurable identified above implies a unique set of measurement specifications (planetary coverage, resolution, repetition rate, etc.) and consequently a unique set of instrument capabilities. In practice, a great deal of overlap exists between the different measurables. For example, in operational terms the measurable "surface appearance" is scarcely distinguishable from "structure of features" or "surface topography". Thus in order to facilitate a listing of measurement specifications, it is useful to group the specifications according to instrumental techniques, rather than by individual measurables. This section reviews the measurement specifications related to those instruments which are likely to be useful on an <u>orbiting</u> spacecraft. The instrument techniques considered are imagery, spectroscopy, photometry, radiometry, and miscellaneous techniques including magnetometry, particle detection, and ranging.

The measurement specifications for planetary and atmospheric orbiter instruments are summarized in Table 2. Particle and field experiments are summarized later; extraterrestrial biology experiments require a lander and are not appropriate for an orbiter. The upper third of Table 2 presents planet-oriented

TABLE 2
ORBITAL MEASUREMENT SPECIFICATIONS

	IMAGERY						RADIOMETRY	
	VISUAL			IR & MICROWAVE				
SCALE	regional	local	detailed*	regional		local	regional	
GROUND RESOLUTION	1 km	0.1 km	1 m	3 km		0.3 km	30 km	
VERTICAL RESOLUTION	1 km	0.1 km	5 m	--		--	--	
SCENE AREA	800x800 km	100x100 km	1 x 1 km	800x800 km		100x100 km	--	
POSITIONAL ACCURACY	10 km	1 km	10 m	10 km		1 km	30 km	
PLANETARY COVERAGE	global	10%	1%	global		10%	10%	
DISTRIBUTION OF COVERAGE	global	--	--	global		--	global	
REPETITION RATE	--	--	--	10 hr		10 hr	5 hrs at terminator	
SENSOR TYPE	visual (shadows)	visual (color)	visual (stereo)	near IR	far IR	passive microwave	IR radiometer	microwave radiometer
SPECTRAL REGION	0.4-0.7 μm	0.4-0.7 μm	0.4-0.7 μm	1-2 μm	3-30 μm	2-20 cm	2.5-50 μm	0.3-100 cm
NUMBER OF BANDS	1	3	1	1	2	1	3	3
BANDWIDTH	0.3 μm	0.1 μm	0.3 μm	1 μm	5 μm	--	--	--
SPECTRAL RESOLVING POWER	--	--	--	--	--	--	5	--
IMAGE OVERLAP	20%	20%	60%	20%	20%	20%	--	--
SOLAR ELEVATION ANGLE	10-30°	40-80°	60-90°	40-80°	--	--	--	--
PHOTOMETRIC ACCURACY	3%	3%	3%	--	--	--	--	--
TEMPERATURE RESOLUTION	--	--	--	--	5°K	5°K	5°K	5°K
MEASURABLES	requiring vertical resolution: surface elevations surface topography structure of features not requiring vertical resolution: rotation axis lithologic contacts surface appearance			lithologic contacts thermal anomalies				

* Detailed scale imagery is not appropriate for a first-generation orbiter mission.

TABLE 2 (Continued)

SPECTROSCOPY							ALTIMETRY	
ULTRAVIOLET		INFRARED			γ-RAY & X-RAY			
regional		regional			regional		regional	
100 km		30 km			100 km		5 km	
10 km		--			--		0.1 km	
--		--			--		--	
10 km		30 km			50 km		5 km	
limb (2500 pts.)		global			global		global	
10° x 10° grid		global			global		global	
5/Mercury day		--			--		--	
spectrometer	photometer	near IR spectrometer	far IR spectrometer	photometer	γ-ray spectrometer	x-ray spectrometer	radar altimeter	laser altimeter
0.05-0.4 μm	0.05-0.4 μm	0.8-2.5 μm	2.5-100 μm	0.8-2.5 μm	0.1-3 Mev	0.2-10 keV	0.3-10 cm	0.4-10 μm
--	10	--	--	10	--	--	1	1
--	--	--	--	0.1-0.3 μm	--	--	--	--
200	50	100	200	20	100	500	--	--
--	--	--	--	--	--	--	--	--
day	day	40-80°	night	40-80°	--	--	--	--
0.2%	0.2%	0.5%	0.5%	0.5%	1%	0.2%	--	--
--	--	--	--	--	--	--	--	--
atmospheric elements and molecules total surface pressure		lithologic contacts petrology surface appearance			surface elements		radius oblateness surface elevations surface topography density distribution	

parameters, the middle third presents instrument-oriented parameters, and the lower third lists the relevant measurables. The term "scale", occurring in the upper third of the table, refers to the level or scale of exploration: regional, local, or detailed. Each level corresponds to a characteristic size (extent) of the measurable based on terrestrial and lunar experience and implies a class of resolution or coverage capability of the measuring instrument. Positional accuracy refers to the allowable location error relative to Mercury's surface. For example, the 10 km entry in the first column indicates that a regional scale image of Mercury's surface should portray a ground area whose location (geographical coordinates) should be known within 10 km. Distribution of coverage pertains to the manner in which the desired amount of coverage is distributed over the planet. The distribution requirements of local and detailed scale exploration cannot be determined a priori, but must await the acquisition and analysis of regional scale data. Repetition rate refers to geographical areas, not the entire amount of planetary coverage. The term "spectral resolving power", as used in the middle third of the table, is defined as the reciprocal of the fractional spectral resolution, i.e., as $\lambda/\Delta\lambda$. Other terms used in the table are self-explanatory.

2.4.1 Imagery

Three levels or scales of exploration are defined: regional, local, and detailed. Thus regional scale imagery implies scene areas of roughly 800 x 800 km, ground resolutions of one to three km, and 70 to 100 percent planetary coverage. Similarly, local scale imagery implies scene areas of about 100 by 100 km, ground resolutions of 50 to 150 meters, and roughly ten percent planetary coverage. As noted above, the exact amount of coverage desired, and its location, cannot be adequately specified until the regional scale imagery is acquired and interpreted. Detailed scale imagery implies scene areas of about one by one km and ground resolutions of approximately one to five meters. Less than one percent surface coverage at this scale should be satisfactory (with a one km^2 scene area nearly one million pictures would be required for one percent coverage of Mercury). Detailed scale exploration has been defined here only for visual imaging techniques. For a first-generation orbiter, the emphasis should be placed on acquiring regional and local scale imagery. The resolution and scene area specifications appearing in the table are in the nature of upper and lower bounds, respectively. That is, imagery providing better resolution or larger scene areas would be equally acceptable. However, imagery providing poorer resolution or smaller scene areas would not be as satisfactory.

When required, as noted in the lower third of the table, detection of vertical height differences may be accomplished in an imaging format by measuring shadow lengths and inferring vertical heights, or by using two images of the same area taken under similar illumination conditions and measuring stereo parallax. Imagery for determining surface appearance would be more effective if stereoscopic coverage were achieved. Both surface appearance and structure of features interpretation would be facilitated by color imagery. It may be noted that the measurable "layering" has been omitted. Effective imagery for study of layering requires ground resolutions of one meter or less. This capability does not appear feasible for an early orbiter mission.

Stereo coverage is best obtained at solar elevations angles higher than 60 degrees. At lower sun angles, shadows may interfere with stereo parallax measurements. Similarly, color imagery is enhanced by solar elevations between 40 and

80 degrees. At lower sun angles, definition is lost in the shadows, while at noon sun the total lack of shadows hinders interpretation. When shadow measurements are desired, solar elevations of 10 to 30 degrees are most appropriate. In many cases interpretation of structural features is facilitated by the increased contrast and shadows at low sun angle.

Radar imagery could be used, in most cases, as well as visual imagery. Furthermore, no constraints need be placed on solar illumination conditions for proper interpretation of radar imagery. However, other studies (Klopp, 1970) have indicated that even low resolution measurements (5-10 km) would require side-looking radar imagers of about 100 kg. Therefore radar imagery has not been considered further in this study.

Near infrared imagery would be useful for mapping of lithologic contracts, while far infrared and passive microwave imagery would be useful for detection of thermal anomalies. The measurement specifications for these experiments are also given in Table 2. The repetition rate specification given for infrared and microwave imagery applies only to the thermal anomaly imagery. The repetition rate is not important when interpreting imagery for lithologic contracts.

2.4.2 Spectroscopy and Photometry

The primary value of an ultraviolet spectral instrument would be in the determination of elemental and molecular abundances in Mercury's atmosphere. The measurement specifications are summarized in Table 2. Vertical profiles, which could be obtained by scanning the limb, are desired; a vertical resolution of ten km corresponds to estimates of the atmospheric scale height. Data should be acquired at about ten degree intervals in latitude and longitude, except near the poles, hence something on the order of 2500 different vertical profiles are desired. This modest coverage will determine if there are significant variations over the planet or, if repetitive measurements are made, variations associated with changes in surface temperature. Either a continuous scanning spectrometer or a narrow-band photometer (with detection bands placed at the resonance lines of potential atmospheric constituents) could be used.

Both near and far infrared spectroscopy experiments would be useful for study of lithologic contacts and petrology. The ground resolution of 30 km, as shown in Table 2, is considerably relaxed from that required in the visual imagery. If feasible, it would be helpful to achieve the same ground resolution as in the visual imagery, as this would facilitate comparison of data. On the other hand, such a high resolution spectrometer is likely to be prohibitively heavy. An IR photometer would contribute to measurements of surface appearance and might provide some useful contacts data as well.

Measurement of some surface elemental abundances might be achieved by x-ray or gamma-ray spectroscopy. The x-ray spectral band was chosen to include the K-shell lines of all atoms of $6 < Z < 30$, while the gamma-ray instrument is intended to detect radioactive isotopes (both natural and induced). The gamma spectra of induced activity should be correlated with solar activity which can be measured at the spacecraft.

2.4.3 Radiometry

Simple non-imaging radiometers would be useful in inferring thermal properties of the surface and have limited applicability in temperature mapping and thermal anomaly detection. The radiometer measurement specifications are given in Table 2, and may be compared to those given for the imaging radiometers. In the interests of determining gross thermal properties of the surface and reducing the instrument weight and size, spatial resolution has been sacrificed for better frequency resolution and coverage. Measurements repeated near the terminator would be particulary useful in investigating the temperature dependence of the surface thermal properties.

2.4.4 Altimetry

Ranging measurements would be useful in determining Mercury's radius and oblateness. A limited amount of topographic data could also be obtained. Although in principal a radar or laser altimeter could be used to completely map the surface, such measurements are more likely to supplement, rather than duplicate, the imagery data. Table 2 provides measurement specifications for both radar and laser ranging. To avoid interference from naturally reflected sunlight, it may be necessary to restrict laser ranging to the dark side of Mercury.

2.4.5 Particles and Fields Measurements

If Mercury has a magnetosphere, the emphasis in particles and fields measurements will be placed upon determining the nature, geometrical configuration, and energy spectrum of the trapped particle population, mapping the magnetic field within the magnetosphere, and examining the interaction between the solar wind and the magnetosphere. If Mercury does not have a magnetosphere, the emphasis will be placed upon magnetometer measurements at the edge of the solar wind cavity in an attempt to detect surface magnetic anomalies as has recently been done from lunar orbit (Mihalov et al., 1971). Both eventualities are covered by the particles and fields measurement specifications given in Table 3. Study of the internal density distribution and discontinuities may require emplacement of a landed surface magnetometer. This technique, recently successful on the moon (Dyal et al., 1970), requires an orbiting magnetometer to provide time-dependent background level calibration.

TABLE 3

PARTICLES AND FIELDS MEASUREMENT SPECIFICATIONS

Instrument Technique	Magnetometry	Plasma Detection	Energetic Particles
Sensor Type	Vector Magnetometer	Plasma Analyzer	High Energy Particle Telescope
Measurement Range	$1 - 10^4\ \gamma$	e: 5-200 ev p: 0.1-5 kev $Z>2$: > 0.2-5 kev	e:E > 20 kev p:E > 50 kev $Z>2$: E>1 Mev/n
Frequency Response or Counting Rate	DC - 10 Hz	10^{10} particles/ (cm^2-sec-ster)	10^7 particles/ (cm^2-sec-ster)
Measurement Accuracy	2%	5%	5%
Measurables	Magnetic Field Vector Solar Wind Interaction Density Distribution Internal Discontinuities	Radiation Belts Solar Wind Interaction	Radiation Belts

SECTION 3

PAYLOADS AND SPACECRAFT

3. PAYLOADS AND SPACECRAFT

Previous sections of this report have defined specific scientific objectives for the exploration of Mercury and identified various "measurables" in support of these objectives. Those measurables which might profitably be observed or measured from a spacecraft orbiting Mercury have been defined further in terms of measurement specifications providing guidance as to desired values of resolution, planetary coverage, surface illumination conditions, etc. The purpose of this section of the report is to explore the relationships (a) between measurement capabilities and instrument size, weight, power requirements and other characteristics and (b) between the instrument support requirements and the spacecraft subsystems. The term "support requirements" refers to the support which must be provided to the measuring instrument by the rest of the spacecraft. Orbital instrument capabilities and support requirements are discussed first. In the second subsection, the instruments are grouped together into several candidate payloads representing different classes of capability and weight. Finally, the third subsection estimates the spacecraft subsystem parameters and defines several candidate spacecraft.

3.1 Instrument Capabilities

This section describes the capabilities of various instruments which are most likely to achieve the measurement specifications given earlier. The instrument capabilities in turn are related to instrument support requirements, in particular weight, power consumption, and data recording or collection rate. The techniques for estimating these support requirements have been provided by Klopp (1970) and North

American Rockwell (1970). The results are summarized in Table 4. Although orbit selection is not discussed until Section 4, the instrument capabilities and support requirements are clearly dependent upon the orbit from which the measurement is attempted. Except for the particles and fields instruments, the results shown in the table are based on a nominal 500 km altitude circular orbit. Data will be provided later in this section to indicate how the support requirements vary with altitude. These data are used in Section 4 to assist in orbit selection for the candidate spacecraft.

3.1.1 Visual Imaging Systems

The measurement specifications given earlier for regional scale imagery imply a need for imaging systems having formats of at least 800 by 800 resolution elements. In practice more resolution elements must be used to allow for reasonable amounts of resolution loss in various components of the system. Visual imagery systems likely to provide such capability include slow scan vidicons, return beam vidicons, and photographic film systems, and are discussed here in that order. It will be shown that although slow scan vidicons do not provide the desired scene area-resolution capability, they do have relatively modest weight, power, and data handling requirements, and are likely to provide the best compromise between instrument capability and instrument support requirements. The return beam vidicon systems provide better resolution capability, but have high data handling requirements in this application. Photographic film systems (with telemetered data return to Earth) provide the best resolution capability, but are likely to require inordinately massive amounts of radiation shielding.

TABLE 4

CANDIDATE SCIENCE INSTRUMENTS

INSTRUMENTS	RESO-LUTION (km)	MASS (kg)	POWER (watts)	DATA RECORDING RATE (kbps)
1½"SLOW SCAN VIDICON	2.5	11	24	80
2" RETURN BEAM VIDICON	1	15	32	1,000
70mm FILM CAMERA	0.005	110	40	80
2-CHANNEL IR LINE SCANNER	3	3	3	16
MICROWAVE LINE SCANNER	3	80	80	1
SIDE-LOOKING RADAR	3	100	130	7.5
UV SPECTROPHOTOMETER	10	2	4	0.15
NEAR IR SPECTROMETER	20	8	10	1.8
10-CHANNEL IR SPECTROPHOTOMETER	30	5	5	0.01
FAR IR SPECTROMETER	30	12	10	8
X-RAY SPECTROMETER	300	5	5	0.1
GAMMA-RAY SPECTROMETER	300	5	5	0.1
3-CHANNEL IR RADIOMETER	30	2	6	0.005
3-CHANNEL MICROWAVE RADIOMETER	30	9	24	0.005
RADAR ALTIMETER	5	10	10	0.01
LASER ALTIMETER	5	12	120	0.01
MAGNETOMETER	--	3	5	0.02
PLASMA ANALYZER	--	7	13	0.1
ENERGETIC PARTICLE TELESCOPE	--	5	3	0.1

The limiting resolution of a 1½-inch slow scan vidicon camera tube is about one thousand TV lines. Although this might imply that a ground resolution of 0.8 km could be achieved over a scene area of 800 x 800 km, in practice allowance must be made for loss of resolution due to the effects of image smear, low scene contrast, the optical lens system, and non-uniform response of the camera tube faceplate. The loss of resolution capability is demonstrated in Figure 5, which compares the assumed modulation transfer function (MTF) of the 1½" vidicon camera tube with the MTF of the entire camera system (excluding the effects of low scene contrast). The system MTF must equal or exceed 0.04 for adequate imagery. The limiting resolution of the camera system is about 850 lines. For low scene contrast (1.6:1), resolution comparable to only 600 lines could be achieved. Allowing for the effects of the raster quality of the image and the curvature of the planetary surface as seen from 500 km altitude, a ground resolution of 3.5 km over an 800 x 800 km scene area would result. In this case, the scene area meets the measurement specifications, but the ground resolution does not. A reasonable compromise would appear to result in a ground resolution of about 2.5 km over a 600 x 600 km scene area. At the center of the scene, a ground resolution of 1.7 km would be achieved. Measurement of shadow lengths at low sun angle illumination could be used to infer vertical height differences of less than one km. The 600 x 600 km scene area is consistent with a 60 degree field of view and a 15mm focal length. The camera system would have a mass of about 11 kg and an average power requirement of 24 watts. Image motion compensation is not necessary.

From a low-altitude circular orbit, the cycle time for regional scale imagery, i.e., the interval between subsequent pictures, is about 210 sec for 20 percent forward overlap. The slow

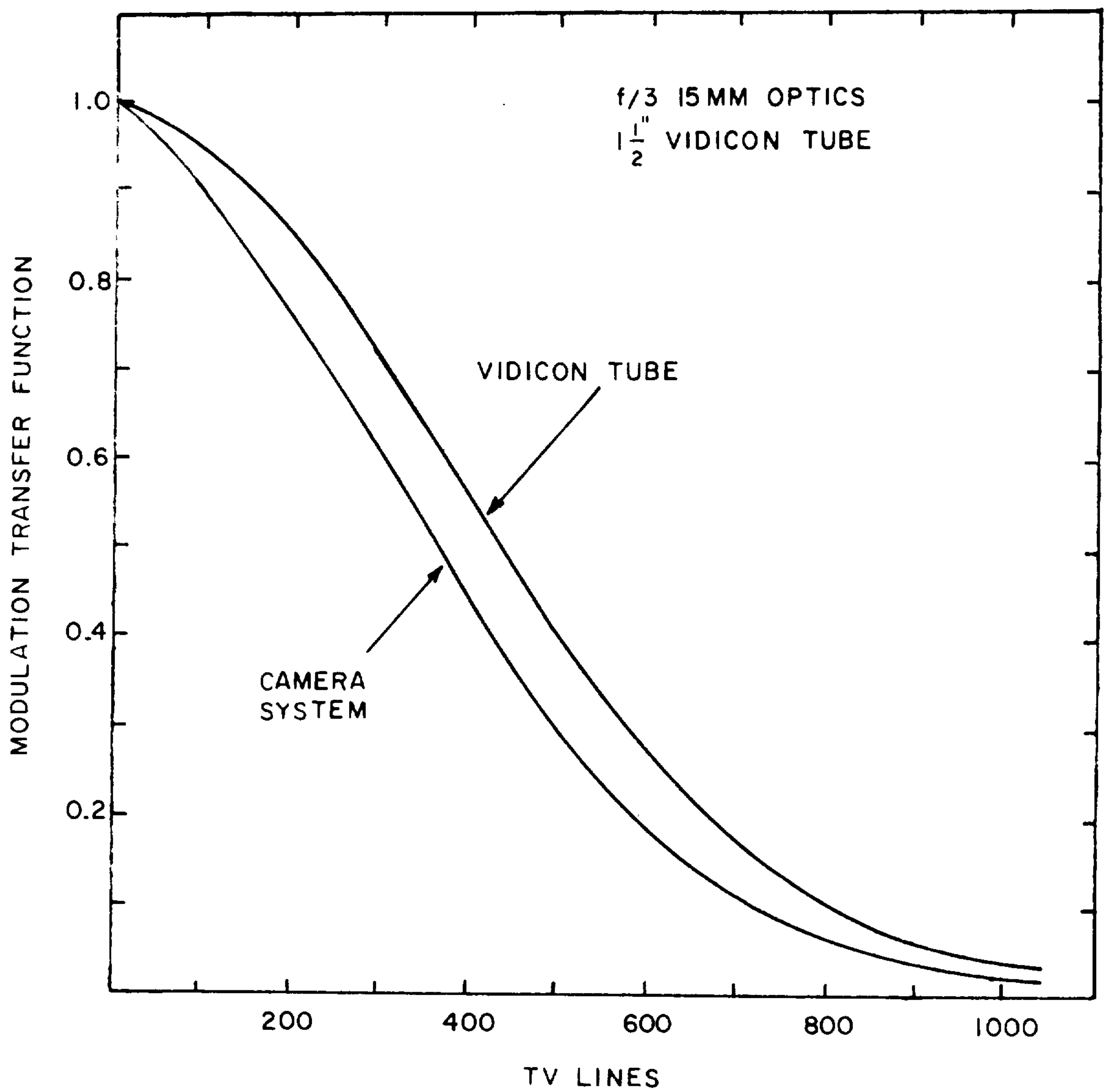

FIGURE 5. VIDICON CAMERA SYSTEM MTF

scan vidicon cannot retain the picture for this length of time without significant loss in image quality. Image retention time should be limited to approximately 100 sec or less, and therefore it is the image retention time which controls the data recording rate. In this case, assuming eight-bit encoding, the data recording rate is about 80 kilobits per second.

Equipping the vidicon system with a 10:1 zoom capability would permit 120 meter resolution over a 60 x 60 km ground area from an altitude of 500 km. Under good lighting conditions and high contrast, less than 100 meters resolution would be achieved. The camera system could acquire regional scale imagery equally well from higher altitudes. A redesign for 2000 km altitude would result in a 57mm focal length system, but similar scene areas and resolutions would result. However, zoom systems become less attractive since a 10:1 zoom would now imply an effective focal length of over five meters. That is, it would be difficult to acquire local scale imagery from this altitude.

A two-inch return beam vidicon (RBV) would provide better resolution capability than the slow scan vidicon, but at some expense in system weight and power requirements and a greatly increased data recording rate. From 500 km altitude, a two-inch RBV system would provide effective ground resolution of one km over an 800 x 800 km scene area. For high contrast scenes near the center of the image, a resolution of 300 meters should be achieved. The camera system would have a mass of about 15 kg and an average power requirement of 32 watts. As with the slow scan vidicon system, image motion compensation is not required. In addition to increased resolution, one of the most important characteristics of currently available RBV's is the reduced image retention time. After about ten seconds, lateral charge leakage appreciably affects picture quality. Thus for regional scale imagery, the data recording rate is about 10^7 bits per second for eight-bit encoding.

If the RBV were equipped with a 10:1 zoom capability, increasing the focal length to 150mm, local scale imagery could be acquired by the same camera. At maximum zoom, the scene area would be about 75 x 75 km with a ground resolution of about 50 meters. The shutter time must be limited to six milliseconds or less to avoid loss of resolution due to image smear, but with an f/3 lens this should be adequate down to sun angles of 15 degrees. Obtaining 20 percent image overlap along the orbital track would require a new picture every 26 seconds, so that again the data recording rate is determined by the RBV storage time.

Operating the camera system from higher altitudes, say 2000 km, would not change the situation as far as the regional scale imagery is concerned. Less allowance would be needed to compensate for planetary curvature and the resolution at the scene center would be about 0.6 km, dropping off to 1 km at the edges. However, a 10:1 zoom would result in only 90 meter resolution over a 160 x 160 km area.

Photographic film systems of the Lunar Orbiter type offer the promise of much higher resolution than the television systems, permitting <u>detailed</u> scale imagery of Mercury's surface. For example, a 70mm film system using SO-243 film could provide 5 meter ground resolution (at low contrast) over a 46 x 46 km area from 500 km altitude. An f/2 350 mm focal length optical system would be required with a ten degree field of view. At this high resolution, image motion compensation would be required. The complete camera system (exclusive of shielding) would have a mass of about 35 kg, including 100 meters of film and processing, flying spot scanner, IMC, and V/H sensor. The 100 meters of film would provide nearly 1500 photographs of Mercury. The major uncertainty is the amount of radiation shielding required to prevent fogging of the film. Bashe and Kennedy (1967) have estimated that about 3 kg of shielding would be necessary on a 330 day Mars mission using 100 meters of 70 mm SO-243 film. Since this estimate assumes the film damage is due to high energy solar protons, it might not be unreasonable to scale this estimate inversely with the square of the heliocentric distance. This implies that roughly 75 kg of shielding would be required for a Mercury mission of similar duration. Unless a radiation resistant film can be developed, it appears that film systems are not feasible for an early Mercury mission.

The weight, power, and data recording rates of the visual imaging systems considered here were summarized in Table 4, along with other instruments discussed later in this section. For comparison, the ground resolution capability of each instrument is also given. The estimates appearing in the table are based on a 500 km altitude circular orbit, except for the particles and fields instruments. It will be shown later that this is the preferred orbit for imaging and spectroscopy experiments.

3.1.2 Infrared Imaging Systems

Near infrared (1-2 μm) imaging systems would be most useful in the mapping of lithologic contacts on both a regional and local scale, while far infrared (3-30 μm) imagery would be most useful in thermal mapping. It may be noted that for the hot poles the peak of the spectral radiance is expected to occur at about 4 μm, while the dark side spectral radiance peak would occur at about 30 μm. The basic problems in designing a conceptual infrared line-scanning device are (a) estimating the required aperture of the collector, and (b) selecting a detector of sufficient sensitivity and response time.

A relatively modest two-channel (1-2 μm and 15-20 μm) line scanner will satisfy the regional scale imagery requirements. A 3 kg instrument consuming 3 watts of power (average) should provide 3 km ground resolution from 500 km altitude over an 800 km scan line. The data acquisition rate would be about 8000 bits per second per channel, assuming eight-bit encoding. The collector aperture of about two cm is determined by spatial resolution requirements, not energy collection requirements. In fact, a brightness temperature resolution of one degree K should be attainable. The instrument weight is dominated by the electronics. Flying the instrument at a somewhat higher altitude, and changing the angular resolution to maintain the same ground resolution, would not increase significantly the instrument weight and power at altitudes up to 800 km. Assuming uncooled thermistor bolometers for each channel, with a response time of 0.5 milliseconds, an additional detector would have to be added to each channel at altitudes above 800 km and hence the instrument mass would increase to about four kg. From an altitude of 2000 km, five detectors per channel would be required, and weight and power requirements would grow to about six kilograms and seven watts (average). The data rate, per detector, would remain approximately constant with altitude.

An instrument designed to achieve the local scale requirements of 300 m resolution over a 100 km scan line from 500 km altitude would have a mass of about 11 kg and an average power requirement of about 14 watts. Again the instrument mass is dominated by the detector arrays and associated electronics (a 21-detector array of 4.5 kg for each channel). In this case the data rate would be approximately 120,000 bits per second per channel. As the flight altitude increases, the number of thermistor detectors required per channel would increase linearly with altitude. The electronics mass and power scale approximately with the square root of the number of detectors, and hence with the square root of the altitude. The mass of the collecting optics (0.6 kg at 500 km) scales with the square of the altitude, while the scanning system mass (0.6 kg at 500 km) grows proportionately to the cube of the altitude. Thus an instrument of the same capability, but flying at 2000 km, would have a mass of about 60-70 kg, an average power consumption of about 25-30 watts, and a data rate of about 500,000 bits per second per channel. The angular momentum associated with the scanning system mirror assembly is likely to lead to some attitude control problems when such large instruments comprise part of the science payload.

3.1.3 Passive Microwave Imaging Systems

The thermal channel of the infrared imager discussed above could be replaced by, or supplemented with, a passive microwave imaging system. However, unless some remarkable advancements are made in microwave technology, a microwave imager of capability comparable to the infrared thermal imager will be larger, heavier, and unlikely to meet the requirements for regional scale imagery. In order to achieve three km spatial resolution from an altitude of 500 km, a mechanically-scanning antenna must be about 3 meters in diameter (at an operating wavelength of 1.5 cm or 20 GHz). Assuming an areal density of 1.5 pounds per square foot, the antenna would have a mass of about 50 kg.

An additional problem arises when the integration time is considered. The integration time required to achieve a specified temperature resolution depends upon the operating frequency and the receiver noise temperature according to (Klopp, 1970)

$$\tau \geq \frac{850}{f} \cdot \left(\frac{T + T_N + T_L}{\Delta T} \right)^2$$

where f is the operating frequency, T is the brightness temperature of the target, T_N is the noise temperature, T_L is the resistive loss temperature (usually on the order of 100°K), and ΔT is the desired temperature resolution. The amplifier noise temperature T_N generally increases with increasing frequency in a nonlinear manner. Thus there is some optimum operating frequency, dependent upon T, which results in a minimum required integration time. Assuming noise temperatures representative of currently available tunnel diode amplifiers (for example, 1100°K at 20 GHz), the optimum operating frequency for observing a hot (700°K) scene is about 20 GHz. At this frequency, an integration time of six milliseconds is required to achieve a temperature resolution of five degrees K. The integration time available depends upon the ground resolution (antenna beamwidth), the linear extent of the scan line, and the speed of the spacecraft. At a ground speed of two km/sec and a ground resolution of three km, only 1.5 seconds are available to sweep out the entire scan line. If the scan line is 800 km in length, only 5.6 msec are available per resolution element. This is almost equal to the integration time required, but with a continuously moving mechanically-scanned antenna only about half the available dwell time can be used if smearing effects are to be avoided. An electrically-scanned antenna would permit a 4.1 msec integration time, since only 1.5 msec are required to shift from one resolution element to the next. The electrically-scanned antenna would have a mass of about 75 kg and achieve a temperature resolution of about six degrees K at Mercury's hot poles, compared to about 7.5 deg K for the mechanically-scanned antenna. The average power requirements are about 75 watts for the electrically-scanned antenna and something in excess of one kilowatt to slew the 50 kg mechanical antenna. The system mass is dominated by the antenna. The receiver has a mass of only 5 kg and consumes only 5 watts of power (average).

The length of the electrically-scanned antenna scales inversely with angular resolution. That is, the size increases linearly with altitude if the ground resolution is fixed. The antenna mass varies as the square of the length, while the power requirement varies linearly with the length. Thus an increase in flight altitude will very rapidly increase the system mass if the system resolution capability is to be maintained.

3.1.4 Radar Imaging Systems

Active microwave (radar) imaging systems are prohibitively massive for consideration on an early Mercury orbiter mission. For example, previous studies (Klopp, 1970) have shown that regional scale (three km resolution over a 600 x 600 km area) imagery requires a radar system of 100 kg mass, an average power requirement of 130 watts, and a data acquisition rate of 7500 bits per second. In addition to the large mass, a 50 meter antenna is required (at 10 cm wavelength). The antenna length could be decreased by decreasing the operating wavelength, but this would also result in increased power requirements. It is worth noting, however, that a radar imaging system would alleviate the solar illumination constraints so that complete planetary coverage could be obtained in about thirty days (from a low circular orbit).

3.1.5 Ultraviolet Spectroscopy

An ultraviolet spectral instrument is likely to be quite useful in determining elemental and molecular abundances in Mercury's atmosphere, if an atmosphere exists. However, because of the present uncertainty in our knowledge of the atmosphere, the desired capabilities of such an instrument cannot be formulated with sufficient detail to permit accurate estimation of the instrument's mass, power requirement, or data collection rate. A ten km resolution at the limb from a 500 km altitude orbit can be achieved by a very modest optical system, hence spatial resolution requirements are not expected to be a major constraint in instrument design. Because of the uncertainty in the atmospheric properties, there is no reliable way to estimate the strength or intensity of the emission or absorption spectra. The resonant emission lines of argon at 1048 and 1067 Å, of krypton at 1165 and 1236 Å, and of xenon at 1296 and 1470 Å would be of particular interest. An approximate estimate of the support required for an ultraviolet instrument is provided by noting that the UV spectrometer selected for the 1973 Venus/Mercury flyby has a mass of two kg, a power consumption of four watts, and a data collection rate of 150 bits per second.

3.1.6 Infrared Spectroscopy and Photometry

Infrared spectrometers and photometers would be especially useful in studying surface appearance, lithologic contacts, and petrology. A seven kg interferometer spectrometer, similar to the Nimbus III Michelson interferometer, operating in the near infrared (0.8-2.5 μm) should provide 30 km ground resolution from an orbital altitude of 500 km. The desired spectral resolving power ($\lambda/\Delta\lambda$) of 100 can be achieved easily requiring a data acquisition rate of about 1200 bits per second assuming eight-bit encoding. The average power requirement of this instrument is about ten watts. The single thermistor bolometer requires no cooling. This instrument provides a spectrum of the infrared radiation from Mercury's surface; it is not sensitive enough to provide thermal energy spectra on the dark side. Actually, at high surface temperatures (400-500 deg K or more) the energy detected near the long wavelength end of the passband (2.5 μm) will be predominantly due to thermal emission rather than reflected solar energy. By increasing the size of the collecting optics, and hence increasing the mass to eight kg, a ground resolution of 20 km could be achieved. The power requirement of this more capable instrument would still be ten watts, but the data acquisition rate would increase to 1800 bits per second. Improving the ground resolution beyond this point increases the instrument mass rapidly. Although it would be quite useful to have an instrument capable of three km resolution, i.e., comparable to that of the imaging systems discussed earlier, the mass would increase to about 65 kg. Neglecting changes in apparent ground speed, the collecting optics mass increases as the square of the altitude. Thus the eight kg instrument (one kg of optics) grows to a 23 kg instrument if flown at 2000 km, rather than 500 km.

A small ten-channel infrared spectrophotometer might be a useful alternative. An instrument using a linear array of ten thermistors operating over the spectral region 0.8-5 μm would have a mass of only five kg and achieve a ground resolution of 30 km from 500 km altitude. Each of the ten channels would have a spectral detection bandwidth of about 0.4 μm. The average power consumption would be about five watts, and the instrument data collection rate would be about 12 bits per second. By increasing the altitude to 2000 km, but maintaining the 30 km ground resolution, the instrument would grow to 17 kg. An 11 kg instrument would provide ten km ground resolution from 500 km altitude. Either instrument could also be used in the visible portion of the spectrum by replacing one of the thermistors by a CdS detector (0.45-0.8 μm) with no significant change in the instrument mass or power requirements.

Estimating the performance of a far infrared (2.5 - 100 μm) interferometer spectrometer is somewhat more complicated. Achieving a spectral resolving power of 200 over such a broad spectral range implies the use of a detector with a fast response time. However, the only currently available detector capable of operating over such a broad range is the thermistor bolometer, which is a relatively slow detector. The thermistor response time is a minimum of about 0.5 milliseconds, and with a 30 km ground resolution there is not enough time to sweep out the entire interferogram (or spectrum) before the apparent ground spot becomes smeared out due to the orbital speed of the spacecraft. Thus the spectral range of the instrument is confined to 2.5-85 μm. This spectral range is believed to be quite adequate, although it could be extended by the use of image motion compensation devices. Another problem associated with the detector arises because the detector sensitivity decreases with response time and hence increases the collector aperture (and mass) consistent with maintaining high signal to noise ratios. An 18 cm aperture will provide signal to noise ratios of 200 or more from 15 to 85 μm on the cold side (100°K) of Mercury. The peak of the thermal radiation spectrum occurs at about 30 μm. At 10 μm the signal to noise ratio has dropped to approximately ten and falls off quite rapidly at shorter wavelengths. However, on the warm side of the planet, there is sufficient thermal energy collected to achieve good signal to noise ratios down to 2.5 μm. The complete spectrometer package has a mass of 12 kg, an average power consumption of ten watts, and collects data at an 8000 bit per second rate. The ground resolution (30 km from 500 km altitude) could be improved only at the expense of increasing the mass and decreasing the operating spectral range. Similarly, increasing the flight altitude while maintaining the ground resolution will also increase the instrument mass. For example, at 2000 km altitude an instrument of the same capability would have a mass slightly more than 100 kg and require a 72 cm aperture.

An attempt to combine the near and far infrared capability into a single instrument would destroy the far IR detection capability. That is, in order to extend the range of the far IR spectrometer down to 0.8 μm, the long wavelength limit must decrease to about 26 μm. This "mid-range" instrument would have essentially the same support requirements (mass, power, data rate) as the far infrared spectrometer.

3.1.7 Gamma and X-Ray Spectroscopy

As with the ultraviolet spectroscopy experiments, there appears to be no reliable way to estimate source strengths and hence the energy-collection requirements of potentially useful instruments. Therefore it is assumed here that the support requirements of either a gamma-ray or x-ray spectrometer are similar to those of instruments designed or suggested for lunar orbiter use; namely, a mass of about five kg, an average power consumption of about five watts, and a data acquisition rate of 100 bits per second. These instruments have poor ground resolution capability, but should be adequate for gross survey work.

3.1.8 Infrared and Microwave Radiometry

A two kg three-channel (3-3.5, 12-15, and 27-33 μm) infrared radiometer would provide 30 km ground resolution from 500 km altitude and be useful for studying surface thermal properties and thermal anomalies. Temperature differences of five deg K could be detected reliably on both the cold and hot sides of Mercury using the two longer wavelength channels. The short wavelength channel would achieve a five deg K temperature resolution only for surface temperatures of about 400°K or higher, even though a PbSe detector is used to increase the sensitivity. Neither this detector, nor the two thermistors used for the other two channels, require cooling. The collecting optics is sufficiently small that the instrument mass is essentially independent of flight altitude, at least over the range 500 - 2000 km. The power consumption is six watts (average), and the instrument data collection rate is about five bits per second.

A nine kg three-channel (20, 30, and 40 GHz) passive microwave radiometer would also be useful in this regard. The ground resolution is 30 km, while the temperature resolution is less than one deg K (significantly better than the infrared radiometer discussed in the previous paragraph). The antenna diameter is about 30 cm. If an altitude of 2000 km were chosen, the antenna diameter would increase to 120 cm and the instrument mass would increase to 16 kg (including the antenna). In either case, the average power consumption would be 24 watts, and the data collection rate about five bits per second, the same as the IR radiometer. A single-frequency system would have slightly less demanding support requirements, depending upon the operating frequency. A 40 GHz system with a 15 cm antenna would have a mass of six kg and a four watt power requirement.

3.1.9 Altimetry

Either radar or laser ranging combined with precision spacecraft tracking would provide copious data on Mercury's radius, figure, and oblateness. Such data might also supplement topographic information deduced from visual imagery. A 120 GHz

(0.25 cm wavelength) radar altimeter would provide range accurate to at least 50 meters. A five km ground spot size would require a 36 cm diameter antenna with a mass of about one kg. The system mass would be about ten kg (including the antenna), the average power requirement about ten watts, and the data rate about ten bits per second. The antenna diameter would increase linearly with altitude. Thus at 2000 km altitude a 13 kg antenna would be required. A radar altimeter could be designed to utilize the same antenna as the passive microwave radiometer by operating at 40 GHz. However, the antenna diameter would have to be increased to 110 cm to provide the desired ground resolution. Of course, the radiometer would be gated off during reception of the radar pulse return. The combined radiometer-altimeter instrument would have a mass of about 20 kg with a 30 watt average power consumption. Thus the combined instrument offers no weight or power savings over the separate instruments.

Laser ranging does not appear to be competitive with radar because of interference with sunlight reflected from the planet. A Neodymium-YAG system operating at 1.06 μm would have an average power consumption of approximately 120 watts using a ten nanosecond pulse width yielding a ranging accuracy of about two meters. The laser energy must be about 1.3 joules in order that the reflected laser energy be ten times larger than the reflected solar energy. The system mass would be approximately 12 kg and the data rate about ten bits per second. A CO_2 laser operating at 10.6 μm avoids the sunlight problem, but the short response time detector required must be cooled to at least 77°K. Cooling systems operating at this temperature tend to be massive, or consume large amounts of power, or both. The cooling problem is aggravated by operation at Mercury where the solar intensity is high. A ruby laser is even less efficient then a neodymium laser and even more sunlight interference would occur at 0.7 μm than at 1.06 μm.

3.1.10 Particles and Fields Instruments

As noted earlier, the types of particles and fields instruments likely to be most useful on a Mercury orbiter mission depend upon whether or not Mercury has a magnetosphere. Magnetometers would be useful in either event, although the desired dynamic range of the instrument may be different in the two cases. A helium vapor magnetometer with triaxial Helmholtz coils is estimated to have a mass of three kg, an average power consumption of five watts, and a data collection rate of about 20 bits per second. This instrument would measure the field components and the total scalar field at frequencies from zero to ten Hz. A rubidium vapor magnetometer of smaller mass could be used, but would be less accurate and more sensitive to temperature.

A solar plasma analyzer package would be useful for studying the solar wind or the interaction of the wind with Mercury's magnetosphere. The plasma instrument package which has been suggested for the 1973 Venus/Mercury flight consists of: 1) an electrostatic analyzer, 2) a low energy electron flux detector, 3) a suprathermal particle detector, and 4) a plasma composition instrument. The total package has a mass of seven kg and an average power consumption of 13 watts. For an orbiter application, the data rate is likely to be about 100 bits per second.

If Mercury is found to have a trapped particle population, some type of charged particle spectrometer would be necessary to study the radiation belt characteristics. The most appropriate type of instrument cannot be selected until the results of the 1973 flyby are available. However, except for specialized application, most radiation detection instruments have masses in the range one to five kg and average power consumptions of two or three watts. Thus a typical instrument might be an energetic particle telescope of five kg mass, a three watt power requirement, and a 100 bit per second data collection rate.

Mass, average power, and data recording requirements of the particles and fields instruments are summarized in Table 4 (p. 51).

3.2 Selected Payloads

Typical mission payloads may be conceptually constructed on the basis of instrument mass and performance estimated in the previous section. In order to facilitate quantitative estimates of the variation of science payload, and ultimately total spacecraft weight, with scientific capability and function, three different science payloads have been formulated. These are: 1) a baseline planetology payload, which emphasizes surface imagery but includes other experiments of modest support requirements which are likely to be useful on an early orbiter mission, 2) a minimum planetology payload, which also emphasizes surface imagery but includes a minimum number of additional experiments, and 3) a particles and fields payload. Table 5 summarizes these payload selections. As discussed later, the planetology experiments tend to be most useful when operated from a low altitude circular orbit, while the particles and fields experiments tend to be most useful when operated from an eccentric orbit which explores the magnetosphere and its interaction with the solar wind. The

TABLE 5

CANDIDATE SCIENCE PAYLOADS

INSTRUMENT TYPE	INSTRUMENT MASS (KG)		
	BASELINE PLANETOLOGY	MINIMUM PLANETOLOGY	PARTICLES AND FIELDS
$1\frac{1}{2}$" VIDICON(S)	22 (2)	11	--
IR LINE SCANNER	3	3	--
UV SPECTROPHOTOMETER	2	2	2
NEAR IR SPECTROMETER	8	8	--
10-CHANNEL SPECTROPHOTOMETER	--	--	5
X-RAY SPECTROMETER	5	--	--
GAMMA-RAY SPECTROMETER	5	--	--
MICROWAVE RADIOMETER	9	--	--
RADAR ALTIMETER	10	--	--
MAGNETOMETER	3	3	3
PLASMA ANALYZER	--	--	7
ENERGETIC PARTICLE TELESCOPE	--	--	5
TOTAL SCIENCE PAYLOAD	67 KG	27 KG	22 KG

three selected payloads are not mutually exclusive, since the interplanetary bus vehicle might deliver more than a single orbiting spacecraft.

3.2.1 Baseline Planetology Payload

This payload instrument selection emphasizes visual imagery of Mercury on both a regional and local scale, and also provides infrared imagery on a regional scale. Two separate $1\frac{1}{2}$-inch slow scan vidicon camera systems are used; one for regional scale imagery, the other for local scale. The regional scale camera (15 mm focal length) covers a 600 x 600 km surface area for each frame from a nominal 500 km altitude orbit. The ground resolution achieved by the system depends both upon the apparent scene contrast and the location of the resolution element. Approximately 2.5 km resolution will be achieved for a low contrast (1.6:1) scene near the edge of the 60 degrees field of view, while approximately 1 km resolution will be achieved for a high contrast (10:1) scene near the center of the field of view. The limiting resolution provided by the 1000 line camera tube is 0.6 km. Although a new ground area will come into view every three minutes, the camera tube will retain the image without serious resolution degradation for only about 100 seconds, hence the data recording rate must be about 8×10^4 bits per second as noted previously. The local scale camera (153 mm focal length) provides ground scenes of 55 x 55 km. A ground resolution of about 150 meters will be achieved for a low contrast scene near the edge of the six degree field of view, while 100 meters resolution will be achieved for a high contrast scene near the center of the field. If twenty percent image overlap is desired along the flight path, pictures must be taken every twenty seconds, hence the data recording rate must be about 4 x 10^5 bits/second. This is twice the currently feasible recording rate for a small recorder, but presumably the recording rate capability will improve before a Mercury orbiter mission is actually flown. Each camera consumes 24 watts (average) power and has an 11 kg mass. The mass estimates (assuming a 500 km altitude circular orbit) for each instrument selected for the baseline planetology payload are summarized in Table 5.

The two-channel infrared imager has been described above. The 1-2 μm channel is used to map reflectivity differences and infer the location of lithologic contacts, the second channel (15-20 μm) is used to obtain a thermal map of the surface and is sensitive enough to detect temperature differences of five deg K on the cold side of Mercury. The three km ground resolution (800 km scan length) provided by the three kg instrument is felt to be quite adequate for an early orbiter mission. The other candidate imaging systems, microwave (80 kg) and radar (100 kg), are prohibitively massive.

The ultraviolet spectrophotometer may not be useful if earlier missions indicate that there is no atmosphere. In this case, the two kg three-channel infrared radiometer might replace this instrument. The microwave radiometer (three channels) is included to provide some exploration capability in the millimeter portion of the spectrum. If this is not considered especially useful, this instrument might also be replaced by the three-channel infrared radiometer with a ten percent reduction in total science payload. The recommended baseline planetology package has a mass of 67 kg and an average power consumption of 114 watts if all instruments were "up" simultaneously. This might occur on daytime orbital passes, but at night the vidicon cameras and the IR spectrometer would be off, reducing the power requirement to 56 watts. The data collection profile is dominated by the television cameras, most notably the local scale camera (4 x 10^5 bits per second).

3.2.2 Minimum Planetology Payload

This package, summarized in Table 5, provides regional scale visual and near infrared surface imagery. A UV spectrophotometer and near IR interferometer spectrometer have been added to this basic imaging package. The magnetometer is also included for mapping the magnetosphere if there is one, or studying gross internal properties and surface magnetic anomalies if there is not. If no atmosphere is found from an earlier flyby, the UV spectrophotometer might be replaced by the three-channel infrared radiometer (three kg). The minimum planetology payload has a mass of 27 kg, an average power consumption of 46 watts, and a data collection rate dominated by the television camera (8 x 10^4 bits per second).

3.2.3 Particles and Fields Payload

This package, also summarized in Table 5, deals with particles and fields measurements and with planetology experiments which do not involve high data collection rates. That is, imaging and interferometer spectrometer experiments have not been considered. The particles and fields instruments include a magnetometer, plasma analyzer package, and an energetic particle telescope; the planetology instruments include both a UV and ten-channel spectrophotometer. The ten-channel instrument covers the spectral region 0.4-5 μm. Thus the particles and fields package should be interpreted as a minimum all-purpose payload which includes both particles/fields and non-imaging planetology experiments. This payload has a mass of 22 kg, an average power consumption of 30 watts, and a data collection rate on the order of 400 bits per second. These support requirements correspond very closely to those of the "minimum planetology" payload excluding the data rate associated with the imaging experiments.

3.3 Orbiter Spacecraft

This subsection examines the characteristics of those spacecraft subsystems required to support the selected science payloads. That is, using the previously defined science payloads as a basis, estimates will be provided of the class of spacecraft implied by each of the science payloads. The spacecraft class is determined by considering each of the major subsystems (communications, data handling, power, attitude control, etc.) essential to the proper functioning of the science payload. This will ultimately permit determination of the class of launch vehicle implied by each science payload.

Throughout this section it will be assumed that the orbiting spacecraft configuration can be defined independently of the mode of interplanetary transfer (direct ballistic, Venus swingby, and solar electric low-thrust) and the Mercury arrival conditions. This is not a rigorously correct procedure, but it is a useful and logical approximation for this type of preliminary study. In particular, the propulsion system employed for orbit capture is not considered in this section. Thus the spacecraft concepts which emerge here are only determined by the nature of the selected science payloads. The effects of variable orbits (discussed later in Section 4) have also been removed by considering only one altitude, 500 km.

Unless otherwise stated, the semi-empirical relationships used in this section to estimate spacecraft subsystem characteristics are due to Kennet and Spear (1969) or to Edsinger (1971). Table 6 summarizes the mass estimates of the different spacecraft subsystems and the total spacecraft mass. A five percent contingency allowance is included in the total mass estimate.

3.3.1 Communications and Antenna

The communications subsystem consists of a radio assembly, a telemetry assembly, and two S-band TWT Amplifiers. The data storage subsystem and the antenna subsystem are considered separately, although the antenna subsystem is closely related to the communications subsystem. The size of the communications subsystem is directly related to the amplifier rated power, which in turn is related to the effective radiated power (ERP) and the antenna gain. The effective radiated power is a function of mission characteristics, such as communications range and data transmission rate. Assuming use of the 210-foot Goldstone antenna and the employment of coded data, the effective radiated power is related to the data transmission or bit rate according to Stein (1967) as

$$\text{ERP (db)} = \text{H (db)} + 6$$

where H is the bit rate in db and a communications range of 1.47 AU has been assumed. This range corresponds to the maximum distance between Mercury and the Earth.

The regional scale vidicon camera images a scene area of 600 x 600 km and 207 frames are required for complete planetary coverage. It will be shown in Section 4 that 176 days in

TABLE 6

ORBITER SPACECRAFT SUBSYSTEMS

(MASS INVENTORY)

SUBSYSTEM TYPE	SUBSYSTEM MASS (KG) BASELINE PLANETOLOGY SPACECRAFT	MINIMUM PLANETOLOGY SPACECRAFT	PARTICLES AND FIELDS SPACECRAFT
SCIENCE INSTRUMENTS *	67	27	22
SCAN PLATFORM	18	9	--
COMMUNICATIONS	32	17	13
ANTENNA	15	15	8
DATA STORAGE	14	7	1
CC & S	16	12	10
ATTITUDE CONTROL	50	45	40
SOLAR PANELS	16	8	5
BATTERY	34	16	13
POWER CONDITIONING	22	11	8
CABLING	23	13	10
THERMAL CONTROL	13	7	6
STRUCTURE	96	67	53
SUBTOTAL	416	254	189
CONTINGENCY ALLOTMENT	21	13	9
TOTAL SPACECRAFT	437 KG	267 KG	198 KG

*BASED ON 500 KM PERIAPSE ALTITUDE

orbit are required to achieve complete visual coverage. If the Goldstone antenna can be used for data reception two hours each day, then the average data transmission rate is estimated as 1.3 kilobits per second. Assuming that data equivalent to three complete coverages are required (for example, at high, medium, and low solar elevation angles), the average data transmission rate implied by the minimum planetology payload is about four kilobits per second. Similarly, the average data transmission rate for the baseline planetology payload may be estimated as approximately 16 kilobits per second. This estimate is based on achieving ten percent planetary coverage with the local scale vidicon camera operating over a 176 day period. For the particles and fields payload, the average data transmission rate is estimated to be 200 bits per second.

At a frequency of 2300 MHz, the antenna gain in db may be represented by (Stein, 1967)

$$G \text{ (db)} = 24.3 + 8.67 \ln D$$

where D is the diameter in meters of the transmitting antenna, and thus the transmitted power can be expressed as

$$P_T \text{ (db)} = H \text{ (db)} - 8.67 \ln D - 18.3$$

The antenna mass may be estimated by

$$M_A \text{ (kg)} = 2.5 + 2.9D + 0.23D^2 + 0.12D^3$$

where D is the antenna diameter in meters. This scaling relationship is based on empirical data and presumes that antennas larger than about three meters diameter will employ some sort of fold-out deployment mechanism. The mass estimates should be fairly accurate for antenna diameters less than about seven meters.

The mass of each TWT amplifier is empirically related to the transmitted power according to

$$M_{TWT}\ (kg) = 2 + 0.075\ P_T\ (watts) \quad .$$

For redundancy, two identical amplifiers are used aboard each orbiter.

The radio assembly mass is approximated by

$$M_R\ (kg) = 3.6 + 0.26\ P_T\ (watts) \quad ,$$

while the telemetry assembly mass is roughly

$$M_T\ (kg) = 5 + 0.22\ P_T\ (watts) \quad .$$

Thus when using two identical TWT amplifiers, the mass of the communications subsystem is taken as

$$M_c\ (kg) = 12.6 + 0.63\ P_T\ (watts).$$

The equations given above have been used to optimize the antenna diameter such that the mass associated with a specific value for the data transmission rate is minimized. The results are shown in Figure 6. The mass which has been minimized includes the communications subsystem mass M_c, the antenna mass M_A, and that portion of the solar panel and power conditioning mass which is related to the power required by the communications subsystem. The total mass of the solar panel and power conditioning subsystems is estimated as described in Section 3.3.5 below. The bottom half of Figure 6 shows the optimum antenna diameter as a function of data transmission rate, while the upper half shows the sum of the communications subsystem mass, the antenna mass, and the associated solar panel and power conditioning subsystem masses also as a function of data transmission rate. At data transmission rates higher than

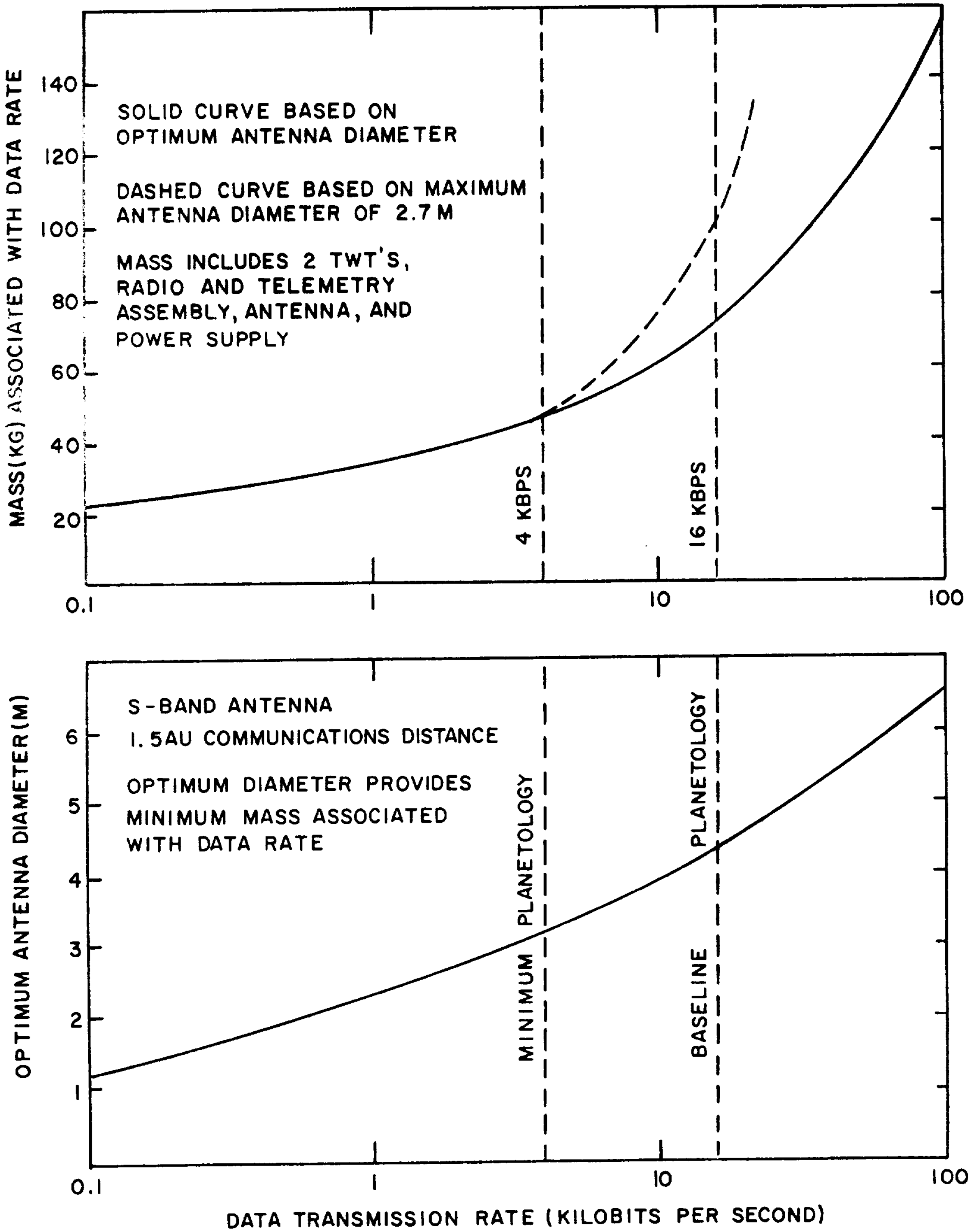

FIGURE 6. OPTIMIZATION OF COMMUNICATIONS AND ANTENNA SUBSYSTEMS

four kilobits per second, the optimum antenna diameter exceeds nine feet (2.74 meters), the maximum diameter rigid antenna which can be accommodated by a Titan or Atlas shroud. The dashed line in the upper half of Figure 6 shows the effect of this constraint.

The communications subsystem characteristics implied by the three candidate payloads are summarized in Table 7. The TWT amplifier input power P_{DC} is related to the transmitted power by

$$P_{DC} = 5.54\ P_T^{0.853} \quad ,$$

while the power requirement of the radio and telemetry components of the communications subsystem have been taken as 0.3 watts per kilogram. Thus the total power requirement of the communications subsystem is

$$P_c = 2.6 + 0.14P_T + 5.54\ P_T^{0.853} \quad .$$

3.3.2 Data Storage

Currently available tape recorders have a storage capacity of about 6×10^8 bits and a recording rate of 2×10^5 bits per second. Each recorder has a mass of seven kg and consumes about ten watts of power. Thus a single recorder can store the equivalent of 75 pictures or frames from the 1½-inch vidicon. For the baseline planetology orbiter two recorders are used, while the minimum planetology orbiter uses only one. For the particles and fields orbiter a core memory of 10^5 bits capacity and one kg mass is assumed.

TABLE 7

COMMUNICATIONS SUBSYSTEM CHARACTERISTICS

	BASELINE PLANETOLOGY	MINIMUM PLANETOLOGY	PARTICLES AND FIELDS
DATA TRANSMISSION RATE (kbps)	16	4	0.2
ANTENNA DIAMETER (m)	2.74	2.74	1.5
TWT INPUT POWER (watts)	105	31	6
TRANSMITTED POWER (watts)	32	8	1.3
COMMUNICATIONS SUBSYSTEM POWER (watts)	112	36	10
ANTENNA MASS (kg)	15	15	8
COMMUNICATIONS SUBSYSTEM MASS (kg)	32	17	13

3.3.3 Command, Control, and Sequencer

The mass of the command, control, and sequencer (CC&S) subsystem is generally assumed to be directly related to the total spacecraft mass exclusive of the propulsion system and propellant mass (hereafter called the total dry mass). For dry masses less than 1500 kg, the scaling relationship used by Kennet and Spear (1969) is approximated by

$$M_{CCS}\ (\text{kg}) = 5 + 30M^* - 11(M^*)^2$$

where M_{CCS} is the command, control, and sequencer subsystem mass and M^* is the spacecraft dry mass in thousands of kilograms. Of course, M^* is not known a priori, hence the estimating procedures used here are iterative. Experience has suggested that a useful first approximation is that the spacecraft dry mass is roughly seven times the science payload mass. Thus first estimates of the computer and sequencer subsystem mass are 17, 10, and 10 kg for the baseline planetology, minimum planetology, and particles and fields spacecraft, respectively. Later iterations result in the values listed in Table 6. The power requirement for the CC&S subsystem may be represented by

$$P_{CCS}\ (\text{watts}) = 20 + 34\ (M^*)^{\frac{1}{2}}$$

where again M^* is the spacecraft dry mass in thousands of kilograms.

3.3.4 Attitude Control

The attitude control subsystem consists of the guidance and control electronics, celestial and inertial sensors, thrusters, tanks, valves, actuators, and plumbing. Kennet and Spear suggest that for a three-axis stabilized spacecraft, gimbaled engine thrust vector control, a 700-day mission, an N_2 cold gas system, and six spacecraft maneuvers, the guidance and control subsystem has a mass of about 40 kg for spacecraft dry masses in the range 200-500 kg. Thus the mass of the attitude control subsystem for the particles and field orbiter is estimated as 40 kg. For the larger spacecraft carrying imaging experiments, additional mass is allowed for orbit trim and additional pointing maneuvers. The estimates for these spacecraft are 45 kg for the minimum planetology mission and 50 kg for the baseline planetology mission. The attitude control subsystem power requirement, largely due to sensors and electronics, is assumed to be twenty watts for all three spacecraft.

3.3.5 Power

The components of the power subsystem are sized considering the total power requirements of the spacecraft. Estimation of the power requirements has been discussed above for each of the spacecraft subsystems; the results are summarized in Table 8. The power delivered by the solar cells must be larger than the power requirement shown in the table in order to recharge the batteries which power the spacecraft during solar occultation. Thus if the orbital period is T and the period of occultation is T_D, the solar cells must provide a power output which is $1 + 2\ T_D/(T-T_D)$ times the total spacecraft power shown in Table 8. For power estimation purposes, the orbital period has been taken as two hours, the occultation period as one hour. Assuming a solar panel specific output of 59 watts/kg at Mercury (corresponding to 20 watts/lb at one AU), the mass of the solar panel array may be estimated with the results previously shown in Table 6.

TABLE 8

ORBITER SPACECRAFT SUBSYSTEMS

(POWER INVENTORY)

	SUBSYSTEM POWER REQUIREMENT (WATTS)		
	BASELINE PLANETOLOGY SPACECRAFT	MINIMUM PLANETOLOGY SPACECRAFT	PARTICLES AND FIELDS SPACECRAFT
SCIENCE INSTRUMENTS	114	46	30
COMMUNICATIONS	112	36	10
DATA STORAGE	20	10	2
CC & S	42	37	35
ATTITUDE CONTROL	20	20	20
TOTAL SPACECRAFT POWER	308 WATTS	149 WATTS	97 WATTS

The battery subsystem mass may be estimated on the basis of the power requirement during solar occultation and the length of the occultation period. For an orbiter mission, which is likely to involve many charge-discharge cycles, nickel-cadmium batteries are preferred. The specific energy of nickel-cadmium batteries is about 26.4 watt-hours per kilogram, and assuming a maximum discharge depth of 0.5 and an overdesign factor of 1.75, the battery subsystem mass M_B is estimated by

$$M_B(\text{kg}) = 0.13 \times (\text{watt-hrs required})$$

with the results previously shown in Table 6. It should be noted that the television cameras are unlikely to be operated during periods of solar occultation so that the science instrument power requirements are reduced from the values in Table 8.

The mass of the power conditioning subsystem M_{PC} has been estimated by a scaling law due to Edsinger, i.e.,

$$M_{PC}\ (\text{kg}) = 0.045\ (P_B\ P_{SP})^{\frac{1}{2}}$$

where P_B is the maximum power demand on the battery subsystem and P_{SP} is the solar panel design power.

3.3.6 Other Subsystems

The mass of the scan platform has been estimated as 18 kg for the baseline planetology spacecraft and nine kg for the minimum planetology spacecraft. The particles and fields spacecraft is assumed to have no scan platform or one of negligible mass. The masses of the cabling and thermal control susbystems are estimated as percentages of the spacecraft equipment which is defined as the sum of the science, scan platform, communications, data storage, CC & S,attitude control, battery, and power conditioning subsystem masses. It does not include the antenna or solar panel subsystems. In particular, the mass allocated for cabling is taken as 8.9 percent of the spacecraft equipment mass, while the mass of the thermal control subsystem is taken as 5.2 percent of the spacecraft equipment mass. These percentages are simply averages of empirical data relevant to planetary spacecraft. It might be argued that this procedure underestimates the thermal control subsystem mass for a Mercury mission, but a more detailed analysis is beyond the scope of this study. Finally, the structure subsystem mass M_S is approximately

$$M_S(\mathrm{kg}) = 320\ M^* - 216\ (M^*)^2 \quad .$$

SECTION 4

ORBIT SELECTION

PRECEDING PAGE BLANK NOT FILMED

4. ORBIT SELECTION

Mercury rotates slowly bringing new areas of the planet into view from a fixed direction in space at a slow rate. Even the most simple analysis in which the orbital plane is fixed in space and the planet is regarded as rotating underneath the orbit would imply, without regard to lighting conditions, that 59 days would be required to obtain complete coverage of Mercury. A more realistic and useful analysis involves consideration of the fractional area of Mercury illuminated by the Sun during a given time period. This places some upper bounds on the amount of coverage actually achievable in that time period. Figure 7 shows the percent of Mercury's surface which is illuminated at solar elevation angles equal to or higher than some minimum value over a 176-day period (one Mercury day). Very nearly all of Mercury's surface is illuminated at elevation angles suitable for shadow measurements at some time or other during this period, while 75 percent of the surface is illuminated under conditions desirable for color imagery, and only 50 percent under conditions desirable for stereoscopic coverage. That is, no matter what orbit is selected (or how many spacecraft are used), good stereo imagery (requiring solar elevation angles higher than 60 degrees) can be obtained for only half the planet. In order to achieve the potential area coverage it is necessary to remain in orbit at least one planetary day, which for Mercury is 176 Earth days. These conclusions are based on the assumption that the rotation axis of Mercury is normal to the orbital plane. If this were not the case, more of the surface would be properly illuminated.

An additional factor which must be considered in proper orbit selection for imaging experiments is the interplay between the orbit period, planetary rotation rate, and sensor

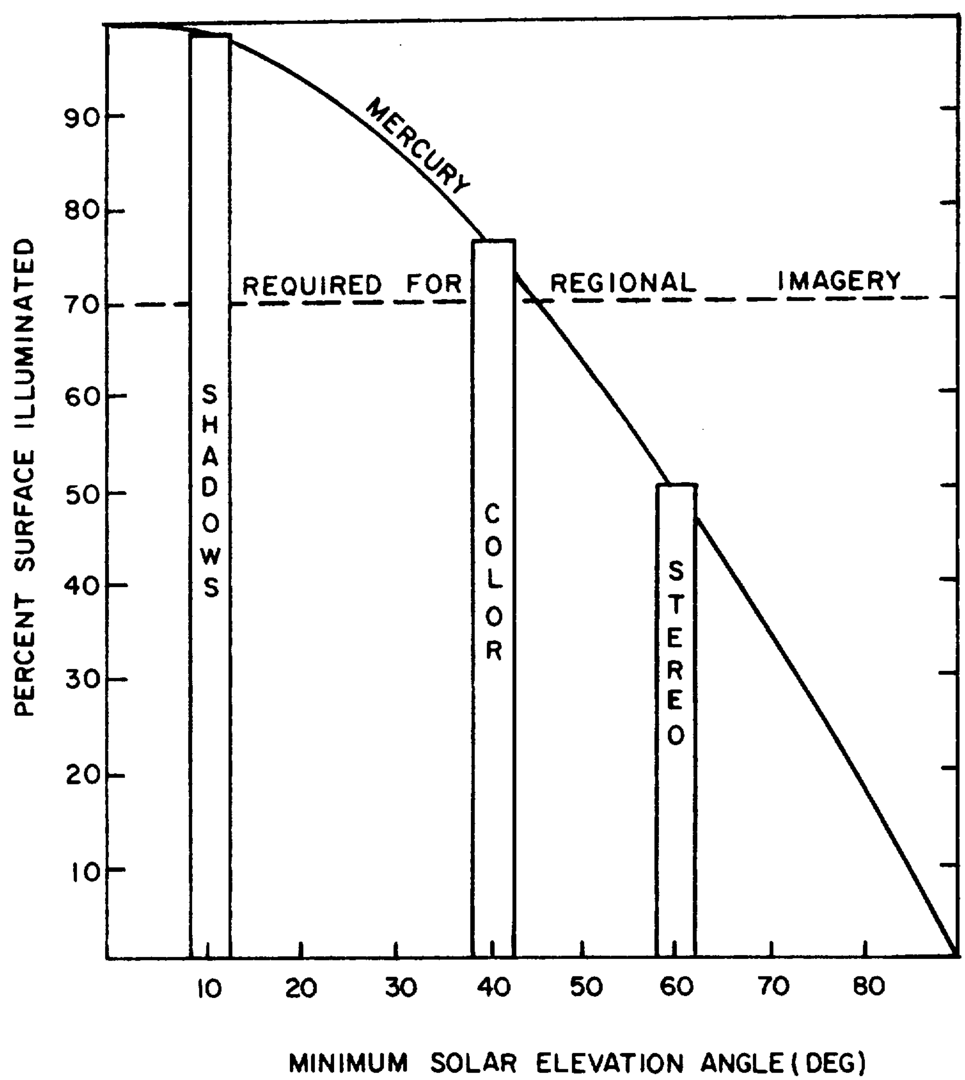

FIGURE 7. COVERAGE AND SOLAR ILLUMINATION

field of view. If the orbit period is very long and the sensor field of view very small, the planetary surface may rotate far enough underneath the orbit so that the imagery acquired at the equator on the nth orbital pass will not overlap with the imagery acquired on the n + 1st orbital pass. In other words, gaps may appear in the coverage. These gaps must be filled in at some later time if complete coverage is required, or if coverage is required of a geographical area which is larger than the instantaneous field of view. Figure 8 shows the coupling between the equatorial lapse rate, orbital period, and mean altitude. The equatorial lapse rate is the distance measured along the equator between two successive orbital ground tracks; the mean altitude is the average of the periapse altitude and apoapse altitude, also equal to the orbit semi-major axis minus Mercury's radius. For example, the dashed lines show that an orbit period of 1.9 hours corresponds to an orbit of 500 km mean altitude with an orbit lapse rate of 20.5 km at the equator. If a single image covers a 600 km equatorial swath, commensurate with regional scale imagery, and 20 percent side overlap is desired, a net ground displacement of 480 km between images is desired. Since the lapse rate is about 20 km/orbit, pictures need only be taken every 24th orbit.

Yet another consideration important in orbit selection is that of orbit lifetime. Because of the current lack of knowledge of Mercury's oblateness and atmospheric properties, it is impossible to do much more than speculate on orbit lifetimes at Mercury. However, because of Mercury's proximity to the Sun, it might be expected that solar perturbations on the orbit would be more significant than at the other planets. In general, the effect of solar perturbations will increase with orbit eccentricity, so that in addition to facilitating imaging experiments, selection of a circular orbit would tend to reduce the effect of

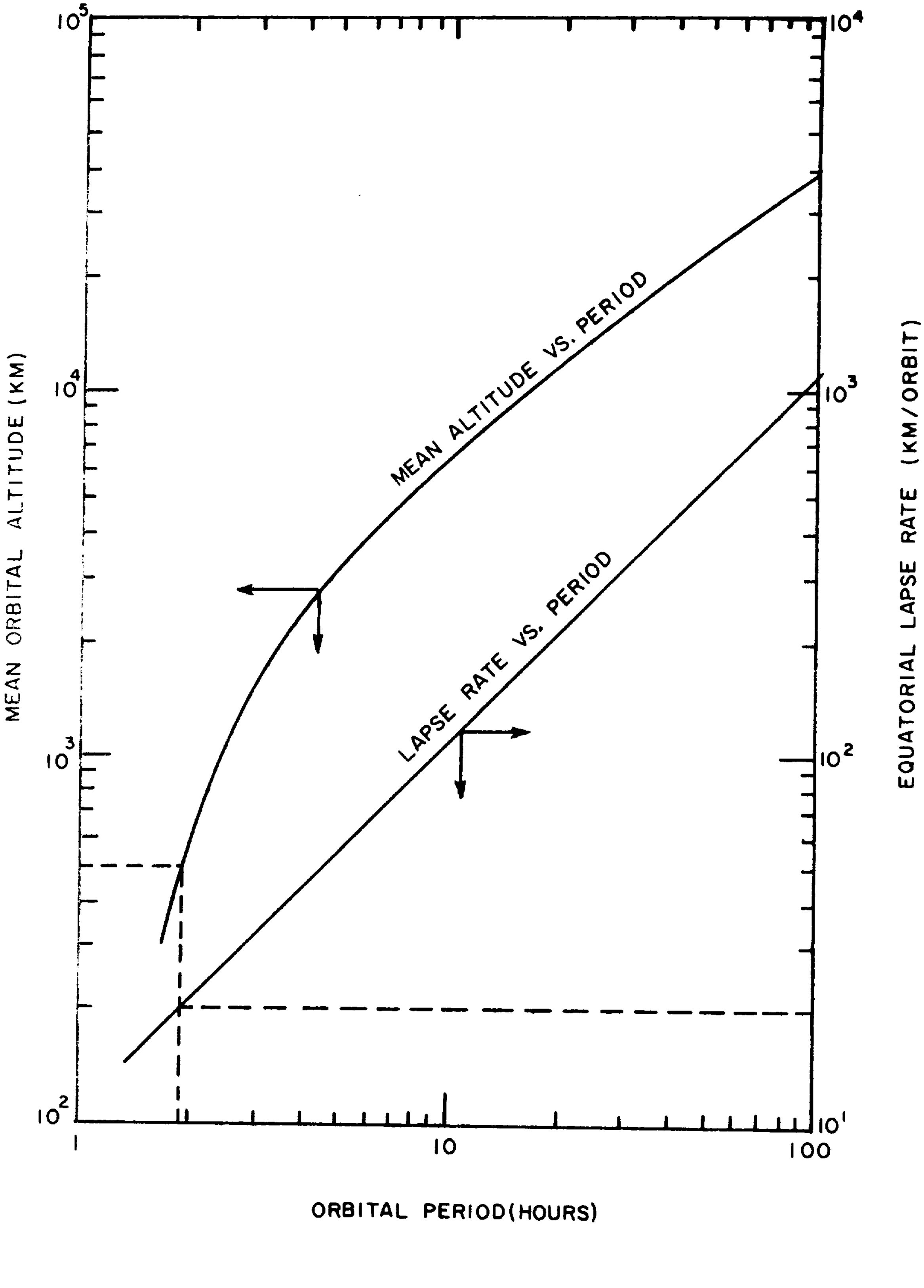

FIGURE 8. ORBITAL LAPSE RATE

solar perturbations. Uphoff (no date) has estimated effects of solar perturbations, oblateness, and atmospheric drag on Mercury-orbiting satellites. It would appear from Uphoff's calculations that orbital altitudes should be maintained above 400-600 km to avoid atmospheric drag. Indeed, Uphoff's data implies only about a one year lifetime for a 500 km altitude circular orbit (based on a C_D A/M of 0.03 m^2/kg). However, these results were based on Vaughan's maximum density model atmosphere (Vaughan, 1969) which corresponds to a 5 millibar surface pressure, and are therefore in the nature of a conservative estimate.

Section 3.2 has identified three science payloads which represent different levels of scientific capability: a baseline planetology payload (67 kg), a minimum planetology payload (27 kg), and a particles and fields payload (22 kg). As indicated in Section 3.1, the payload mass has been estimated based on an orbital altitude of 500 km. If the altitude is increased above 500 km, the payload mass must increase to achieve the same measurement specifications (most notably the ground resolution) from higher altitude. The increase in science payload mass with altitude is shown in Figure 9. The instrument weights most sensitive to an increase in altitude are associated with the near infrared spectrometer (baseline and minimum planetology), the radar altimeter (baseline planetology), and the ten-channel spectrophotometer (particles and fields payload). This increase in payload mass with altitude is reflected in an increase in the orbiting spacecraft mass with altitude, which is also shown in Figure 9. The estimation of orbiting spacecraft mass at 500 km altitude was discussed in Section 3.3. The spacecraft subsystem weights which increase as a result of increasing the science payload mass include those associated with the scan platform and cabling, thermal control, and structure subsystems. Of course, the fractional increase in

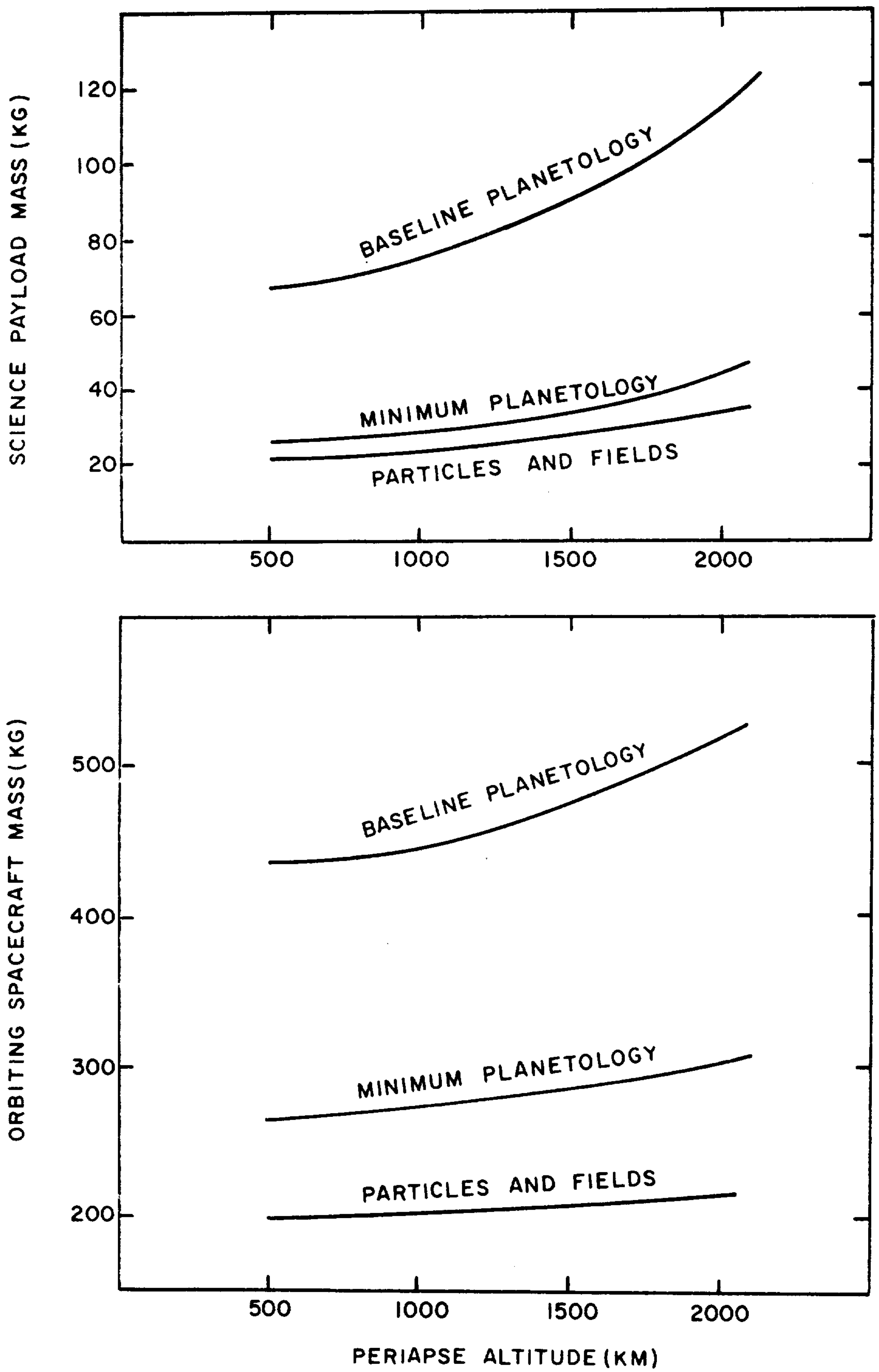

FIGURE 9. VARIATION OF SCIENCE PAYLOAD AND SPACECRAFT MASS WITH ALTITUDE.

spacecraft mass with altitude is not as large as the fractional increase in the science payload mass.

Another major influence on orbit selection is the size of the orbit capture retro-propulsion stage, which depends upon the orbit itself, the net injected spacecraft mass, and the approach conditions at Mercury. As discussed further in Section 5, approach conditions are characterized by approach velocities (in terms of the hyperbolic excess velocity at Mercury, VHP) of 8 to 11 km/sec in the case of ballistic transfers to Mercury and by approach velocities of zero to 4 km/sec in the case of solar electric low-thrust transfers. Figure 10 shows the variation of the required spacecraft mass approaching the planet as a function of orbit altitude for the baseline planetology payload. For the high approach velocities characteristic of ballistic transfer a three-stage chemical retro system of 300 second specific impulse has been assumed. A circular orbit is desired for both planetology missions to facilitate imaging experiments from all positions along the orbit. These results show that for ballistic missions to Mercury and circular orbits, the approach mass is minimized by choosing a 500 km altitude orbit. Although the figure pertains to the baseline planetology payload, similar results have been obtained for the minimum planetology payload. The increase in approach mass with increasing orbit altitude is a consequence of both an increase in the required injected mass with altitude, as shown in Figure 9, and an increase in the retro maneuver energy requirement (ΔV). A two-stage chemical retro system would result in a less complex capture maneuver, but the required approach mass would increase by 13-16 percent even for the minimum ballistic approach velocity of eight km/sec. The penalty would be more severe at higher approach velocities.

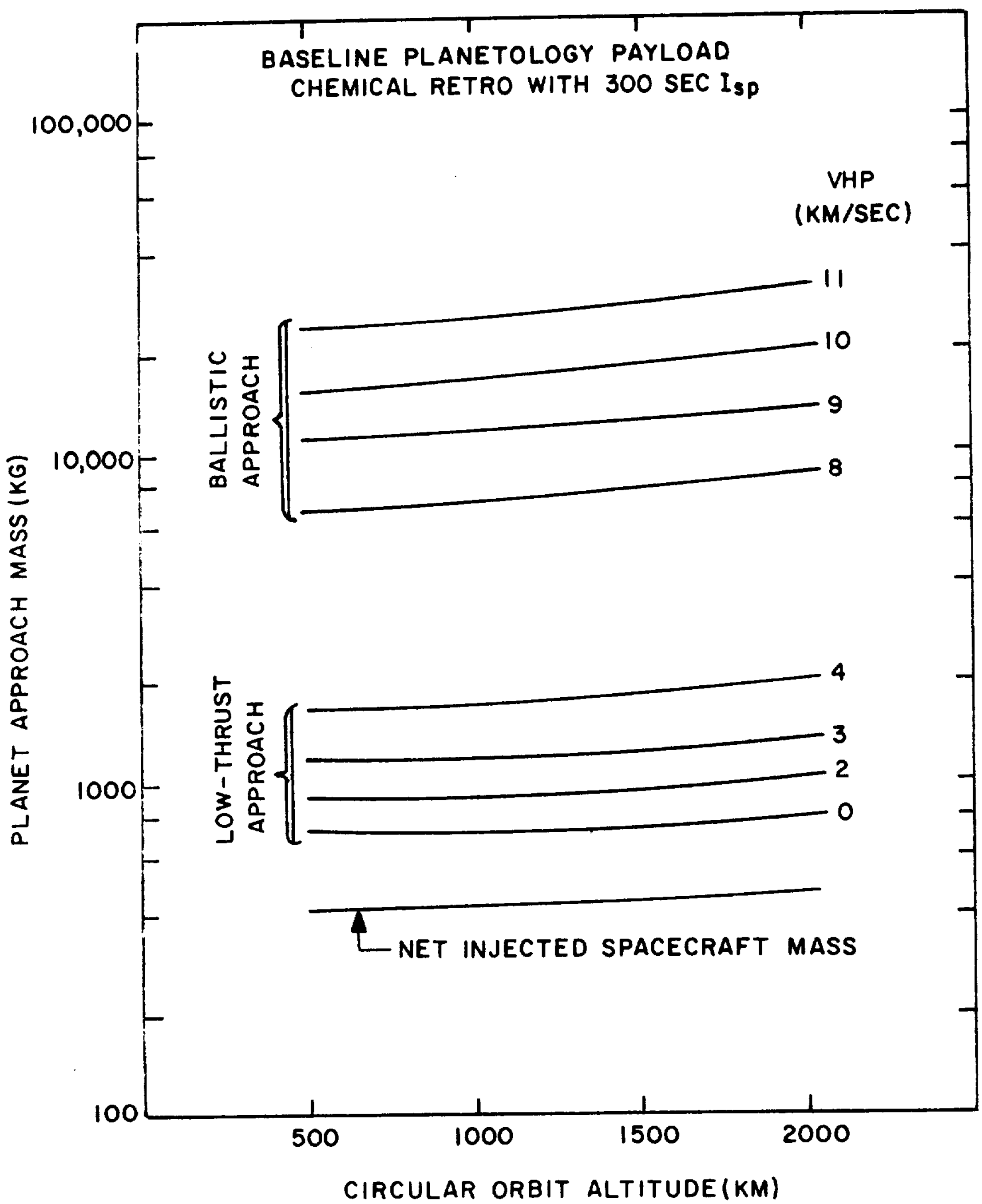

FIGURE 10. SPACECRAFT MASS AT MERCURY ARRIVAL FOR BASELINE PLANETOLOGY PAYLOAD

For the low-thrust mission mode a one-stage chemical retro system has been assumed, again with the results shown in Figure 10. For approach velocities of less than three km/sec, the approach mass is actually minimized at orbit altitudes of about 1000 km, but the approach mass is very nearly independent of orbit altitude from 500 to 1500 km. Even for the rendezvous case (VHP of zero km/sec), choice of the 1000 km orbit altitude reduces the approach mass by only 12 kg from the 500 km orbit case. Similar results are obtained in the case of the minimum planetology payload. Thus a useful generalization appears to be that for orbiting missions at Mercury involving extensive imagery of the surface, the total spacecraft mass is minimized by selecting a 500 km altitude orbit.

This conclusion, however, is only valid for low-thrust approaches if the required payload mass in orbit increases with altitude in much the same manner as shown in Figure 9. For low approach velocities (three km/sec or less), the orbit capture ΔV requirement for circular orbits actually decreases with increasing orbit altitude in the range 500-2000 km, and hence the retro system mass would decrease with increasing orbit altitude if the injected mass were constant. However, for both the minimum and baseline planetology orbiting spacecraft the required orbiting mass does increase with orbit altitude and the net effect is as shown in Figure 10. It should also be noted that the low-thrust mode analyzed here implies that the solar electric low-thrust propulsion stage is jettisoned prior to the orbit capture maneuver. A typical comparison of impulsive and low-thrust capture maneuvers is given in Section 6.2.1. In general, when low-altitude circular orbits are desired at Mercury, the 50-200 kg improvement in orbiting payload provided by a low-thrust spiral capture maneuver does not appear to justify retention of the solar electric low-thrust stage.

In the case of the particles and fields payload, an eccentric orbit is desired in order to provide data from different points within Mercury's magnetosphere and on Mercury's interaction with the solar wind. In addition, because of the ten-channel spectrophotometer (or alternative low data-rate planetology instruments), the science payload mass is reduced by selection of a low periapse altitude. The variation of the science payload mass and net orbiting spacecraft mass with periapse altitude has been shown in Figure 9. It may be noted that although the particles and fields science payload mass is similar to the minimum planetology science payload mass, the net orbiting spacecraft masses in the two cases differ by 70 kg because of the relatively low data transmission rate utilized by the particles and fields spacecraft. Figure 11 shows the required spacecraft approach mass as a function of orbit periapse altitude and orbit eccentricity for the net injected orbiting spacecraft mass associated with the particles and fields payload. As with the planetology payloads, the approach mass is minimized by selection of a 500 km periapse altitude. It is also seen that the approach mass decreases with increasing orbit eccentricity as might be expected. Uphoff (no date) has estimated the effects of solar perturbations upon the lifetime of satellites in eccentric orbits about Mercury. His data suggest that for a 500 km periapse altitude an orbit of eccentricity 0.8 or larger may have a "very short" lifetime. If the periapse altitude were raised, Uphoff's results indicate that the eccentricity could be increased.

As noted earlier, Good (1967) has suggested that Mercury's magnetic moment might be as large as one-tenth the Earth's moment. This implies that Mercury's magnetospheric radius is about three Mercury radii or about 7500 km. In order to fully explore the magnetosphere using an orbit of 500 km periapse altitude, the orbit eccentricity must be at least 0.4.

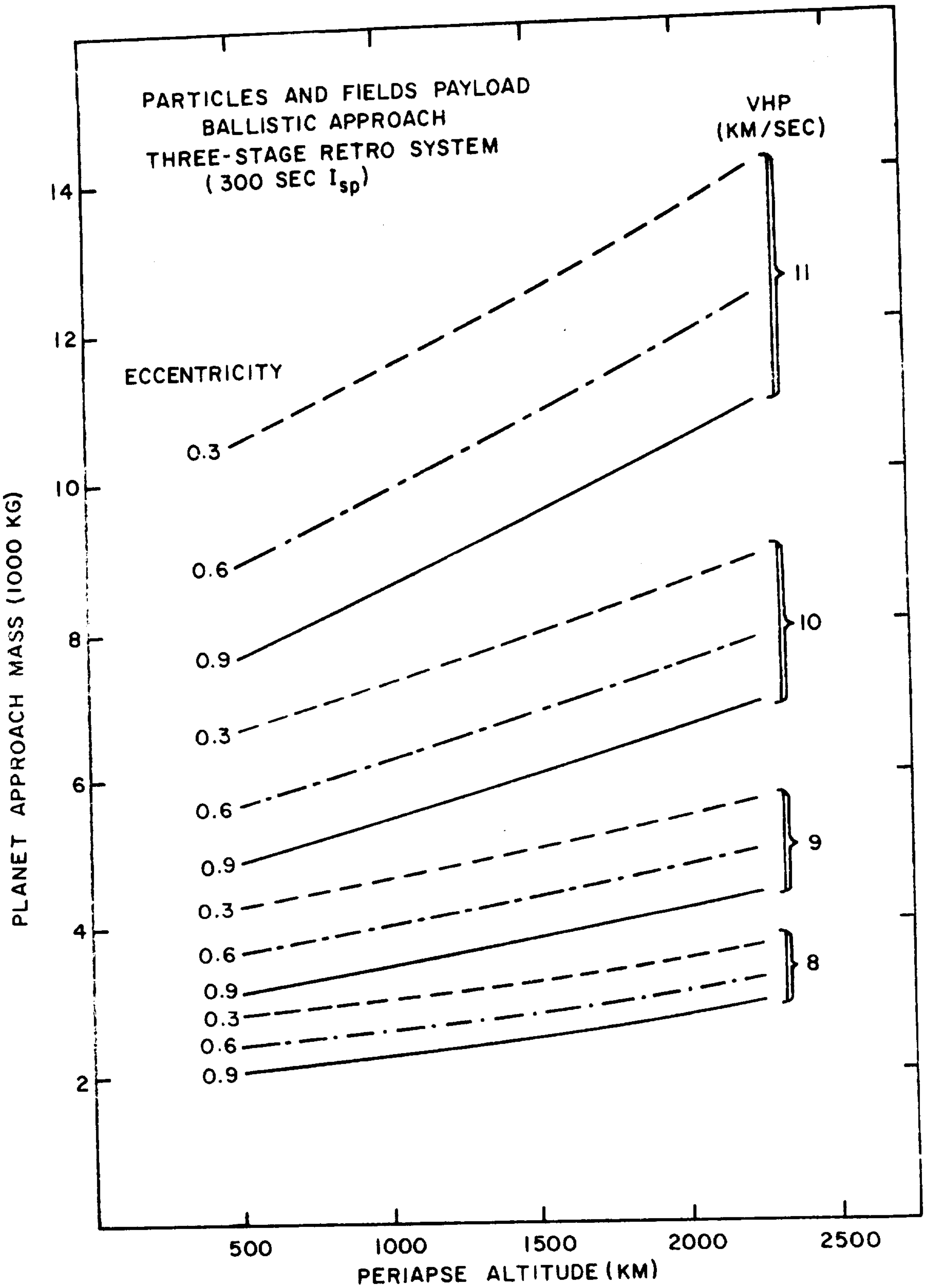

FIGURE 11. SPACECRAFT ARRIVAL MASS AT MERCURY FOR PARTICLES AND FIELDS PAYLOAD (BALLISTIC MODE)

Thus an orbit of eccentricity 0.6 and periapse altitude 500 km would appear to be particularly appropriate for the particles and fields payload. Figure 12, showing the particles and fields spacecraft approach mass for low-thrust arrivals, indicates that this conclusion is equally valid for the low-thrust mission mode.

As yet no comments have been made about orbit inclination. For the imaging payloads, a polar orbit would provide maximum planetary coverage. In fact, a near-polar orbit would also provide adequate planetary coverage and would facilitate the determination of the gravitational field moment by precision tracking of the spacecraft. For this study, a polar orbit has been selected. For the particles and fields spacecraft, where not as much emphasis is placed on achieving complete planetary coverage, a mid-latitude inclination (say 50°) would appear to be appropriate and would simplify gravitational moment determination.

To summarize, the following three classes of orbiting spacecraft have been defined:

a. A "particles and fields" spacecraft of nearly 200 kg, similar to an Explorer class spacecraft, carrying 22 kg of particles and fields instrumentation including a few long data-rate planetology instruments in a moderately eccentric orbit of medium inclination.

b. A "minimum planetology" spacecraft of roughly 250 kg, similar to an outer planet Pioneer class spacecraft, carrying a minimal 27 kg of

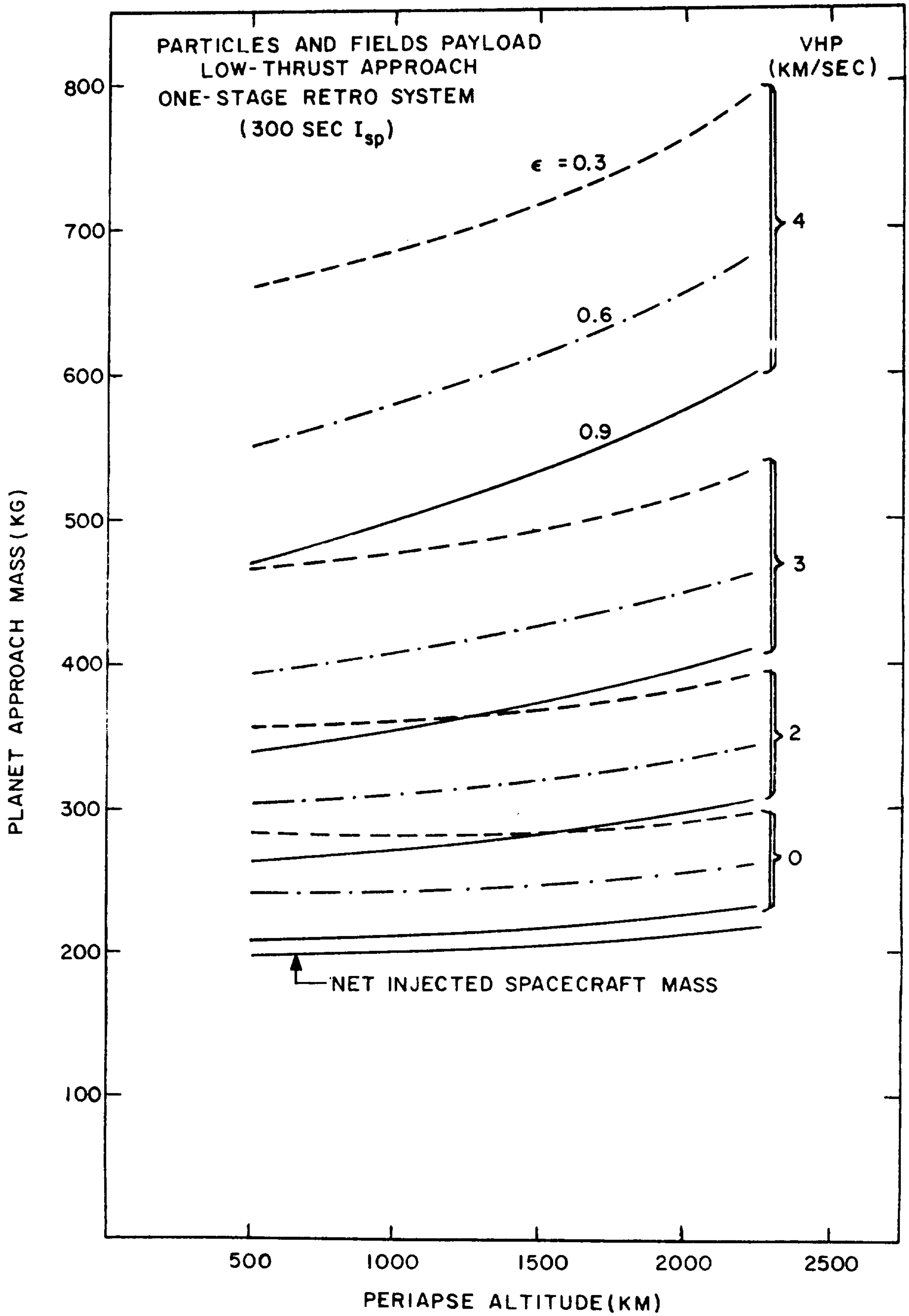

FIGURE 12. SPACECRAFT ARRIVAL MASS AT MERCURY FOR PARTICLES AND FIELDS PAYLOAD (LOW-THRUST MODE)

science instruments, which is dominated by the television camera and infrared spectrometer. The emphasis is upon regional scale surface examination conducted from a low-altitude circular polar orbit.

c. A "baseline planetology" spacecraft of somewhat more than 400 kg, similar to a Mariner class spacecraft, carrying nearly 70 kg of science instruments. Here the emphasis is upon regional and local scale imagery of Mercury's surface, with remote sensing investigations in all regions of the electromagnetic spectrum from gamma-ray wavelengths to the microwave. A low-altitude circular polar orbit is used as with the smaller planetology spacecraft.

If additional launch capability is available, even more complex and massive spacecraft could be considered. Perhaps the most efficient way to utilize increased delivery capability, however, would be to combine the basic spacecraft classes just described. One useful combination would be the baseline planetology spacecraft and the particles and fields spacecraft. Such a combination would provide surface-oriented instruments on an orbit suitable for extensive planet coverage and particles and fields instruments on an orbit facilitating exploration of Mercury's possible magnetosphere. Useful data would be provided for study of all those measurables identified in Section 2.2 as appropriate for study from an orbiting spacecraft. Another useful combination consists of both the baseline and minimum planetology spacecraft. The 1973 Venus/Mercury mission might indicate that particles and fields experiments at Mercury are not likely to be rewarding. Additional capability should then be directed towards planetology experiments. By employing separate spacecraft, one spacecraft could be dedicated to the achievement of obtaining complete coverage of Mercury's surface while the other could be placed in a near-equatorial orbit for repetitive coverage of the hot and warm poles and of other interesting areas in the equatorial or mid-latitudes. Mid-latitude coverage would be enhanced by raising the orbit altitude above 500 km.

Thus two additional spacecraft concepts may be defined:

d. A "broad first look" dual satellite concept consisting of the baseline planetology orbiter and the particles and fields orbiter.

e. A "maximum planetology" dual satellite concept consiting of the baseline planetology satellite in a low-altitude circular polar orbit and the minimum planetology satellite in a circular equatorial orbit of somewhat higher altitude.

These five orbiting mission concepts are summarized in Figure 13.

MISSON	SPACECRAFT MODEL(S)		SCIENCE	ORBITER	PERIAPSE ALTITUDE	ϵ	INCLINATION	ORBIT PERIOD
A	PARTICLES AND FIELDS		22kg	198kg	500km	0.6	50°	7.4^h
B	MINIMUM PLANETOLOGY		27	267	500	0	90	1.9
C	BASELINE PLANETOLOGY		67	437	500	0	90	1.9
D	BROAD FIRST LOOK	(A)	22	198	500	0.6	50	7.4
		(C)	67	437	500	0	90	1.9
E	MAXIMUM PLANETOLOGY	(B)	44	303	2000	0	0	3.4
		(C)	67	437	500	0	90	1.9

FIGURE 13. CANDIDATE ORBITER MISSION SET

SECTION 5

INTERPLANETARY TRANSFER

5. INTERPLANETARY TRANSFER

The previous sections of this report have discussed the reasons for performing a Mercury orbiter mission and have defined a spectrum of mission concepts that seem most appropriate. This section describes the pertinent characteristics of Earth-Mercury interplanetary trajectories suitable for delivering an orbital payload to Mercury. Direct ballistic, Venus swingby, and solar electric low-thrust mission modes are discussed sequentially.

5.1 Direct Ballistic Trajectories

Manning (1966, 1967a, 1967b) has performed a comprehensive survey of both direct ballistic and Venus swingby opportunities in the 1980-1999 time period. The VHL (hyperbolic excess velocity at launch) requirements for direct ballistic missions repeat on a 13-year cycle. Opportunities for orbiter missions may be discovered by searching for minimum values of the sum of VHL and VHP (hyperbolic excess velocity at Mercury). Three launch opportunities occur in each calendar year, except for 1984, 1991, and 1997 which have four launch opportunities. Of the three (or four) opportunities in each year, one opportunity will have a low value for VHL, another opportunity a low value for VHP. These opportunities are never the same, i.e., in any year the opportunity with the lowest VHL is different from the opportunity with the lowest VHP. Except for 1982, 1989, and 1995, the yearly opportunity which has the minimum value for the sum of VHL and VHP is the same opportunity which has the minimum VHP. Consequently, the yearly minimum energy <u>orbiter</u> opportunity is different from the yearly minimum <u>flyby</u> opportunity (except in 1982, 1989, and 1995).

Direct flyby opportunities invariably involve arrival near the descending node of Mercury's orbit (Figure 1, p. 12). Conversely, direct orbiter opportunities invariably (but not in 1982, 1989, and 1995) involve arrival near the ascending node. The ascending node is close to the perihelion point where Mercury's orbital velocity is large, and thus tends to minimize the difference between the spacecraft's velocity and that of Mercury.

Figure 14 shows that the 1982 and 1989 orbiter launch opportunities, involving descending node arrivals, have appreciably higher values for VHP than the other launch opportunities in the 13-year cycle portrayed in the figure. High VHP situations should be avoided because a more energetic orbit capture maneuver will be demanded than for a low VHP mission. This effect has been indicated previously in Figures 10 and 11. Over the 13-year cycle, the minimum value for the sum of VHP and VHL is about 17.5 km/sec (actually 17.8 in 1980, 17.5 in 1986, and 17.4 in 1992) and this favorable value repeats every six or seven years. Flight times over the 13-year cycle range from 85 days (in 1981, 1987, and 1988) to 140 days (in 1983).

Launch vehicle implications will be discussed in detail in Section 6. Suffice it to say, however, that even in the vintage years of 1980, 1986, and 1992, an Intermediate-20 launch vehicle is required to place a 450-500 kg spacecraft into a low-altitude circular polar orbit at Mercury. In the poorer years, such as 1983 or 1990, a Saturn V launch vehicle would be required.

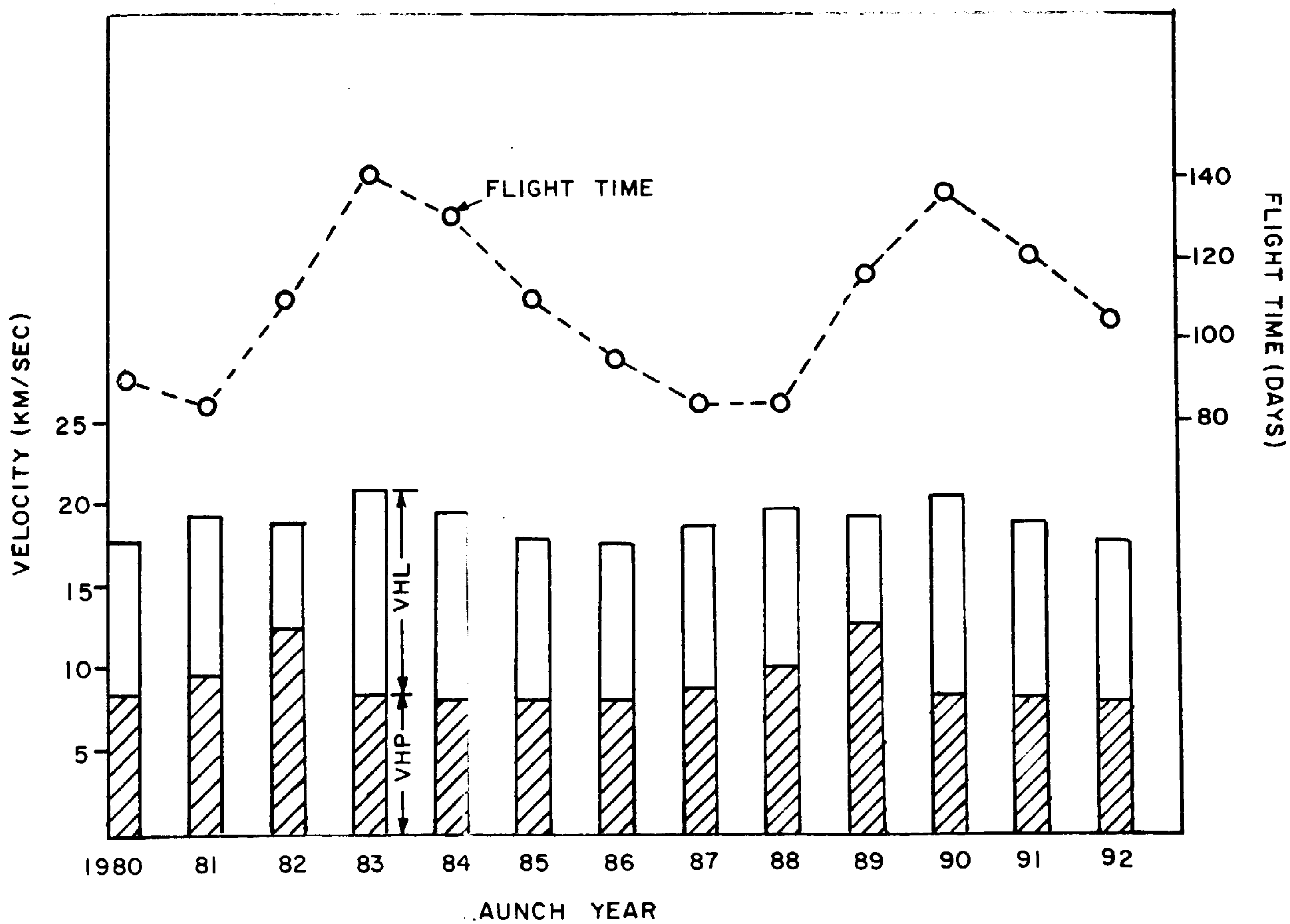

FIGURE 14. DIRECT BALLISTIC OPPORTUNITIES TO MERCURY

5.2 Venus Swingby Trajectories

5.2.1 Unpowered

Opportunities for Earth-Venus-Mercury trajectories can arise no more frequently than opportunities for Earth-Venus trajectories, which occur every 17 months. That is, Venus swingby missions to Mercury cannot be performed every calendar year at reasonable launch vehicle cost. Manning (1966, 1967a, 1967b) has searched for promising Venus swingby opportunities with the results shown in Figure 15. The chances of finding a good Venus swingby opportunity in an arbitrarily selected launch year are somewhat better than "50-50". However, the Venus swingby opportunity (if one exists) may not be better than the direct ballistic opportunity. For example, the value of (VHP + VHL) for the swingby opportunities in 1988 and in 1991 is higher than for the direct opportunity. Furthermore, feasible unpowered swingby trajectories, i.e., those involving miss distances of greater than 250 km at Venus, tend to involve arrival at Mercury aphelion with relatively high values of VHP. Of the swingby opportunities shown in the figure, only the 1982 and 1989 opportunities have a lower VHP than the minimum-energy direct opportunity in the same year. Flight times from Earth to Mercury via Venus range from 136 days (1986) to 435 days (1988). The Venus swingby opportunities do not, of course, repeat on the 13-year cycle of direct missions. There is a particularly good swingby opportunity in 1997 (290-day flight time, 13.8 km/sec for VHP + VHL), for example, which is not shown in the figure.

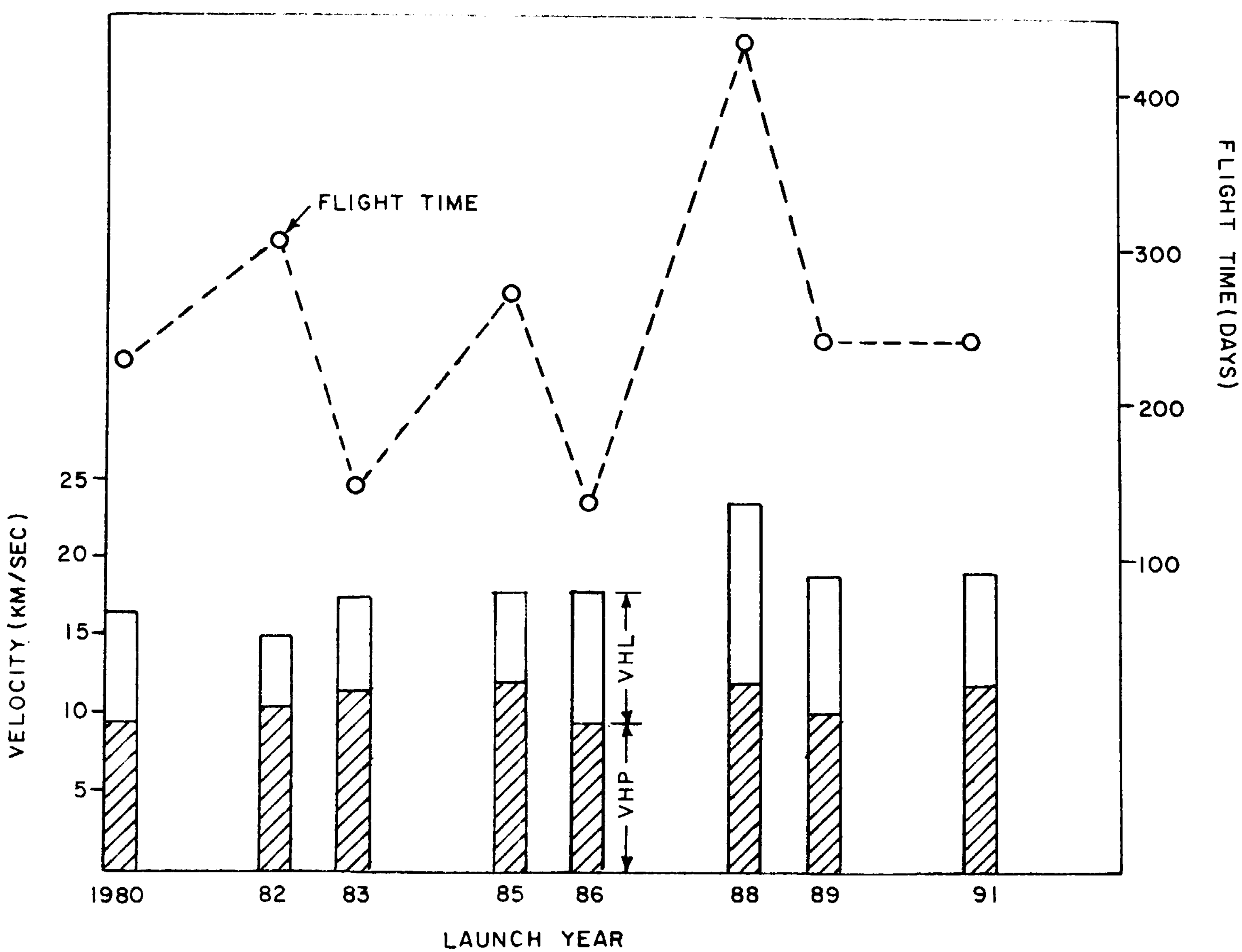

FIGURE 15. UNPOWERED VENUS SWINGBY OPPORTUNITIES TO MERCURY

5.2.2 Powered

For those cases where the optimum miss distance at Venus is less than 250 km, the miss distance can be increased to 250 km by performing a small midcourse maneuver prior to Venus encounter and a larger midcourse directional change after encounter. Atmospheric effects become important at miss distance less than 250 km. Manning's results for those powered swingbys which represent an improvement on the unpowered case are shown in Figure 16. Except for 1985, the powered swingby opportunities shown also result in a smaller VHP than either the unpowered swingby or direct opportunities. The ΔV values shown in the figure refer to the impulsive maneuvers required near Venus encounter to raise the miss distance. Flight times range from 124 days (1980) to 340 days (1991).

The ballistic mission mode opportunities for a Mercury orbiter are summarized by Table 9 which shows, for each calendar year from 1980 to 1999, the "best" opportunity in each year where "best" means the minimum sum of VHL, VHP, and ΔV. It is interesting to note that the lowest approach velocities are achieved by the direct ballistic missions of 1984-1986, which repeat in 1998-2000, and by the direct ballistic mission of 1991. These direct missions all have short flight times (95-130 days) and moderately high values of VHL (9.4-11.4 km/sec). At these opportunities, except for 1984, an Intermediate-20 class vehicle is required to deliver a 450 kg payload into a low-altitude circular polar orbit at Mercury. The relatively high value of VHL in 1984 places this mission out of the capability range of the Intermediate-20. Other opportunities within the Intermediate-20 capability include the Venus swingbys in 1980, 1982, and 1988 and the 1987 direct mission. The 1980 and 1988 powered swingbys represent the most favorable opportunities

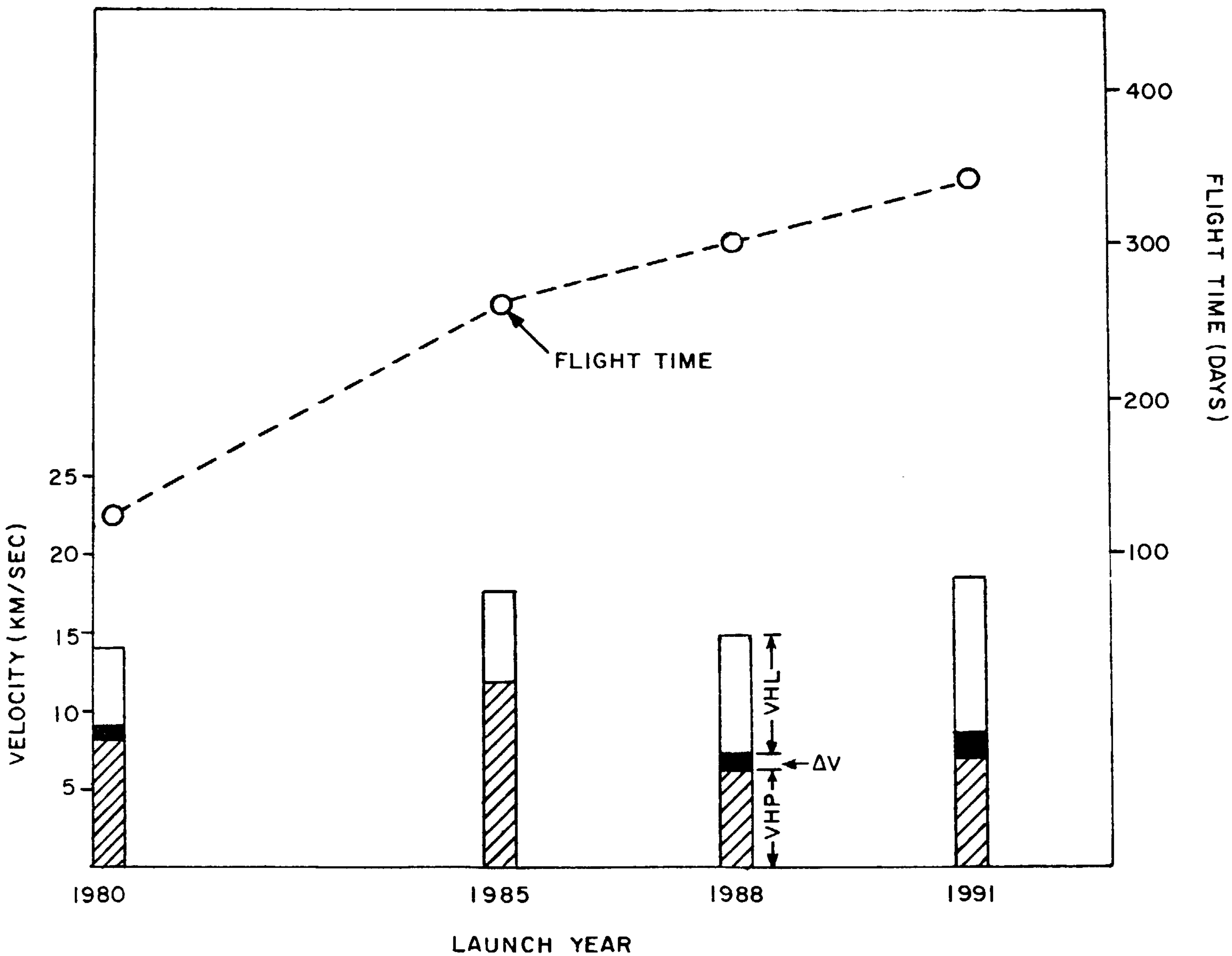

FIGURE 16. POWERED VENUS SWINGBY OPPORTUNITIES TO MERCURY

TABLE 9

YEARLY BALLISTIC MERCURY ORBITER OPPORTUNITIES

LAUNCH YEAR	LAUNCH DATE (JULIAN)	VHL (KM/SEC)	VENUS MISS ALTITUDE (KM)	VENUS ΔV (KM/SEC)	VHP (KM/SEC)	FLIGHT TIME (DAYS)
1980	2444336	4.8	250	0.9	8.2	124
1981	4716	9.7	---	---	9.5	85
1982	5000	4.6	1980	---	10.5	305
1983	5484	6.0	270	---	11.4	144
1984	5828	11.4	---	---	8.1	130
1985	6196	9.8	---	---	8.1	110
1986	6562	9.4	---	---	8.1	95
1987	6918	9.7	---	---	8.7	85
1988	7330	7.5	250	0.9	6.3	300
1989	7680	8.7	1190	---	10.2	242
1990	8022	12.1	---	---	8.2	135
1991	8369	10.7	---	---	8.1	120
1992	8752	9.5	---	---	7.9	105
1993	9116	9.5	---	---	8.3	90
1994	9650	4.6	1360	---	9.5	290
1995	2450020	6.6	---	---	12.3	110
1996	0180	5.3	250	3.0	8.6	210
1997	0810	4.1	3620	---	9.8	290
1998	0946	9.8	---	---	8.1	110
1999	1312	9.4	---	---	8.1	95

NOTE: AFTER MANNING (1967a)

considered since both VHP and VHL are relatively small for both these missions. Something on the order of fifty percent more payload can be delivered on these missions than on the 1984-1986 direct missions. The 1980 powered swingby opportunity is discussed in greater detail in Section 6.1, where a representative ballistic mission is considered.

5.3 Solar Electric Low-Thrust Trajectories

The mission analysis of a solar electric low-thrust Mercury orbiter is more complex than the ballistic mode analysis considered above. In essence, an additional stage is added to the vehicle, and consequently the mission designer has more variables to manipulate in his search for an "optimum" mission. In order to introduce some of these variables, it is convenient to consider an expression for the total interplanetary spacecraft mass as a function of time:

$$m_T(t) = \frac{m_o}{1 + m_o \int_o^t \frac{a^2 dt'}{2P_j}}$$

where $m_T(t)$ is the total spacecraft mass at the time t, m_o is the total spacecraft mass at time equal to zero (the start of the interplanetary journey), a is the magnitude of the thrust acceleration vector, and P_j is the kinetic jet power. Both the acceleration due to the low-thrust propulsion stage and its jet power are functions of time and remain under the integral sign. It is convenient to define a performance index J as

$$J = \int_{o}^{t} a^2 \frac{P_o}{P_J} \, dt'$$

where P_o is the jet power at the start of the trip, and thus

$$m_T(t) = \frac{m_o}{1 + \frac{m_o J}{2P_o}}$$

The variable t may be dropped for notational purposes, if m_T is understood to mean the <u>total</u> spacecraft mass at Mercury arrival and J is found by an integration over the interplanetary flight time.

The performance index J has units of power per unit mass, which is equivalent to $(\text{length})^2/(\text{time})^3$, and is usually quoted in terms of m^2/sec^3. Its value clearly depends upon the details of the interplanetary trajectory, in particular the time history of the square of the (low-thrust) acceleration and relative power. With a thrusting stage, as opposed to a coasting transfer, there are an infinite number of ways of leaving the Earth with some velocity and arriving at Mercury with some other velocity. The trajectory problem is then to select that particular trajectory which minimizes J since the last equation above shows that, other things being constant, the minimum J will result in the maximum spacecraft mass delivered to Mercury. Note that this is not equivalent to optimizing the orbital payload at Mercury, which will be discussed below.

The performance index J is independent of the low-thrust propulsion system power rating, (as long as no constraints are imposed upon the thrust vector) but does depend upon the time history of the <u>relative</u> jet power. The jet power depends upon the solar power available to the spacecraft and the efficiency of the low-thrust propulsion system in transforming the solar power into thrusting power. The low-thrust trajectories calculated during this study are based on Strack's relative solar power curve (Strack, 1967) shown in Figure 17. The solar energy flux incident upon the solar panels is assumed to follow an inverse-square dependence upon heliocentric distance, but the solar panel efficiency decreases with increasing temperature. The net result is that on a trajectory going inward toward the Sun from one AU, the solar panel output power does not increase as rapidly as predicted by the inverse-square law. At solar distances larger than 0.65 AU, the solar panels are oriented normal to the Sun-spacecraft axis. The flat portion of the curve below 0.65 AU is caused by panel tipping to keep the equilibrium temperature constant and the solar panel output power at a maximum. Figure 17 also shows the relative solar power curve used by Horsewood and Mann (1970), who experienced severe convergence difficulties in attempting to find optimum solar electric low-thrust trajectories for Mercury orbiter missions. Their solar power curve falls to zero before the orbit of Mercury is reached. Zola's solar electric study (Zola, 1969) is based on the Strack power curve.

The performance index J, as defined above, is independent of the low-thrust propulsion stage characteristics and therefore can serve as a useful criterion in a general search for favorable solar electric low-thrust flight opportunities. The CHEBYTOP computer program, developed by Hahn, Johnson, and Itzen (1969), has been used to identify launch opportunities

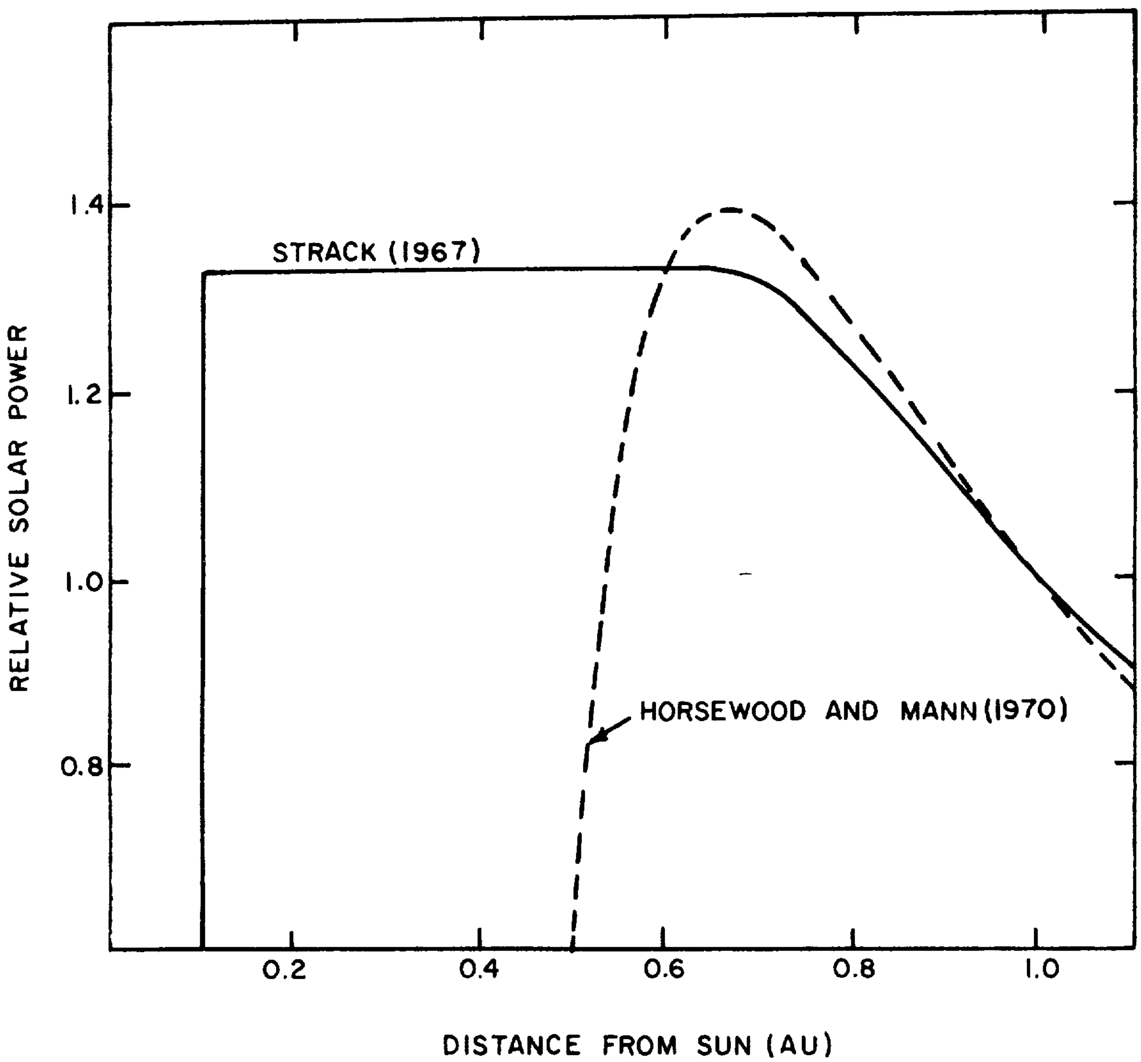

FIGURE 17.
SOLAR POWER CURVE

occurring in 1982. The results of this search which are assumed to be representative of the early 1980's are shown in Figure 18 which shows optimized values of J as a function of arrival date with flight time as a parameter. The dashed curve gives J values for a 300 day flight time, the dashed-dotted curves 350 days, and the solid curves 400 days. The Julian dates of Mercury's perihelion and aphelion are indicated along the x-axis. Apparently there is no correlation between favorable arrival dates and perihelion, aphelion, the descending node, or the ascending node. This is in marked contrast to the ballistic missions where arrival near perihelion is preferred. The trajectories summarized in the figure are all constrained to arrive at Mercury with zero hyperbolic excess velocity relative to Mercury, i.e., the trajectories are all rendezvous trajectories. If anything, this should increase the sensitivity of J to Mercury's velocity or orbital position. Also the launch velocity (VHL) is fixed at five km/sec. As with the direct ballistic missions, there are three opportunities each launch year. Which of the three opportunities is best depends upon the time of flight. For 300 and 350-day flight times, the second opportunity in the figure is superior to the other two opportunities, while for a 400-day flight time, the third opportunity is preferable. All the trajectories shown involve heliocentric travel angles from 400 to 1100 degrees, i.e., two to three loops about the Sun.

Minimizing the performance index J is not equivalent to maximizing the useful payload mass in Mercury orbit. The CHEBYTOP program minimizes J subject to fixed endpoint constraints, and changes in these constraints influence the useful orbital payload. In particular, the initial injected spacecraft mass m_o is sensitive to VHL, while the orbiting mass is sensitive to VHP and the orbital selection. Fortunately, J is not overly sensitive to either VHP or VHL. In the case of

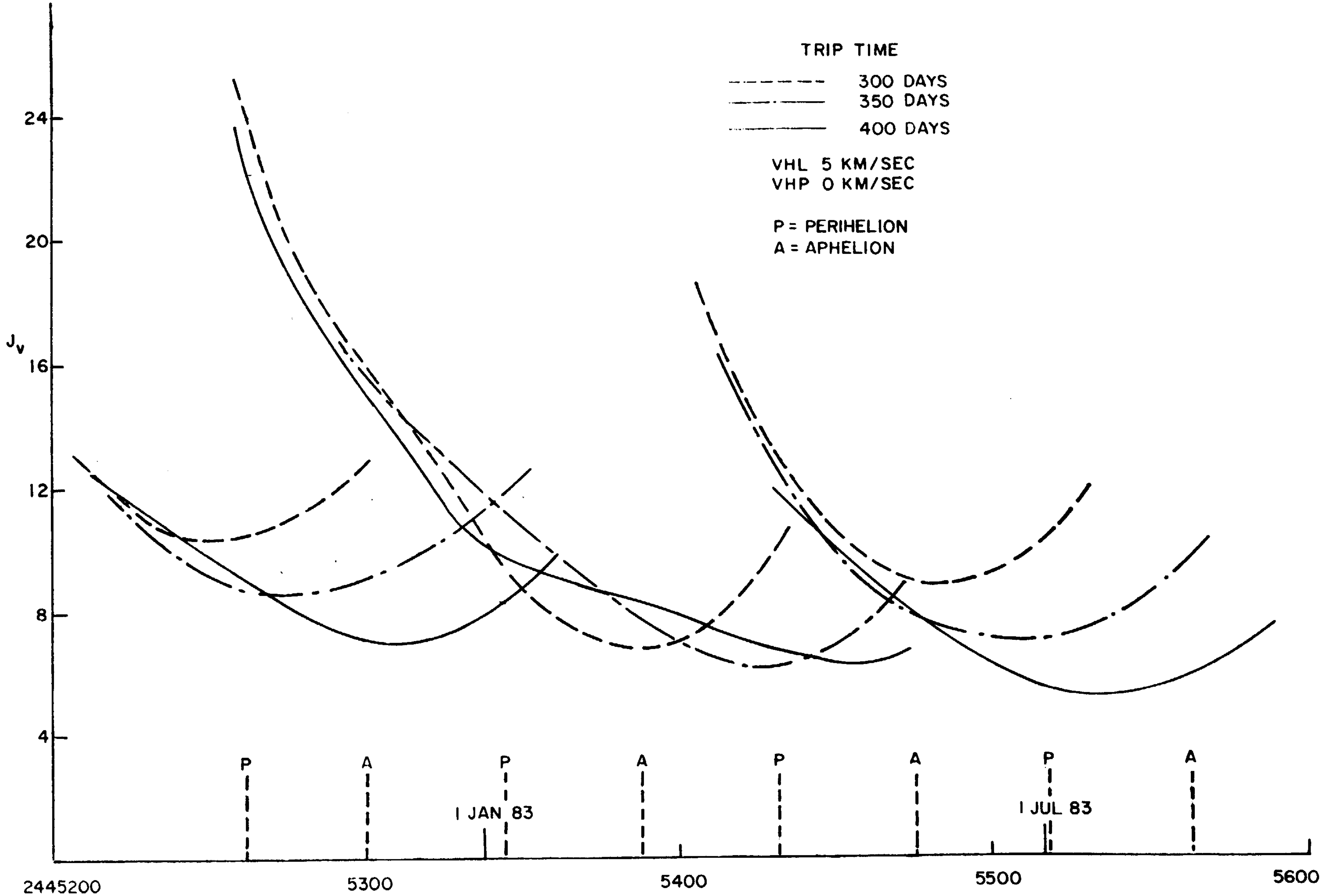

FIGURE 18. PERFORMANCE INDEX J.

the 400-day trajectory arriving at Mercury in July 1983, for example, a ten percent increase in the values of VHL or VHP will result in a two to three percent decrease in the optimum J. Although an increase in VHL will decrease J and hence the low-thrust propellant mass, it will also decrease the initial mass capability of a given launch vehicle. The relations between m_o and VHL used in this study are shown in Figure 19 for three different launch vehicles, and have been taken from Horsewood and Mann (1970). (The SLV3X/Centaur may not be available during the time period considered during this study. Its performance is comparable to, but somewhat less than, that of the Titan IIIC over the VHL range of interest.) Similarly, increasing VHP from zero will decrease J, thus decreasing the low-thrust propellant mass, but will increase the fuel mass required for the orbital capture maneuver. The influence of VHP upon the net orbiting mass is shown in Figure 20, which pertains only to a 500-km altitude circular orbit. A one-stage chemical retro of I_{sp} equal to 300 sec has been assumed. For VHP's higher than 5 km/sec, multi-stage capture manuvers are preferred.

It should be noted that no restriction has yet been placed on the thrust vector of the low-thrust propulsion stage. That is, both the magnitude and direction of the thrust vector are completely free. Values of the performance index shown in Figure 18 refer to this variable thrust case. In practice, the thrust is derived from an engine operating with a constant exhaust velocity (or constant specific impulse). For this constant I_{sp} case, the CHEBYTOP program minimizes J as before, but now the low-thrust acceleration vector is given by

$$a = \frac{a_o m_o}{m_T(t)} \frac{P_i}{P_o} \sigma(t)$$

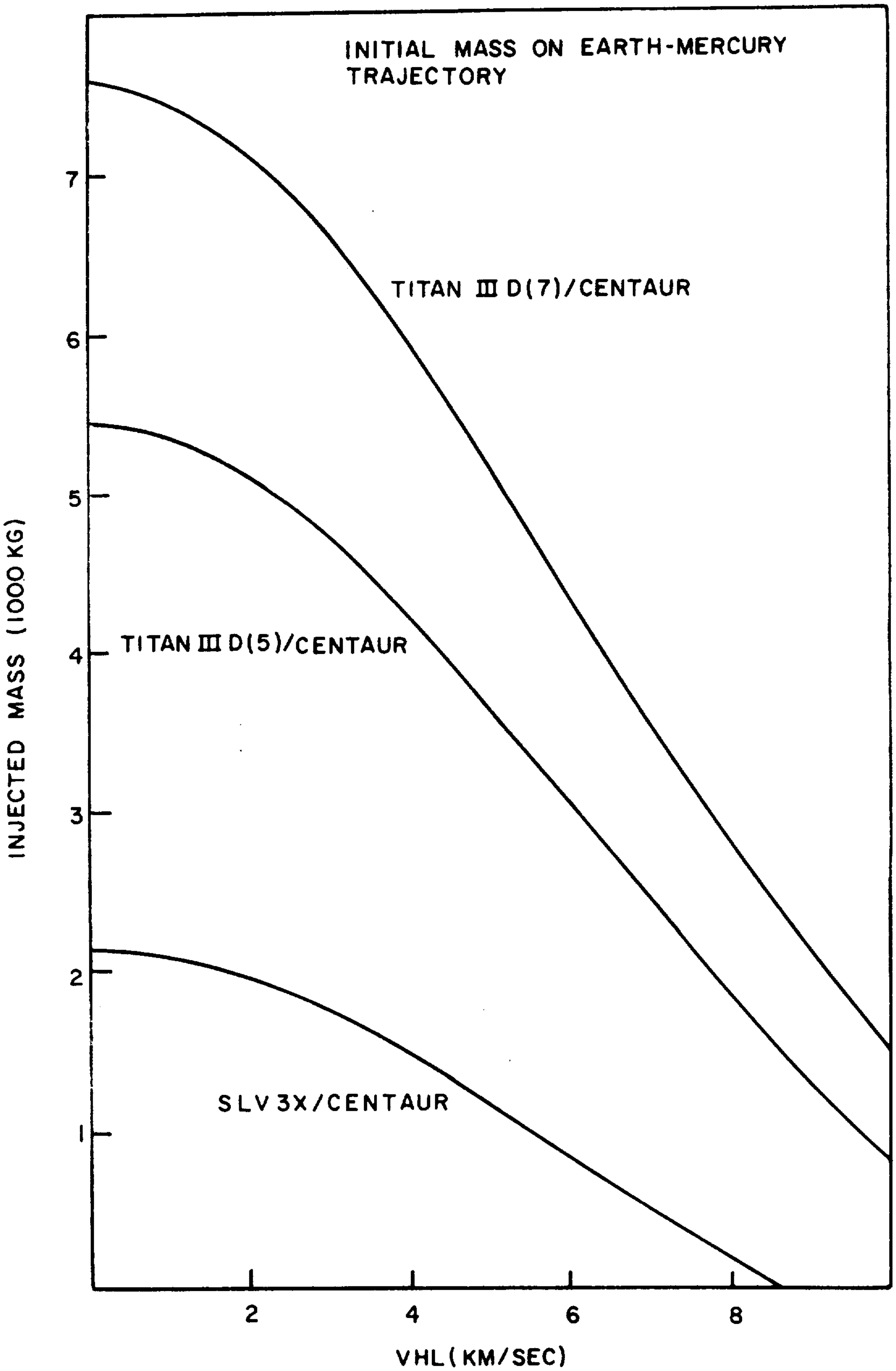

FIGURE 19. EFFECT OF VHL ON INITIAL MASS

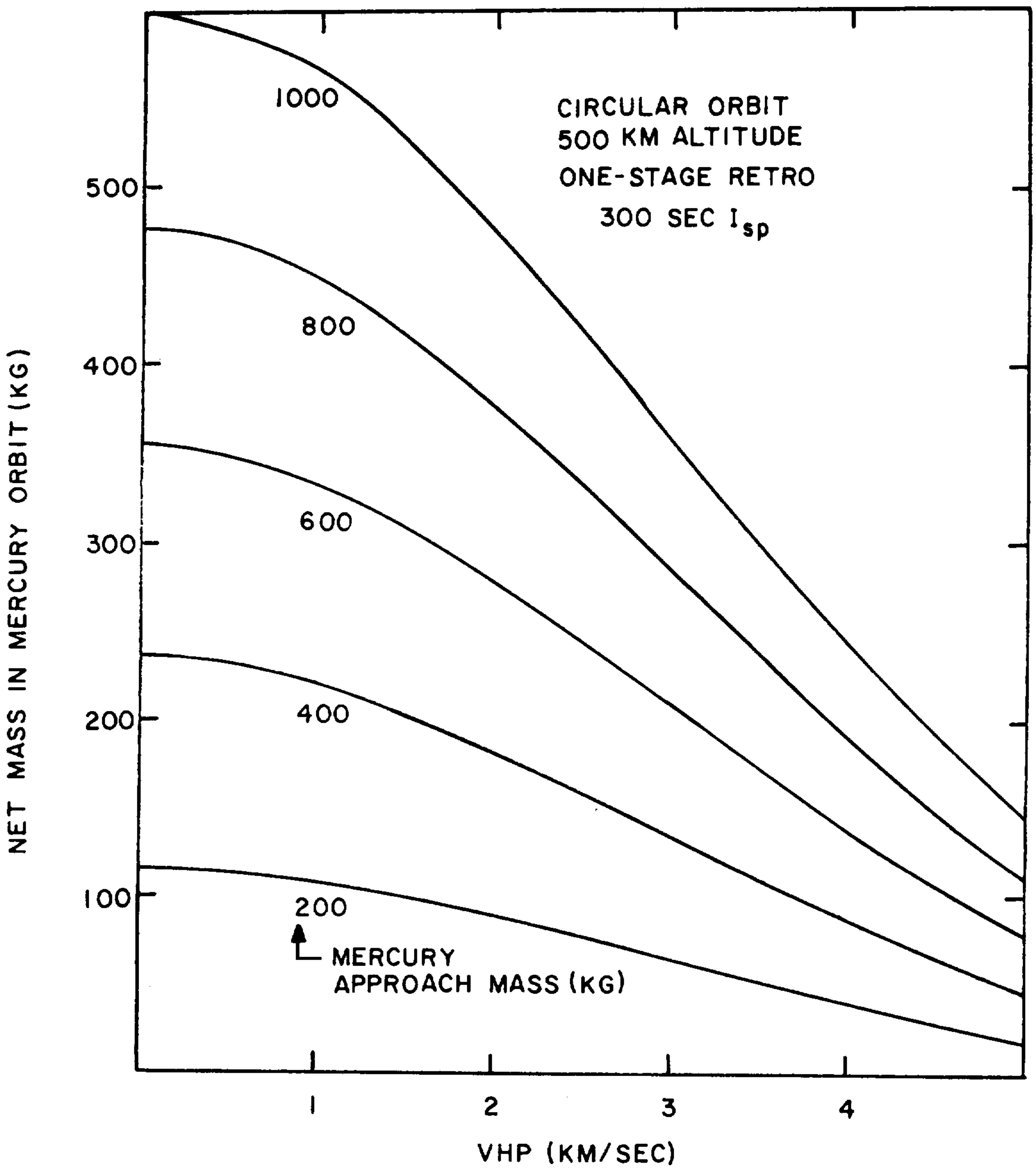

FIGURE 20. EFFECT OF VHP ON ORBIT PAYLOAD

where a_o is the initial acceleration at one AU and σ (t) is unity during thruster operation and zero when the thrusters are off. The direction of the acceleration vector is still a free variable which is used in minimizing J. Minimum values of J obtained in the constant I_{sp} case are necessarily larger than minimum values of J obtained in the variable thrust case. For the trajectories calculated during this study, the constant I_{sp} J's were typically five to fifteen percent larger than the variable thrust J's.

SECTION 6

CANDIDATE MISSION MODES

6. CANDIDATE MISSION MODES

The previous section has outlined the general characteristics of both ballistic and low-thrust interplanetary flights as applied to a Mercury orbiter mission. This section considers the applicability of each flight mode for delivering the scientific payloads described earlier. To permit a detailed quantitative comparison of different mission modes, specific launch opportunities are selected.

6.1 Ballistic Missions

Of all the ballistic opportunities occurring in the 13-year cycle described in the previous section (direct, unpowered and powered Venus swingby), the 1980 powered Venus swingby has the least demanding energy requirements. That opportunity has been selected here to present ballistic missions in their most favorable light. The optimum launch date is November 19, 1980 with an associated VHL of 4.8 km/sec. Figure 19, which can be used for ballistic missions as well as low-thrust missions, indicates that approximately 5300 kg of spacecraft can be injected into the interplanetary trajectory by a Titan IIID(7)/Centaur launch vehicle. Seventy-six days later the spacecraft passes by Venus at only 250 km altitude. This would, of course, permit a close-range study of Venus but this aspect of the mission has not been considered, the emphasis being on Mercury. The powered swingby maneuver requires an impulse of about 0.9 km/sec, and allowing 0.15 km/sec for additional midcourse maneuvers, 3400 kg of spacecraft are left after jettisoning the Venus swingby stage (300 sec I_{sp}). On August 8, 1980, the spacecraft arrives at Mercury with a VHP of 8.2 km/sec after a total flight time of 124 days. Using two retro propulsion stages (300 sec I_{sp}), approximately 240 kg can be placed on a 1.2 x 4.8 orbit at Mercury. This orbit corresponds to that selected for the "particles and fields" orbiter in Section 4 and the delivered 240 kg payload exceeds the requirements of the particles and fields orbiter by 40 kg. On the other hand, the delivered payload estimate is somewhat optimistic in that no allowance has been made for launch window considerations. Manning (1966) has stated that for this particular launch opportunity a five percent increase in the total velocity requirements corresponds to a 40-day launch window. This is somewhat atypical; for most of the ballistic opportunities a five percent increase in total velocity requirements corresponds to a 10 to 20-day launch window. At any rate, even in the very favorable 1980 opportunity the comparatively large Titan IIID(7)/Centaur launch vehicle is required for the particles and fields orbiter. It should also be noted that, in effect, this mission requires three post-launch stages, one at Venus, and two at Mercury, and hence represents a high degree of complexity.

For the 1980 powered swingby opportunity, the delivery capability of other launch vehicles has been estimated along the same lines as described above. The results are shown in Figure 21, as a function of launch vehicle class and Mercury orbit eccentricity. The requirements of the candidate orbiting spacecraft are indicated in the figure by the circled letters. That is, A represents the 198 kg particles and fields orbiter in a 0.6 eccentric orbit, B represents the 267 kg minimum planetology orbiter in a circular orbit, and C represents the 437 kg baseline planetology orbiter in a circular orbit. Thus the particles and fields orbiter mission requires a Titan IIID(7)/Centaur launch vehicle. A Titan IIID(5)/Centaur could be used if the orbit eccentricity were increased past 0.9, but then the orbit lifetime might be short as noted in Section 4. The minimum planetology

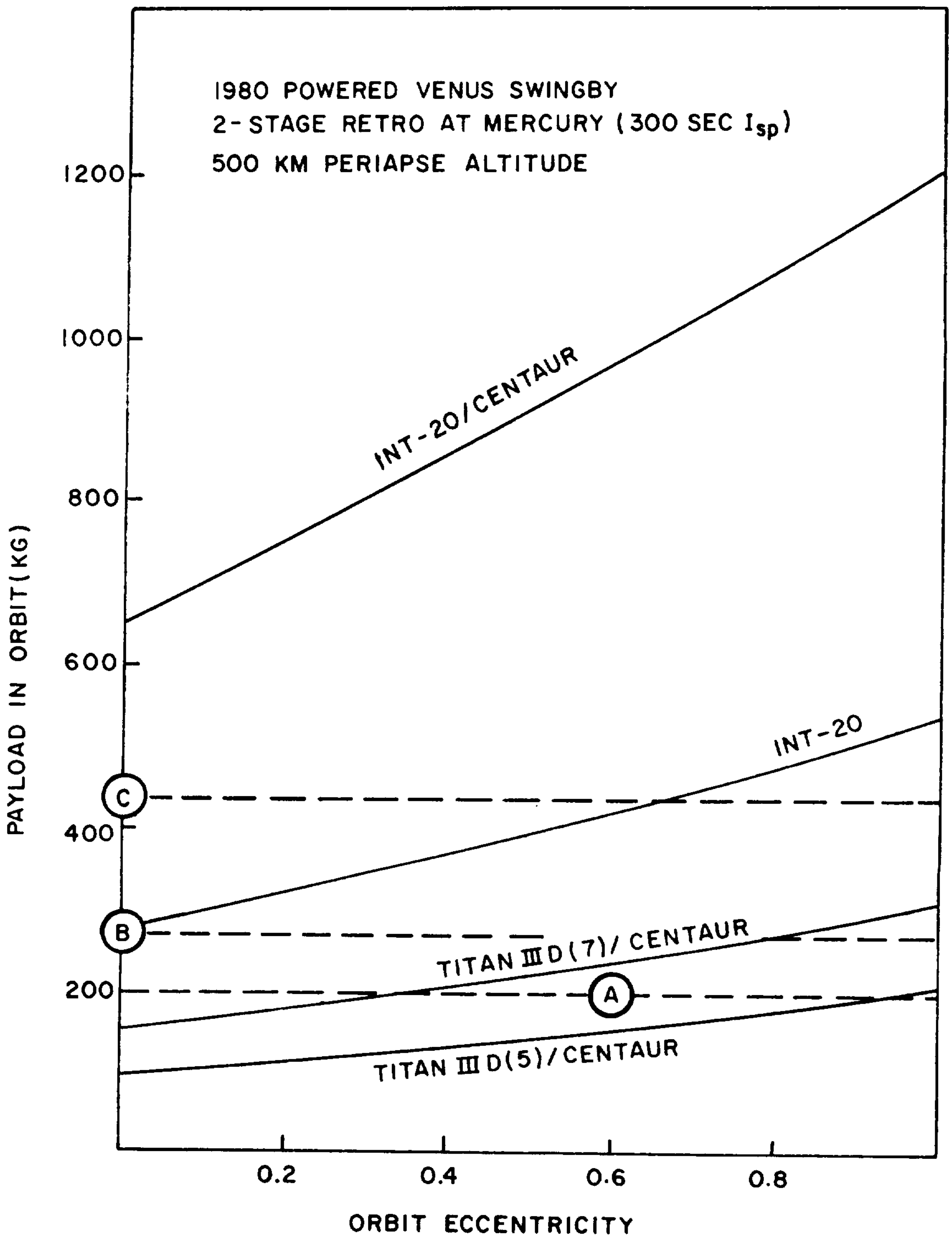

FIGURE 21. BALLISTIC MODE DELIVERY CAPABILITIES

orbiter requires an Intermediate-20 launch vehicle, which is just sufficient for a 500 km altitude circular orbit, unless the orbit eccentricity were increased past 0.8 permitting use of the Titan IIID(7)/Centaur. Again however, this shortens the orbit lifetime. The baseline planetology payload requires the Intermediate-20*/Centaur, unless the apoapse altitude is raised to somewhat more than 10,000 km. Imagery and spectroscopy acquired from this altitude would not meet the scientific requirements unless instrument capability can be significantly increased without a corresponding increase in instrument weight. Although not indicated on the figure, the Intermediate-20/Centaur is capable of delivering either the "broad first look" mission package (consisting of A and C) or the "maximum planetology" package (consisting of B and C). The emergence of an informed preference for one or the other of these packages must await the results of earlier Mercury flybys.

The only other ballistic opportunity in the 1980's which is at all comparable to the powered 1980 swingby in terms of energy requirements, and hence launch vehicle delivery capabilities, is the 1988 powered swingby opportunity. Although this mission involves a significantly longer flight time (300 days), the orbital delivery capabilities of the launch vehicles considered above are slightly improved, because of the smaller VHP associated with the 1988 opportunity. The particles and fields orbiter could probably be delivered by the Titan IIID(5)/Centaur, rather than requiring the Titan IIID(7)/Centaur as in 1980, but this is the only notable shift in delivery capability.

---

* SIC(4-F1)/SIVB(J2S)

6.2 Solar Electric Missions

The performance characteristics of the low-thrust interplanetary propulsion stage are treated independently of the launch vehicle. The stage consists of a low-thrust propulsion system, low-thrust propellant, and propellant tankage and plumbing. The propulsion system mass is simply the specific mass α times the solar panel power level at one AU. The specific mass has been taken as 30 kg/kw in this study. This value may be regarded as 15 kg/kw for a rollout solar array, 7.5 kg/kw for the thruster array, 4.5 kg/kw for power conditioning, and a ten percent contingency factor. The propellant tankage mass is assumed to be three percent of the propellant mass. The propellant tankage mass was ignored in the general discussion of Section 5.3.

The kinetic jet power P_j is related to the solar panel output power P_{sp} by

$$P_j = \eta P_{sp}$$

where η is the efficiency of the low-thrust propulsion stage, and may be regarded as the product of the power conditioning efficiency and the thruster efficiency. For this study the efficiency is taken as

$$\eta = \frac{0.769}{1 + \dfrac{2.126 \times 10^6}{I_{sp}^2}}$$

where I_{sp} is the thruster specific impulse in seconds. The specific impulse is essentially similar to the exhaust velocity, since the exhaust velocity is simply $g_o I_{sp}$, where g_o is the

Earth's surface gravity, 9.80665 m/sec^2. If the power conditioning efficiency is taken as 91 percent, the thruster efficiency implied by the above equation is shown in Figure 22 by the solid curve. The upper dashed curve in the figure shows the efficiency of thrusters in the two or three kilowatt range which has been projected (Lazar, 1969) for mid-1970's. The lower dashed curve shows the efficiency achieved by the one kilowatt Sert II mercury ion thrusters. The thruster efficiency assumed in this study would appear to be quite conservative for a Mercury mission in the early 1980's.

6.2.1 Titan IIID(5)/Centaur Missions

Maximum orbit payloads for Titan IIID(5)/Centaur-launched missions have been computed assuming a constant specific impulse low-thrust stage with the results shown in Figure 23 as a function of flight time. Orbit payload is based on 300 sec I_{sp} chemical capture injection into a circular orbit of 500 km altitude. It will be shown later that use of a chemical retro system (which is small compared to the ballistic case) appears to be more attractive than a low-thrust spiral capture. The upper curve shows orbiting payload masses achieved if the power level and specific impulse of the interplanetary low-thrust stage are permitted to vary in optimizing the orbit payload. In the lower curve, the power level is constrained at 15 kw, while the specific impulse is restricted to 2500 sec or higher. Trajectory calculations were performed only for 300, 350, and 400-day flight times. Reference to Figure 18 shows that for 1982 launches, the best (minimum J) 300 and 350-day opportunities arrive in February and March 1983, while for a 400-day flight time the minimum J opportunity shifts to arrival in July 1983. That is, the solid curves shown in Figure 23 are

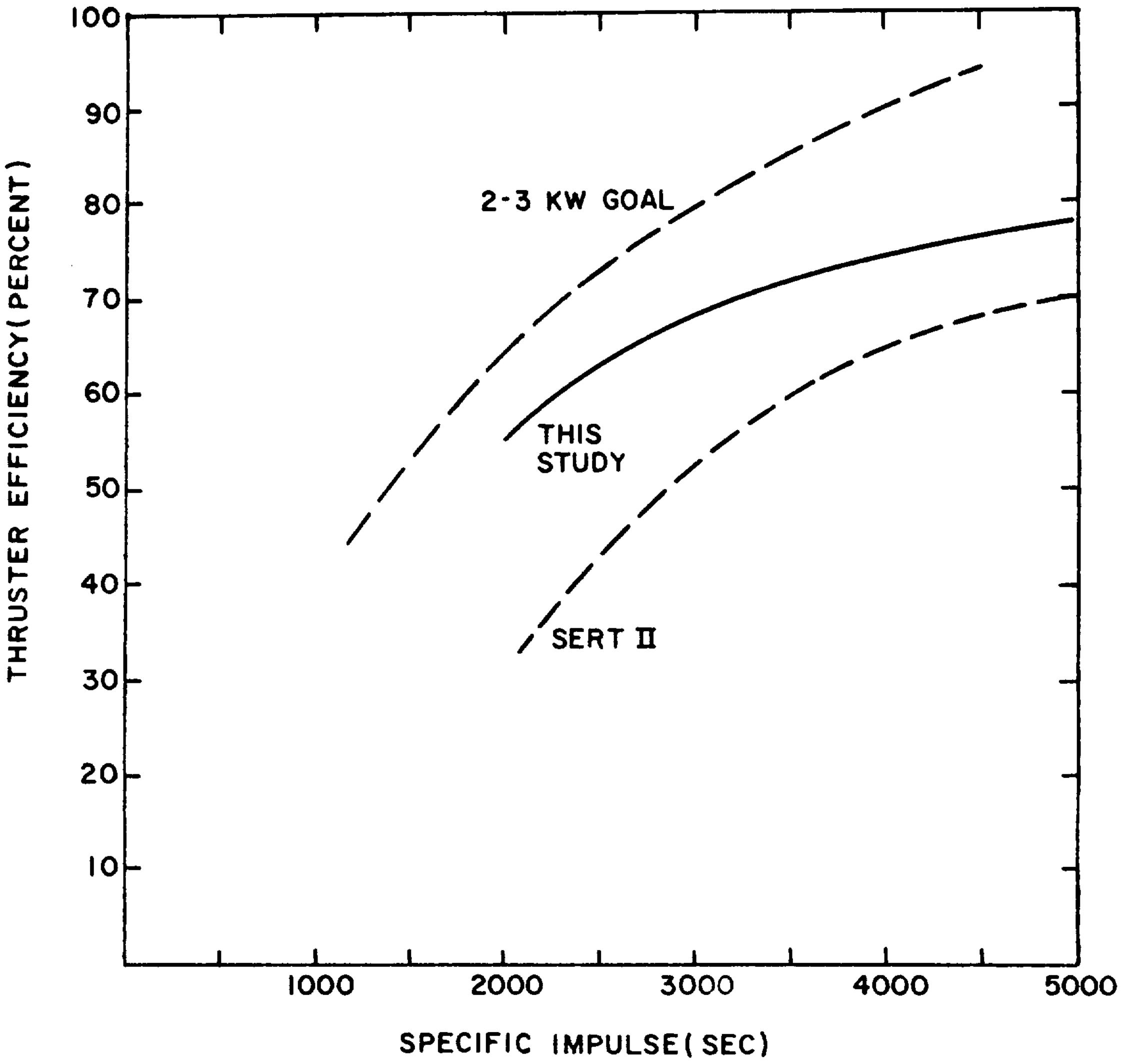

FIGURE 22. ION THRUSTER EFFICIENCY

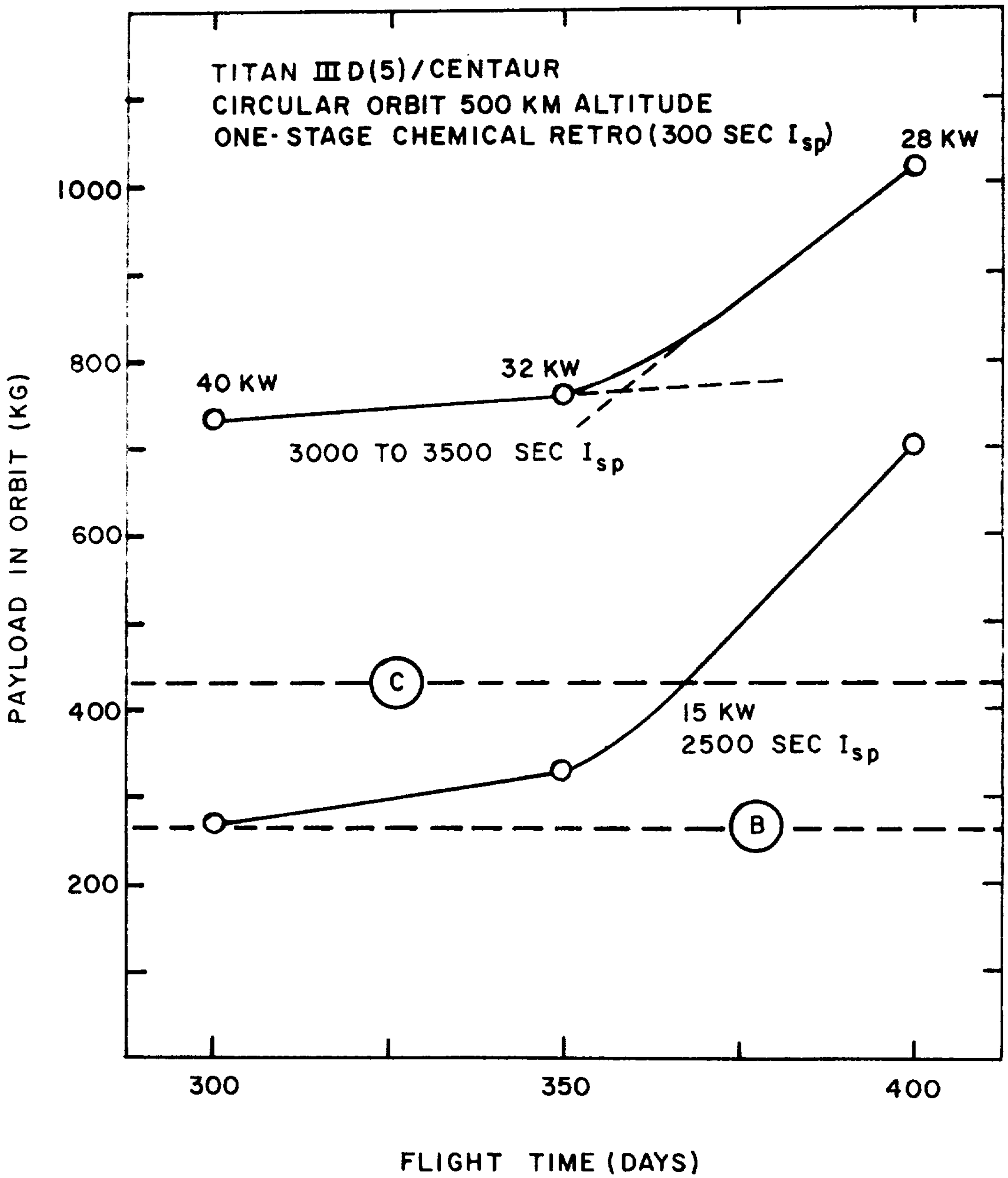

FIGURE 23. SOLAR ELECTRIC MODE DELIVERY CAPABILITIES (TITAN IIID(5)/CENTAUR)

not continuous with respect to launch or arrival date at about 360 days. If the minimum J opportunity is selected for each flight time, the payload mass increases slowly for flight times increasing from 300 to 350 days. Beyond 350 days the payload mass should increase as shown by the dashed line until about 355 or 360 days when the annual minimum J arrival date shifts abruptly from April 1983 to July 1983. This opportunity shift occurs in all the solar electric mode results presented in this section.

The payload results are also sensitive to the power level. That is, decreasing the power level of the low-thrust propulsion stage results in a marked decrease in payload capability. The fractional reduction in payload is nearly proportional to the fractional reduction in power. This effect is aggravated by restricting the specific impulse to 2500 sec or larger. At a power rating of 15 kw, the optimum specific impulse would be less than 2500 sec, and a double penalty is paid.

The horizontal dashed lines in Figure 23 correspond to the candidate orbiter mission payloads selected earlier; B refers to the minimum planetology orbiter, C to the baseline planetology orbiter. Thus for a Titan IIID(5)/Centaur-launched mission and a 15 kw low-thrust stage, the minimum planetology mission requires a 300-day flight time, the baseline planetology mission a 370-day flight time. Either of the multi-satellite missions could be flown with a 15 kw low-thrust stage, but would probably require flight times of 400 days or more.

Some authors, such as Zola (1969) and Bartz and Horsewood (1969), have suggested that for inner planet orbiters the solar electric stage should be retained on the orbiter and used as a power supply subsystem for the orbiting spacecraft.

The effects of this strategy are shown in Figure 24, for payload insertion into a 500 km altitude circular orbit at Mercury. The low-thrust stage power level <u>and</u> specific impulse are optimized for maximum payload in orbit. The payload masses shown do <u>not</u> include the low-thrust stage mass. The curve corresponding to jettisoning the solar electric low-thrust stage is, of course, identical to the upper curve of Figure 23. The lower curve shows that, for low-altitude Mercury orbits and a chemical capture maneuver, a severe payload penalty is incurred by retaining the solar electric stage. But as long as the solar electric stage is retained, the chemical retro stage may be eliminated and a low-thrust spiral capture maneuver performed. This strategy increases both the orbital payload and the flight time, since approximately 50 days are required to complete the spiral capture. A complicating feature of the spiral capture maneuver is the maintenance of the proper solar panel orientation as the spacecraft spirals many times about Mercury. Since the solar panels must be oriented properly with respect to the Sun-spacecraft axis, and the low-thrust vector direction must pass through 360 degrees during each spiral orbit about Mercury, it appears that a low-thrust spiral capture involves a complicated gimballing problem for either the thruster or solar panel subsystem. These considerations suggest that unless exceedingly high power requirements are anticipated for the orbiting spacecraft, as might be the case if a radar imaging system were included in the instrument payload, the interplanetary low-thrust stage should probably be jettisoned prior to the orbit capture maneuver. The in-orbit payload capability of this strategy is more than adequate for all orbiter spacecraft which have been identified in Section 3.

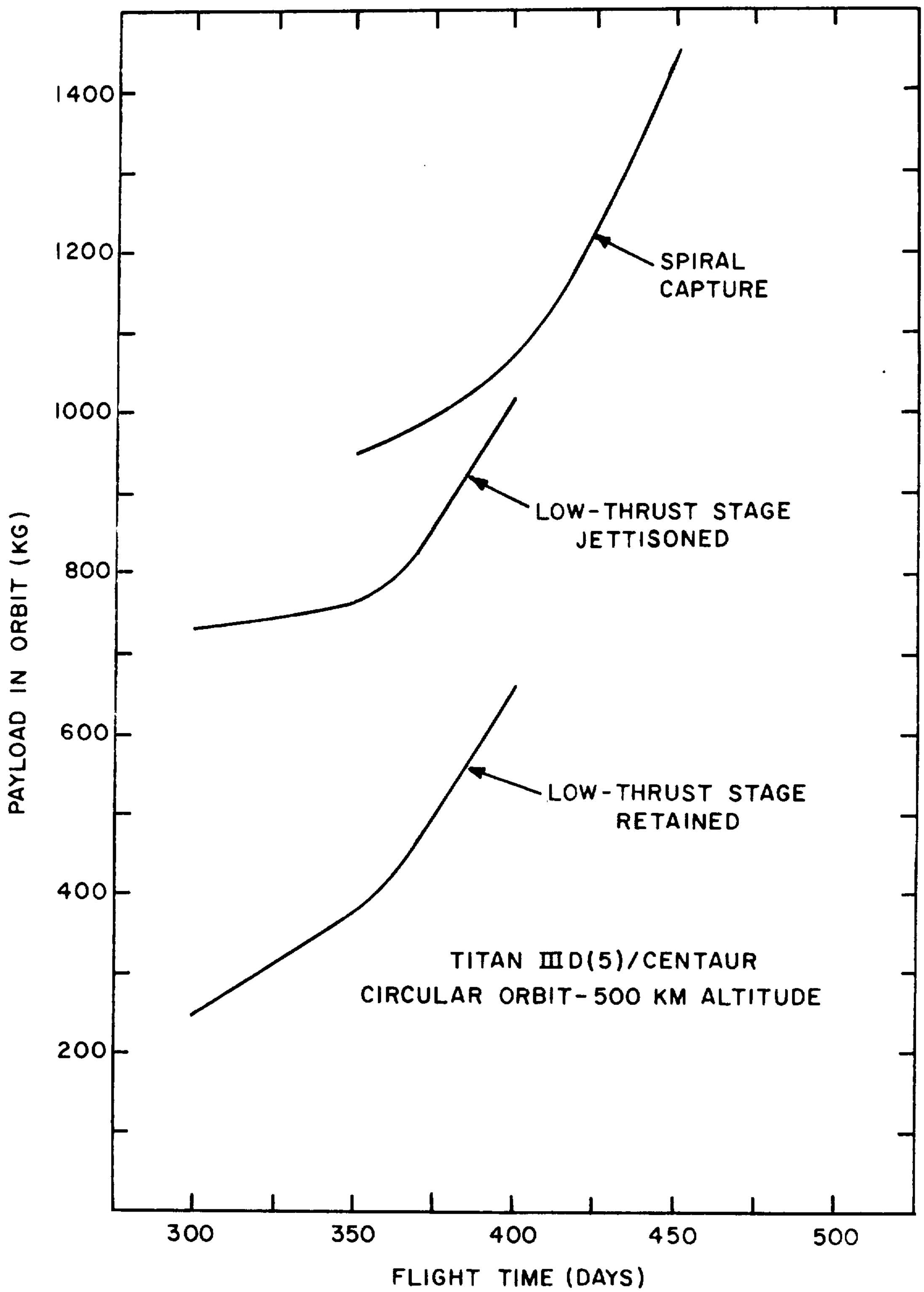

FIGURE 24. ALTERNATE SOLAR ELECTRIC MODES

6.2.2 Atlas (SLV3X)/Centaur Missions

Since the baseline planetology (C) orbiter is well within the delivery capabilities of a Titan IIID(5)/Centaur-launched 15 kw solar electric stage, it is interesting to reduce the size of the launch vehicle. Maximum payloads inserted into a 500 km altitude circular orbit using an Atlas (SLV3X)* /Centaur are shown in Figure 25 as a function of flight time. The low-thrust propulsion stage is jettisoned prior to the chemical capture maneuver. As in the Titan IIID(5)/Centaur results, the upper curve in Figure 25 represents an optimization in which the low-thrust propulsion stage power level <u>and</u> specific impulse are free variables. The lower curve represents the optimized payload results when the power level is constrained to 15 kw or less. Optimized values of specific impulse range from 3500 to 4000 sec when the power level is unconstrained and range from 3000 to 3500 sec when the power level is constrained to 15 kw or less. For flight times of 300 and 350 days, the orbiting payload capability of the SLV3X/Centaur is only ten to twenty percent less than the Titan IIID(5)/Centaur with a 15 kw solar electric stage. However, for 400-day flight times, when the minimum J opportunity shifts from arrival in March 1983 to July 1983, the SLV3X/Centaur-launched payload is only about half the Titan IIID(5)/Centaur-launched payload. Thus for the minimum planetology (B) and baseline planetology (C) missions, the effect of reducing the launch vehicle capability from a Titan IIID(5)/Centaur to an SLV3X/Centaur is to increase the interplanetary flight times from 300 to 350 days for the B mission and from 370 to about 425 days for the C mission. An increase of about 50 days in either case.

---

* As noted earlier, the SLV3X may not be available during the time period of interest. Use of the Titan IIIC should give results comparable to those presented here.

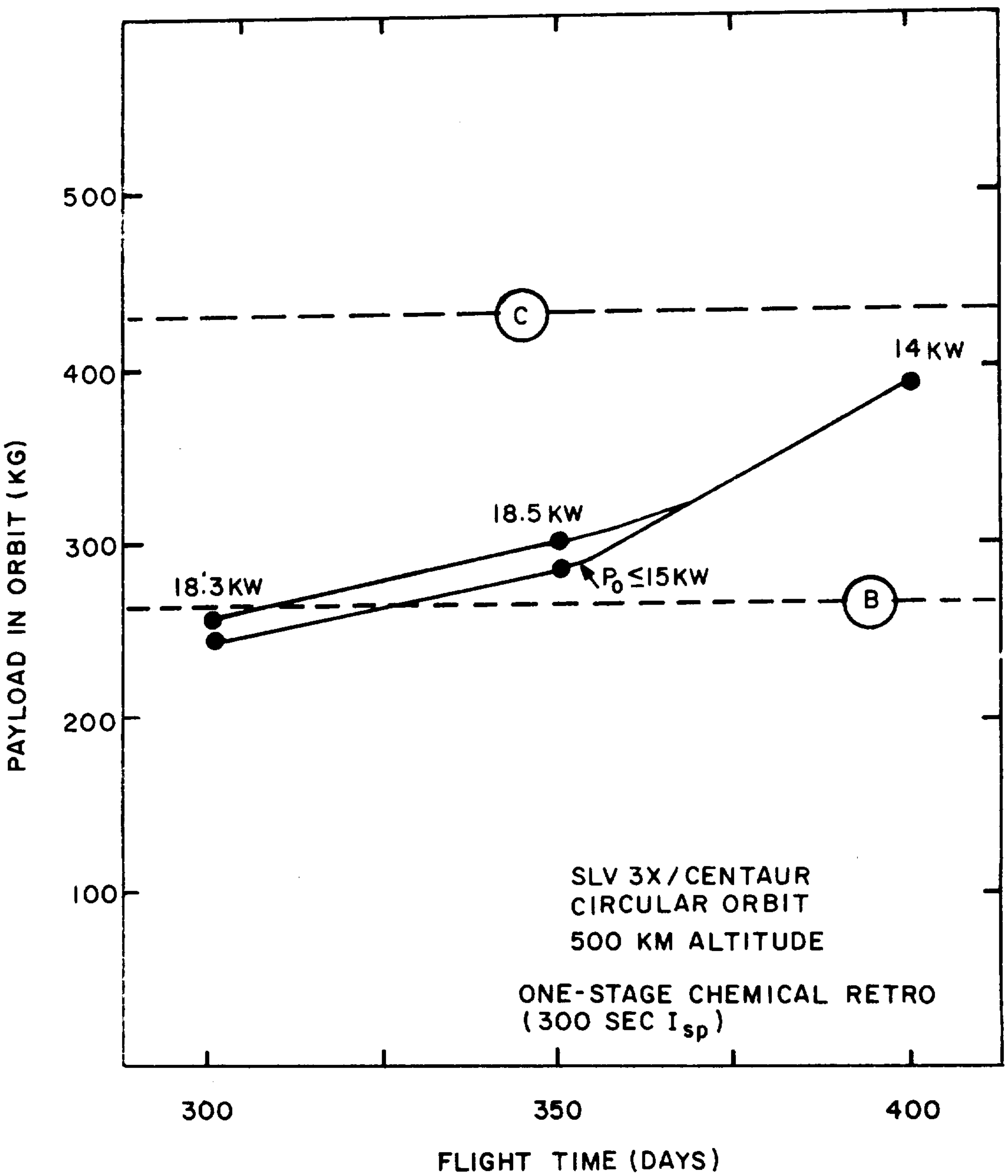

FIGURE 25. SOLAR ELECTRIC MODE DELIVERY CAPABILITIES
(SLV 3X/CENTAUR)

Perhaps the most striking difference between the Titan missions and Atlas missions is the dissimilarity of the constrained power optimizations. The SLV3X/Centaur-launched missions do not suffer greatly from reducing the power level to 15 kw; the Titan IIID(5)/Centaur-launched missions do. That is, the optimum power level for the Titan IIID(5)/Centaur missions is much higher than 15 kw, while the optimum power level for the SLV3X/Centaur missions is close to 15 kw. In fact, for flight times somewhat greater than 350 days, the optimum power for the SLV3X/Centaur is less than 15 kw.

The payload results discussed in this section have indicated that even for the most favorable launch opportunities, an Intermediate-20 class launch vehicle is required to deliver a minimal surface-imaging science package into Mercury orbit using a ballistic mission mode with multiple chemical propulsion stages. On the other hand, employment of a 15 kw solar electric low-thrust interplanetary stage permits delivery of a larger, more capable, surface-imaging science package with either a Titan IIID(5)/Centaur or an Atlas (SLV3X)/Centaur. The next section discusses some of the operational details involved in flying a selected Mercury orbiter mission, with emphasis on data collection and communications once the spacecraft is inserted into Mercury orbit.

SECTION 7

BASELINE MISSION

7. BASELINE MISSION

This section presents operational detail of a representative solar electric Mercury orbiter mission, namely, a 370-day flight launched by a Titan IIID(5)/Centaur and using a 15 kw solar electric low-thrust interplanetary stage. As noted earlier, delivery of a 267 kg spacecraft with 27 kg of science instruments into a low-altitude circular orbit at Mercury using the ballistic mission mode requires an Intermediate-20 launch vehicle. Although ballistic missions are usually regarded as simple and straight-forward even though requiring large launch vehicles, this is not the case for Mercury orbiter missions. Even for the favorable minimum-energy missions in 1980 and 1988, a three-stage chemical propulsion subsystem is necessary (one stage for the powered Venus swingby, and two stages for the Mercury capture maneuver).

A Titan IIID(5)/Centaur launch vehicle is selected for the solar electric mission considered here. An Atlas (SLV3X)/Centaur could have been selected, but the Titan provides a larger orbital payload, is a programmed vehicle for planetary exploration, and has increased growth potential over the "stretched" Atlas in that if the power level of the solar electric stage is upgraded considerably more payload is available. Figure 23 (p. 134) suggests that if the power level of the solar electric stage is limited to 15 kw, a 370-day flight time will be necessary to provide delivery of the 430 kg baseline planetology orbiter. A Mercury arrival date of 25 Jun 1983 (Julian date 2445511), which should not be far from the optimum, has been rather arbitrarily selected fixing the launch date as 20 Jun 1982 (Julian date 2445141). Based on data from optimized 350 and 400-day flights, the optimum end point conditions for maximum orbital payload are a VHL of about 6.7 km/sec and a

VHP of about 1.4 km/sec. The CHEBYTOP computer program was used to optimize the interplanetary trajectory with the results shown in Figure 26. During the 370-day flight, the spacecraft completes more than two loops about the Sun (heliocentric travel angle of 833 degrees). The positions of Earth and Mercury at the launch and arrival dates are shown in the diagram. Since the flight time is very nearly one year, the Earth is nearly in the same position when the spacecraft arrives at Mercury as when the spacecraft was launched. Mercury completes more than four revolutions about the Sun while the spacecraft is enroute.

The total mass of the spacecraft immediately after injection on the interplanetary transfer is about 2620 kg. The solar electric low-thrust propulsion stage provides an initial acceleration of 2.7×10^{-5}g using 15 kw of solar panel output power and mercury ion thrusters of 2500 sec specific impulse.

The power input to the thrusters is 13.7 kw at the start of the interplanetary transfer and increases as shown in Figure 27. If each thruster is rated at 4.5 kw, the power level for each of the four operating thrusters is indicated in the upper part of Figure 27. The lower part of the figure suggests a power switching policy when six thrusters are used. At any given moment, four of the thrusters are operating while two are on standby. The total thrusting time for any individual thruster is only about 6000 hours. Although it is not shown in the figure, the optimum constant specific impulse thrust solution to the trajectory problem involves a twelve-day coasting period near the beginning of the mission (from day 3 to day 15). The small dip in the thruster power level at about 180 days flight time occurs when the spacecraft travels out from and back within 0.7 AU from the Sun (as shown in the southwest quadrant of Figure 26). The thrust vector direction is indicated in Figure 28, which shows the angle between the thruster system ion exhaust

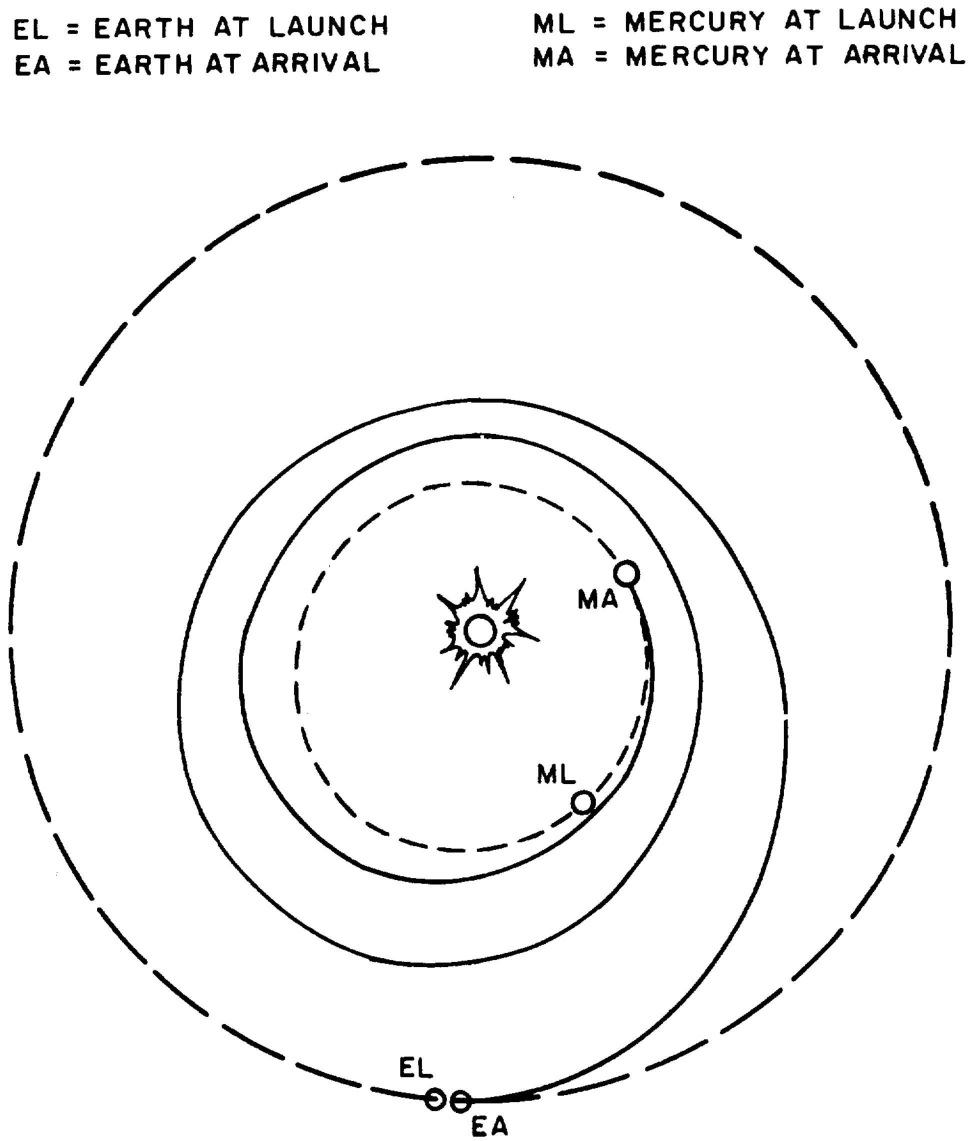

FIGURE 26. SOLAR ELECTRIC EARTH-MERCURY TRAJECTORY

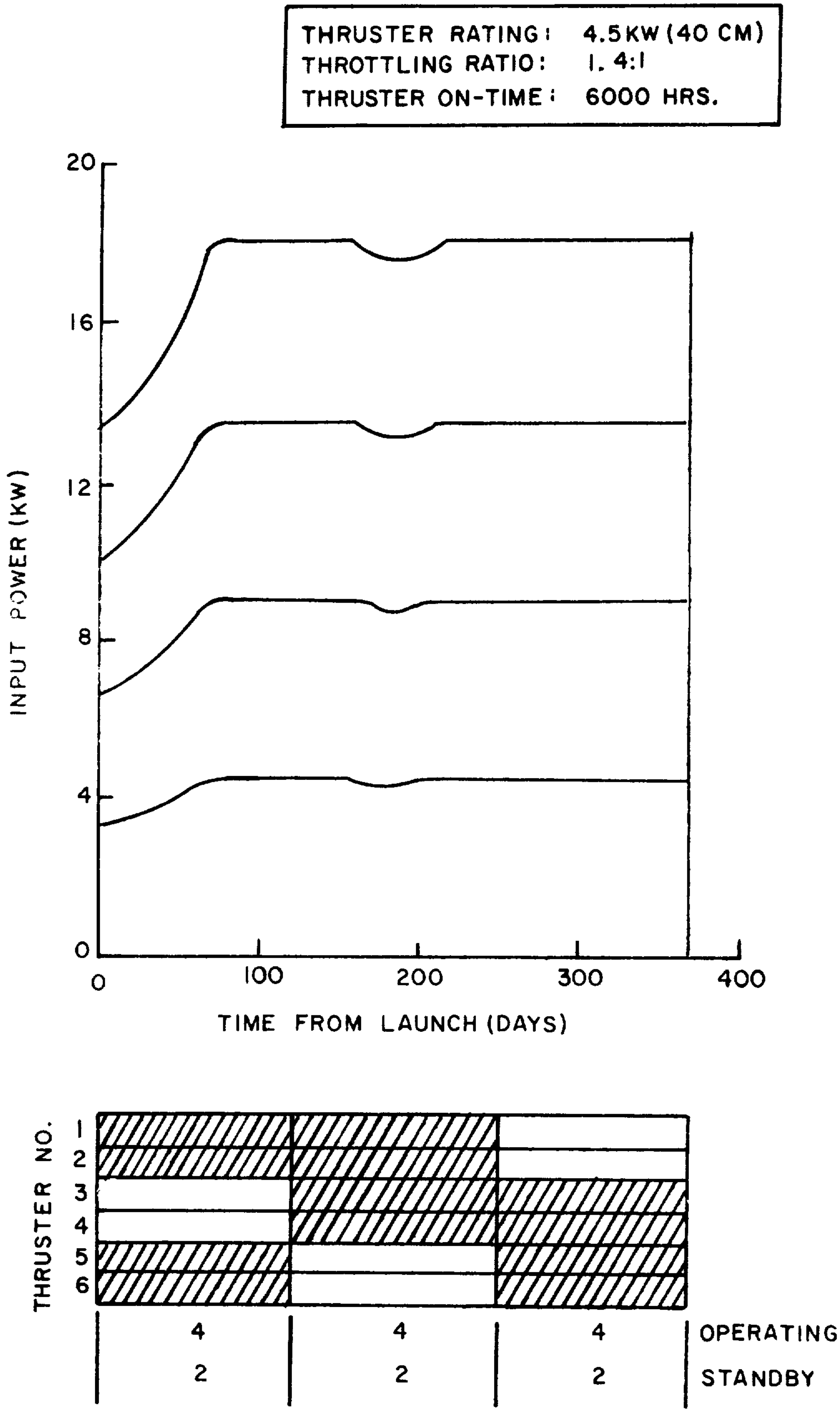

FIGURE 27. THRUSTER POWER PROFILE

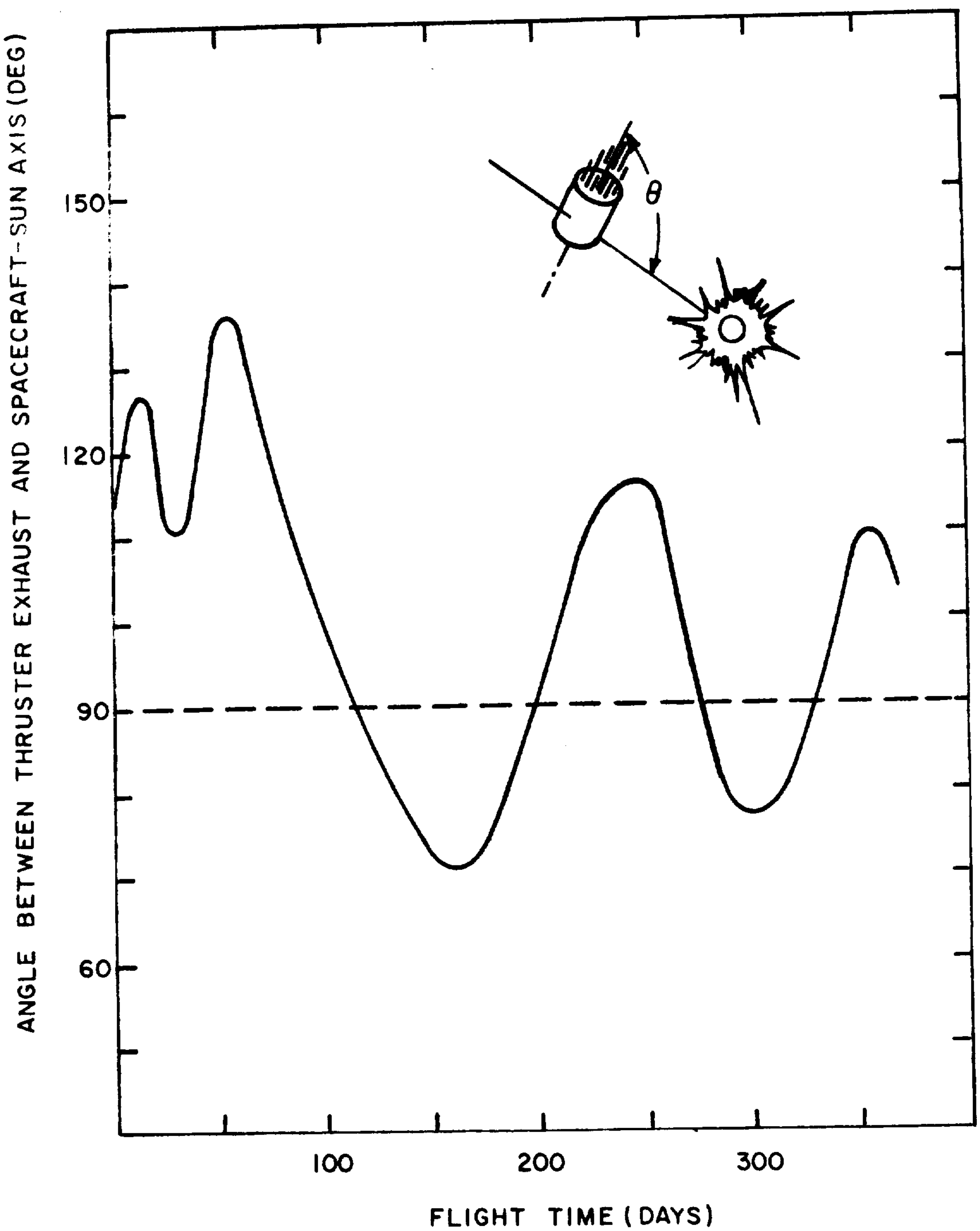

FIGURE 28. THRUST VECTOR ORIENTATION

velocity and the spacecraft-Sun axis. Through most of the mission the thrust vector is within 30 degrees of the normal to the spacecraft-Sun line. A future study might properly consider the penalties incurred by fixing the thrust angle.

Approximately 1150 kg of propellant and 40 kg of tankage are required with the 450 kg low-thrust propulsion system. Something less than three kg of propellant are required for seven guidance corrections, at fifty-day intervals throughout the transfer. The position and velocity errors are estimated to be 3000 km and 3 meters/sec, respectively, at the end of the interplanetary transfer phase. The spacecraft arrives at Mercury five days before the ascending node and nine days before perihelion. After jettisoning the low-thrust propulsion stage the total spacecraft mass is nearly 1000 kg. A space-storable chemical retro system (300 sec I_{sp}) injects the 520 kg spacecraft into a 500 km altitude circular polar orbit at Mercury. This payload mass, determined from a later point-calculation, is approximately ten percent larger than would be anticipated from Figure 23, indicating that some caution must be exercised in interpreting Figures 23 and 25 for flight times other than 300, 350, and 400 days. A mass inventory of the spacecraft is given in Table 10.

Since the data collection rate of the science payload is dominated by the two television cameras, some insight into the time profile of the mission may be gained by considering the solar elevation angle at the subspacecraft point on Mercury's surface. This is shown in Figure 29 as a function of position in orbit and orbital stay time or mission duration. The orbital position can be expressed conveniently in hours, and the length of the y-axis in the figure corresponds to the orbital period of a 500 km altitude polar circular orbit (1.9 hours). Thus, for example, the figure shows that at the start of the orbital mission the solar elevation angle at the subsatellite point is ten degress or higher for about 0.75 hours every orbit (1.8-1.05 hours). Approximately 12.5 orbits are completed every day.

TABLE 10

SPACECRAFT MASS INVENTORY

TITAN IIID(5)/CENTAUR

MASS AFTER EARTH DEPARTURE	2620 KG
SEP STAGE (15 KW, 2500 SEC)	450
SEP PROPELLANT AND TANKAGE	1190
MASS AFTER JETTISON	980
CHEMICAL RETRO STAGE	460
ORBITING PAYLOAD	520
SCIENCE MASS	80

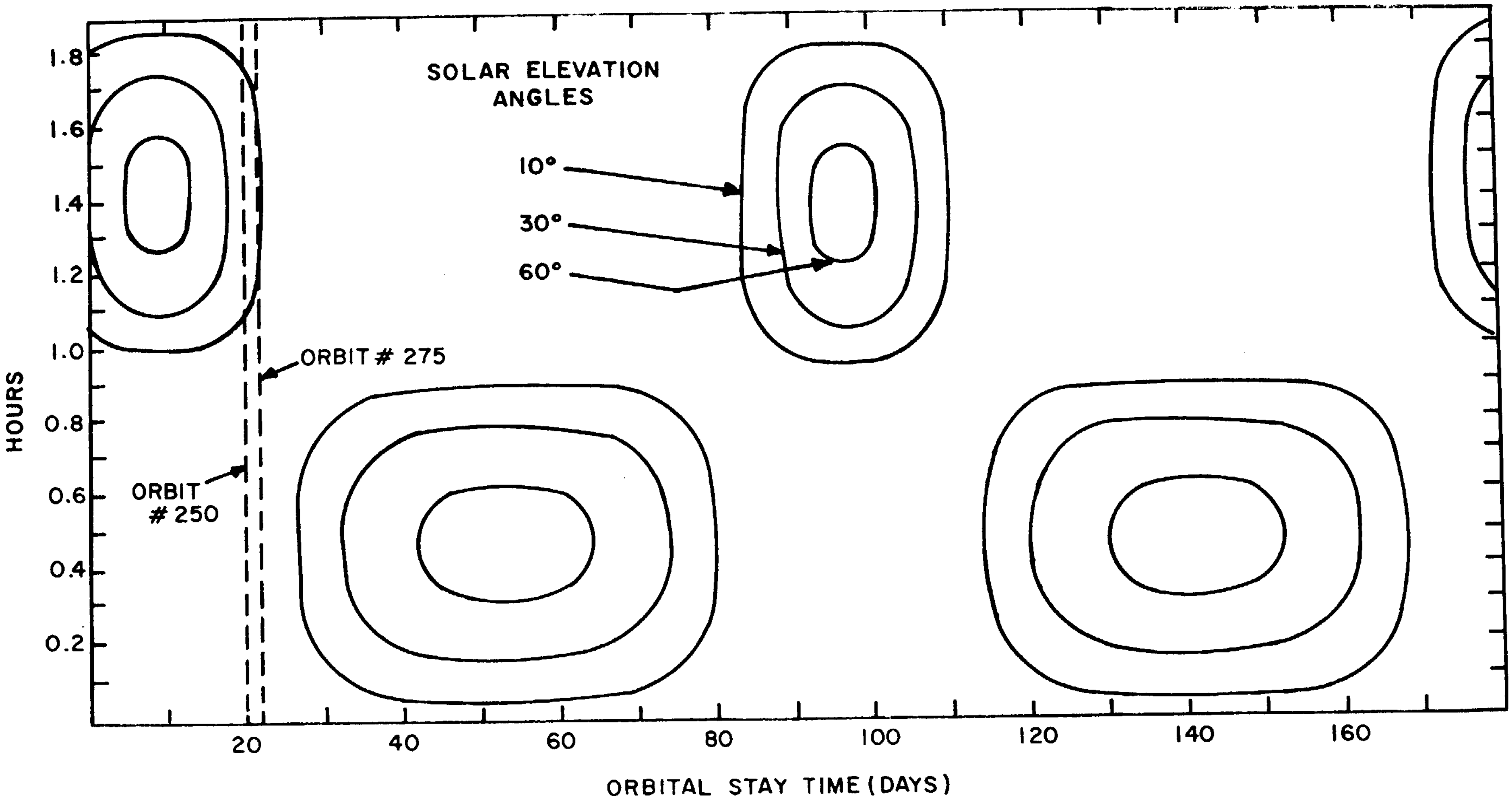

FIGURE 29. SOLAR ELEVATION AT THE SUBSATELLITE POINT

During the first orbital pass, 14 regional scale pictures could be taken at 20 percent forward overlap, representing a data load of about 1.1×10^8 bits. For regional scale imagery, no new areas come into view for 23 orbits (1.8 days). Transmitting the regional scale imagery obtained from one orbital pass to Earth during a two hour period requires a data transmission rate of 1.6 kilobits per second. The communications system is designed to provide a 16 kilobit per second rate, and hence is not stressed by transmission of regional scale imagery. On the other hand, if the local scale camera were used in the period from 1.0 to 1.8 hours, approximately 140 local scale pictures could be collected from a single orbital pass, and a transmission rate of 16 kilobits per second would be required to send these data back in a two hour transmission period. Because of Earth occultation problems, there will be periods when a continuous two hour period is not available and, as discussed below, this is the case at the beginning of the mission.

Visual imagery can be acquired throughout the first 22 days (through the first 275 orbits or so) of the mission at which time the orbit trace is sufficiently close (and approximately parallel) to the terminator that only low-angle lighting is available at the subsatellite point. However, starting with the 27th day, low-angle lighting conditions are obtained on the other side of the orbit. Because of Mercury's 3/2 resonance rotation rate, four lighting cycles are required to achieve complete planetary coverage, and the mission must last approximately 176 days if this is to be accomplished.

For a 500 km altitude circular polar orbit, the maximum period of Earth, Sun, or Canopus occultation is about 0.6 hours. These occultation periods occur during the mission as shown by Figure 30. During a 176-day mission, the Earth is

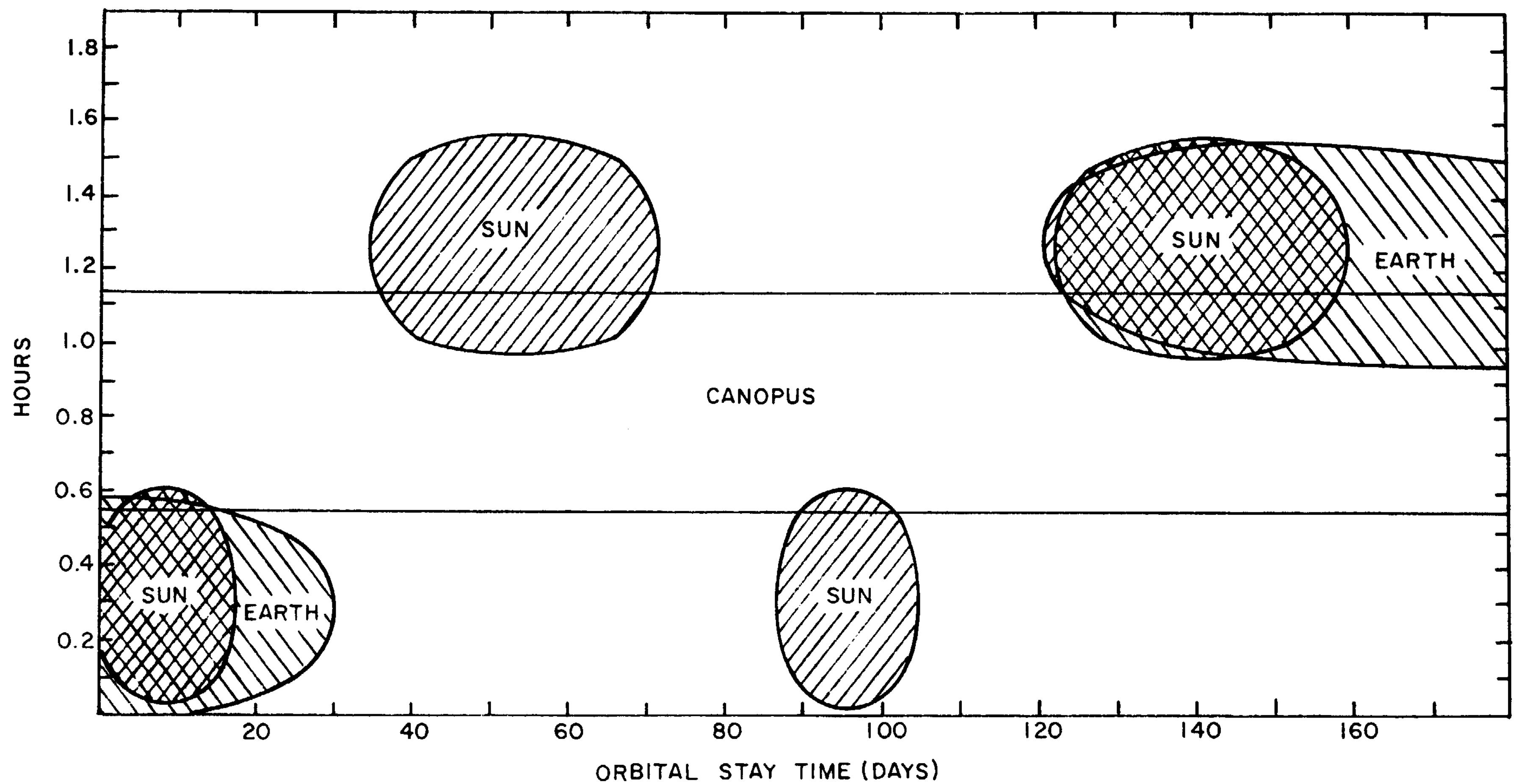

FIGURE 30. OCCULTATION PERIODS

occulted for the first 30 days and again from day 123 through 176. The Sun is occulted for four periods, as shown by the figure, while Canopus is occulted 0.6 hours every orbit.

During the mission, the communication distance to Earth varies from about 0.5 to nearly 1.5 AU as shown by the sine-like curve in Figure 31. As noted earlier, the communications system is designed to achieve a 16 kilobit per second data transmission rate for the maximum communication distance of 1.47 AU. At various periods during the mission, the line-of-sight from Earth to the orbiting spacecraft may pass sufficiently close to the Sun that communications with the spacecraft will be interrupted by solar radio interference. This, of course, is likely to happen near conjunction. Experimental data from S-band communications with Pioneer (Goldstein, 1969) indicate that radio communications with the spacecraft will be interrupted whenever the line-of-sight passes within two degrees of the Sun. Figure 31 shows that during the 176-day mission, three conjunctions occur; Figure 32 shows that two of these result in a loss of communications. In Figure 32 the three conjunctions of concern are numbered 3, 4, and 5, but only 3 and 5 result in the communications line-of-sight passing within two degrees of the Sun. Communications loss occurs for a two-day period centered on 9 July 1983 and again for a six-day period centered on 30 Oct 1983. That is, no communications are possible on days 13-15 and on days 124-130 of the mission.

Periods of high data collection rates during the mission are highlighted in Figure 33. Because of the availability of a variety of solar illuminations, the imagery data is likely to peak at about 10, 52, 96, 130, and 174 days in orbit. These periods are alternatively about 8 and 22 days in duration. A short (two-day) period of communications blackout due to solar interference will occur at the end of the first peak period. The second blackout, of six days duration, occurs just prior to the fourth data collection peak. A 0.6 hour Earth occultation period will occur every orbit during the first, fourth, and fifth data collection peak as shown in the figure.

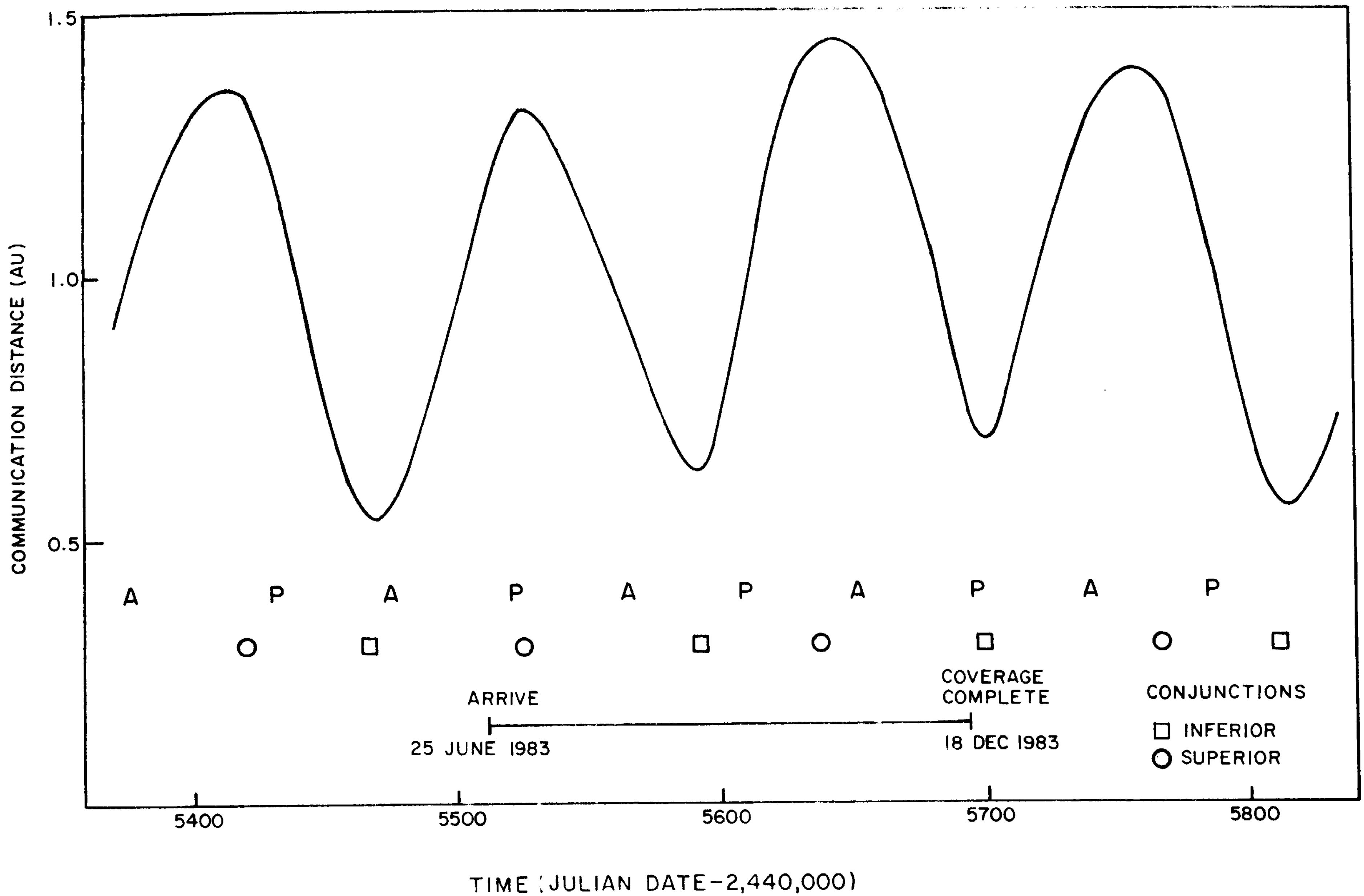

FIGURE 31. COMMUNICATION DISTANCE

ANGULAR DISTANCE BETWEEN MERCURY
AND THE SUN AS SEEN FROM EARTH

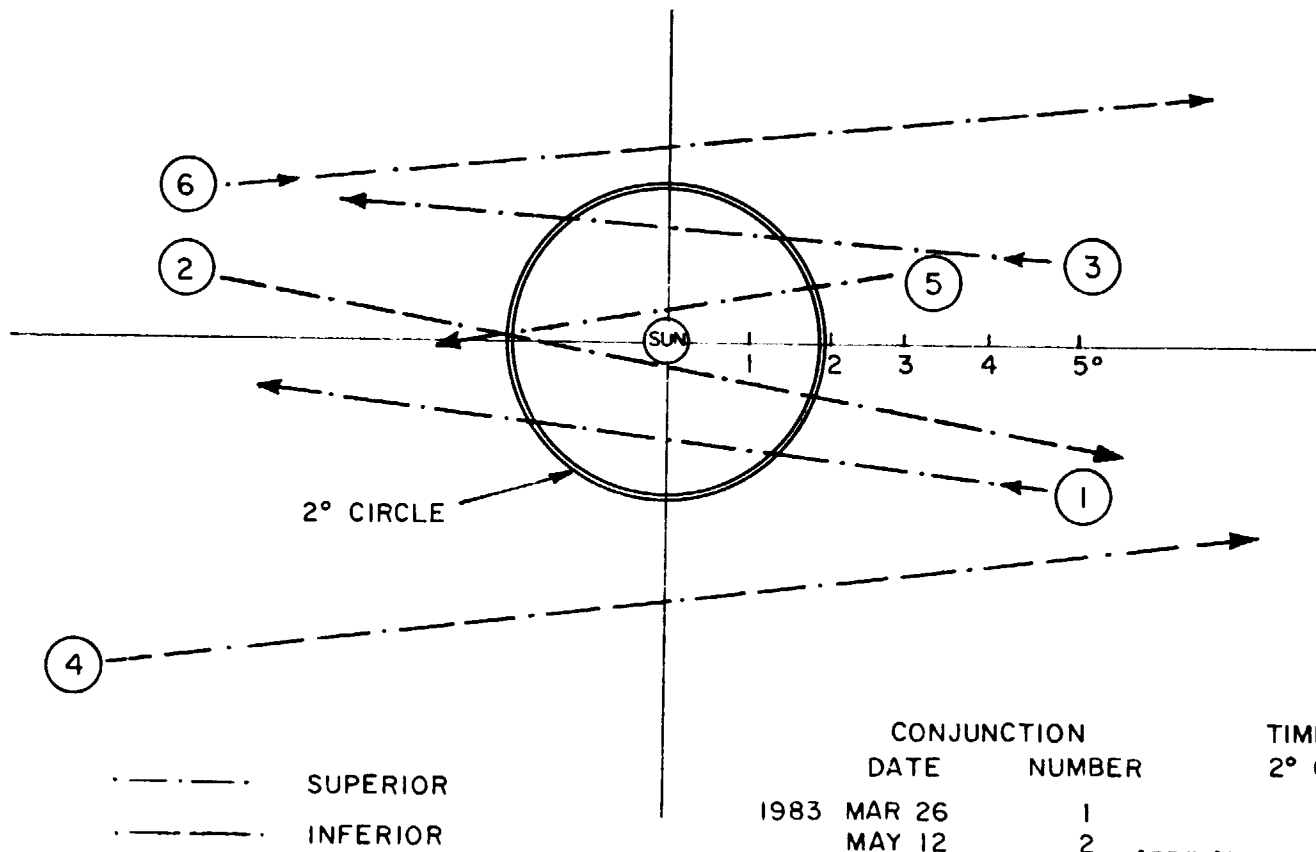

	CONJUNCTION DATE	NUMBER		TIME WITHIN 2° OF SUN
1983	MAR 26	1		3.0^d
	MAY 12	2		2.4
	JUL 9	3	ARRIVAL	2.2
	SEP 15	4	176 DAYS	0
	OCT 30	5		6.0
	DEC 31	6		0

FIGURE 32. COMMUNICATION BLACKOUT PERIODS

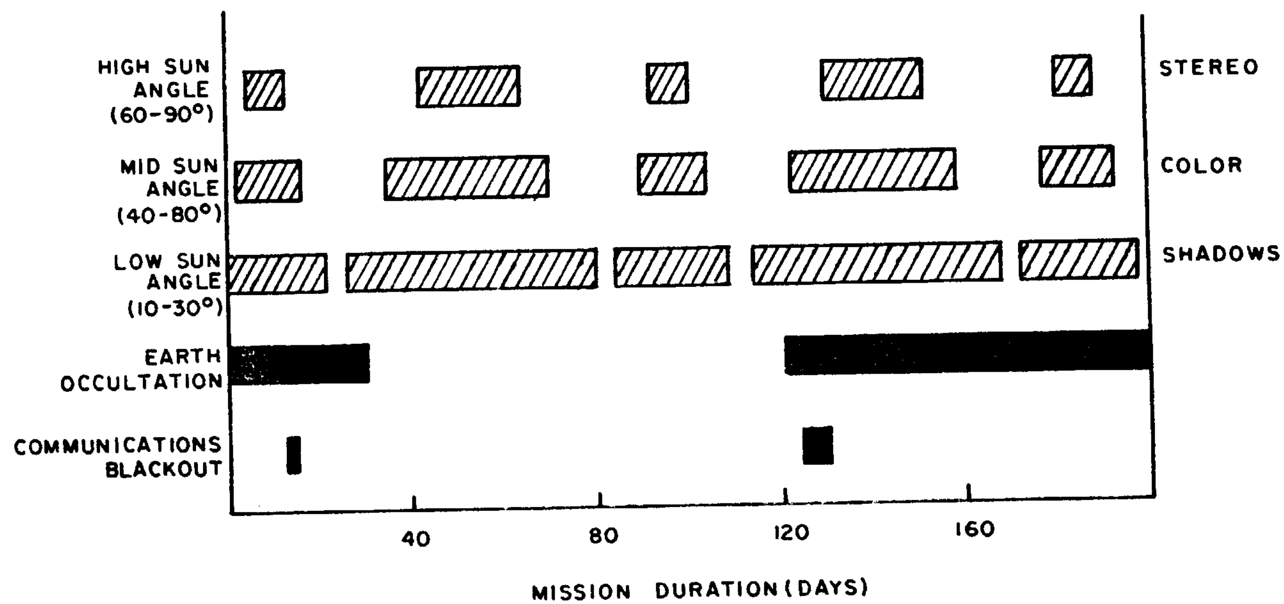

FIGURE 33. ACTIVITY PROFILE

SECTION 8

CONCLUSIONS AND RECOMMENDATIONS

8. CONCLUSIONS AND RECOMMENDATIONS

This report has presented the results of a preliminary study of a Mercury orbiter mission. The research reported here unquestionably indicates that a solar electric low-thrust Mercury orbiter mission deserves further study. That is the basic conclusion and recommedation of this report. Other conclusions, which rest on as firm a footing as is possible to be laid in a pre-phase A study of this type, include:

1. First-generation orbiter missions should emphasize visual surface imagery on at least a regional scale (one to three km resolution) and require 176 days in orbit to achieve complete planetary coverage.

2. A low-altitude (about 500 km) circular polar orbit is preferred for such missions.

3. Ballistic mode orbiter missions, whether direct or Venus swingby, require Saturn-class launch vehicles.

4. A 450-500 kg orbiting spacecraft can be delivered by a Titan IIID(5)/Centaur using a 15 kw solar electric upper stage, although interplanetary transfer times of 300-400 days are required.

5. Unless high-power-consuming radar imaging experiments are to be performed, it appears preferable to jettison the solar electric transfer stage prior to the orbit capture maneuver.

6. New technology requirements include development of high-temperature solar-radiation-resistant solar panels (for orbiter power) and spacecraft subsystem modifications for one-year lifetime in Mercury's environment.

It is noted that the conclusions of other recently completed studies emphasizing the potential advantages of solar electric propulsion might be strengthened by these conclusions. Finally, it is admitted that in this study opportunities for solar electric missions to Mercury have been typified by 1982 launch dates and 300-400-day flight times. Additional studies of solar electric trajectories are required to verify similar potentialities of other launch years and longer flight times. On the other hand, in-depth analysis of Mercury orbiter missions should probably await the completion of the currently programmed Venus-Mercury 1973 mission.

REFERENCES

Ash, M. E., Shapiro, I. I., and Smith, W. B., "Astronomical Constants and Planetary Ephemerides Deduced from Radar and Optical Observations", Astron. J., 74, 338-350, 1967.

Bartz, D. R. and Horsewood, J. L., "Characteristics, Capabilities and Costs of Solar Electric Spacecraft for Planetary Missions", AIAA Paper No. 69-1103, 1969.

Bashe, R. and Kennedy, S., "Martian Orbital Photographic Study, Technical Summary Report", NASA CR-61854, 1967.

Belton, M. J. S., Hunten, D. M., and McElroy, M. B., "A Search for an Atmosphere on Mercury", Astroph. J., 150, 1111-1124, 1967.

Camichel, H. and Dollfus, A., "La Rotation et la Cartographie de la Planete Mercure", Icarus, 8, 216-226, 1968.

Chapman, C. R., "Optical Evidence on the Rotation of Mercury", Earth and Planet. Sci. Letters, 3, 381-385, 1967.

Colombo, G. and Shaprio, I. I., "The Rotation of the Planet Mercury", Astroph. J., 145, 296-307, 1966.

Dollfus, A., "Polarization Studies of the Planets" in The Solar System, Vol. III Planets and Satellites (edit. by G. P. Kuiper and B. M. Middlehurst), U. of Chicago Press, 1961.

Dyal, P., Parker, C. W., and Sonett, C. P., "Apollo 12 Magnetometer: Measurement of a Steady Magnetic Field on the Surface of the Moon", Science, 169, 762-764, 1970.

Dyce, R. B., Pettingill, G. H., and Shapiro, I. I., "Radar Determination of the Rotations of Venus and Mercury", Astron. J., 72, 351-359, 1967.

Edsinger, L., "Parametric Sizing of Unmanned Spacecraft", to be published.

Field, G., "The Atmosphere of Mercury" in The Origin and Evolution of Atmospheres and Oceans (edit. by P. J. Brancazio and A. G. W. Cameron), John Wiley and Sons, New York, 1964.

Goldreich, P. and Peale, S., "Spin-Orbit Coupling in the Solar System", Astron. J., 71, 425-438, 1966.

Goldreich, P. and Peale, S., "The Dynamics of Planetary Rotations" in Annual Review of Astronomy and Astrophysics - Vol. 6, Annual Reviews, Palo Alto, Calif., 1968.

Goldstein, R. M., "Superior Conjunction of Pioneer 6", Science, 166, 598-601, 1969.

Goldstein, R. M., "Mercury: Surface Features Observed During Radar Studies", Science, 168, 467-469, 1970.

Good, R. C., Jr., "The Magnetosphere of the Planet Mercury as a Scattering Center for Solar Flare Protons", AIAA Paper 67-150, 1967.

Hahn, D. W., Johnson, F. T., and Itzen, B. F., "Final Report for Chebychev Trajectory Optimization Program (CHEBYTOP)", Boeing Report No. D2-121308, Boeing Co., Seattle, Wash., 1969.

REFERENCES (Continued)

Hãmeen-Antilla, K. A., Pikkarainen, T., and Camichel, H., "Photometric Studies of the Planet Mercury", Moon, 1, 440-448, 1970.

Horsewood, J. L. and Mann, F. I., "Optimum Solar Electric Interplanetary Trajectory and Performance Data", NASA CR-1524, 1970.

Howard, W. E. III, Barrett, A. H., and Haddock, F. T., "Measurement of Microwave Radiation from the Planet Mercury", Astroph. J., 136, 995-1004, 1962.

Johnson, H. A., "Detection, Sensitivity, and Related Statistics of Microwave Radiometry", Report No. 735, Naval Weapons Center Corona Labs., 1967.

Kellerman, K. I., "11-cm Observations of the Temperature of Mercury", Nature, 205, 1091-1092, 1965.

Kennet, H. and Spear, E. E., "Spacecraft Sizing Technique for Planetary Missions", AIAA Paper No. 69-125, 1969.

Klopp, D. A., edit., "Orbital Imagery for Planetary Exploration, Vol. II, Definitions of Scientific Objectives", NASA CR-73451, 1969.

Klopp, D. A., "Orbital Imagery for Planetary Exploration, Vol. I, Technical Summary", NASA CR-73450, 1970.

Koslovskaya, S. V., "On the Internal Constitution and Chemical Composition of Mercury", Astroph. Letters, 4, 1-3, 1969.

REFERENCES (Continued)

Lazar, J., "Current Status of Electric Propulsion Technology", AIAA Paper No. 69-1107, 1969.

Lieske, J. H. and Null, G. W., "Icarus and the Determination of Astronomical Constants", Astron. J., 74, 297-307, 1969.

Lyttleton, R. A., "On the Internal Structures of Mercury and Venus", Astroph. and Space Sci., 5, 18-35, 1969.

Majeva, S. J., "The Thermal History of the Terrestrial Planets", Astroph. Letters, 4, 11-16, 1969.

Manning, L. A., "Minimal Energy Ballistic Trajectories for Manned and Unmanned Missions to Mercury", NASA TN D-3900, 1966.

Manning, L. A., "Comparison of Several Trajectory Modes for Manned and Unmanned Missions to Mercury: 1980-2000", AIAA Paper No. 67-28, 1967a.

Manning, L. A., "Trajectory Modes for Manned and Unmanned Missions to Mercury: 1980-2000", J. of Spacecraft and Rockets, 4, 1128-1135, 1967b.

Manning, L. A., "Investigation of an Early Flyby Sequence for Imaging of the Planet Mercury", Paper No. VIII c.5, 15th Annual Meeting of Amer. Astronautical Soc., 1969.

McGovern, W. E., Gross, S. H., and Rasool, S. I., "Rotation Period of the Planet Mercury", Nature, 208, 375, 1965.

Melbourne, W. G. and O'Handley, D. A., "Recent Development Ephemerides and the Mass of Mercury", JPL Space Programs Summary 37-53, Vol. III, 1-4, 1968.

Mihalov, J. D., Sonett, C. P., Binsack, J. H., and Moutsoulas, M. D., "Possible Fossil Lunar Magnetism Inferred from Satellite Data", Science, 171, 892-894, 1971.

Morrison, D. and Sagan, C., "The Microwave Phase Effect of Mercury", Astroph. J., 150, 1105-1110, 1967.

Murdock, T. L. and Ney, E. P., "Mercury: The Dark-Side Temperature", Science, 170, 535-537, 1970.

North American Rockwell Corp., "Remote Sensor Systems for Unmanned Planetary Missions", Report SD 70-361-1, Space Division, 1970.

O'Leary, B. T. and Rea, D. G., "On the Polarimetric Evidence for an Atmosphere on Mercury", Astroph. J., 148, 249-253, 1967.

Peale, S. J., "Generalized Cassini's Laws", Astron. J., 74, 483-489, 1969.

Pettingill, G. H. and Dyce, R. B., "A Radar Determination of the Rotation of the Planet Mercury", Nature, 206, 1240, 1965.

Pettingill, G. H., Dyce, R. B., and Campbell, D. B., "Radar Measurements at 70 cm of Venus and Mercury", Astron. J., 72, 330-337, 1967.

Pikkarainen, T., "The Surface Structures of the Moon and Mercury Derived from Integrated Photometry", Publ. No. 14, U. of Oulu, Finland, 1969.

Pirraglia, J. and Gross, S. H., "Latitudinal and Longitudinal Variation of a Planetary Atmosphere and the Occultation Experiment", Planet. and Space Sci., 18, 1769-1784, 1970.

Reynolds, R. T. and Summers, A. L., "Calculations on the Composition of the Terrestrial Planets", J. of Geophys. Res., 74, 2494-2511, 1969.

Soter, S. and Ulrichs, J., "Rotation and Heating of the Planet Mercury", Nature, 214, 1315-1316, 1967.

Smith, B. A. and Reese, E. J., "Mercury's Rotation Period: Photographic Confirmation", Science, 162, 1275-1277, 1968.

Stein, M., "Telemetry Communications Guidelines", Report No. S-3, Astro Sciences Center, IIT Research Inst., Chicago, 1967.

Strack, W. C., "Solar-Electric Propulsion System Performance for a Close Solar Probe Mission", J. of Spacecraft and Rockets, 4, 469-475, 1967.

Uphoff, C., "The Long-Term Motion of Articifial Planetary Satellites", Report MDC G1228, McDonnell Douglass Astronautics Co., Western Div., Santa Monica, Calif., no date.

Vaughan, O. H. Jr., "Model Atmospheres of Mercury", AIAA Paper No. 69-54, 1969.

REFERENCES (Continued)

Winter, D. F. and Saari, J. M., "A Particulate Thermophysical Model of the Lunar Soil", Astroph. J., 156, 1135-1151, 1969.

Zola, C. L., "Interplanetary Probe Missions with Solar-Electric Propulsion System", NASA TN D-5293, 1969.